Development of an agreed set of climate projections for South Australia

Task 4: Development of an application test bed. Reservoir management models

Leon van der Linden and Michael D. Burch

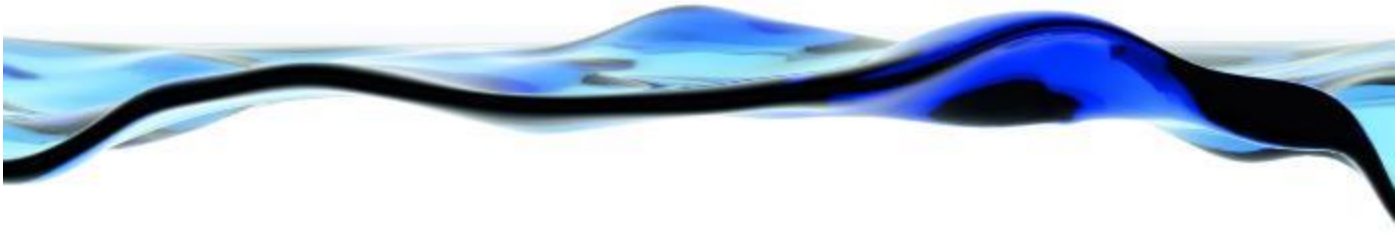

Goyder Institute for Water Research

Technical Report Series No. 16/3

www.goyderinstitute.org

Goyder Institute for Water Research Technical Report Series ISSN: 1839-2725

The Goyder Institute for Water Research is a partnership between the South Australian Government through the Department of Environment, Water and Natural Resources, CSIRO, Flinders University, the University of Adelaide and the University of South Australia. The Institute will enhance the South Australian Government's capacity to develop and deliver science-based policy solutions in water management. It brings together the best scientists and researchers across Australia to provide expert and independent scientific advice to inform good government water policy and identify future threats and opportunities to water security.

Enquires should be addressed to: Goyder Institute for Water Research
Level 4, 33 King William Street
Adelaide, SA, 5000
tel: 08-8236 5200
e-mail: enquiries@goyderinstitute.org

Citation

van der Linden, L. & M. D. Burch (2016). *Development of an agreed set of climate projections for South Australia, Task 4: Development of an application test bed. Reservoir management models,* Goyder Institute for Water Research Technical Report Series No. 16/3, Adelaide, South Australia

Copyright

Disclaimer

Executive Summary

This report is a contribution to the Goyder Institute for Water Research project '*An agreed set of climate projections for South* Australia' (Beecham, 2015). This project sought to deliver well-evaluated climate projections and downscaled data products that could be used by South Australian government, industry and the community alike, to be appropriately prepared and informed for future climate change i.e. be 'Climate Ready'. This report presents two components of work that contribute to the overall goal of demonstrating the application and utility of downscaled climate change projections and reservoir hydrodynamic-water quality models to assess future climate change impacts.

The report general introduction provides the context for the importance and risks of future climate change impacts upon surface water quality and why these risks need to be understood and quantified to effectively plan appropriate adaptive responses.

The project consisted of a two stage assessment:

1. The evaluation of the suitability of a coupled reservoir hydrodynamic water quality model to predict changes in water quality from altered meteorological boundary conditions (Chapter 1). (Also published as van der Linden *et al.*, 2015)
2. The second stage applied downscaling products from Task 3 that developed as part of the larger Goyder Water Research Institute project to determine the impacts on water quality in Mount Bold Reservoir, South Australia using a one-dimensional coupled water quality model. (Chapter 2)

Chapter 1 describes the application of a three-dimensional model (ELCOM-CAEDYM) at Happy Valley Reservoir, South Australia to a range of incremental manipulations of the meteorological boundary conditions. The model was used to determine responses to changes in air temperature, wind and inflow volume, which were evaluated independently (i.e. not factorial combinations). Climate change projections were used to identify and select appropriate changes in these variables. In addition the model was also used to test these variables outside these plausible ranges, so as to fully evaluate model behaviour within potential (but implausible) climate change. The growth of major phytoplankton groups was one of the important modelled outputs. The modelled response of these phytoplankton groups was within competitive growth response behaviour that was expected from an empirical climate sensitivity analysis that was based upon historical data. These modelling scenarios support the currently prevailing scientific theory that cyanobacteria, which produce nuisance tastes, odours and toxins and which compromise raw water quality, will become more successful in a warmer climate. This is consistent with a number of other modelling studies.

Chapter 2 describes the application of the downscaling products from Task 3 in the larger Goyder Water Research Institute project. These projections were used to determine future potential impacts upon water quality in Mount Bold Reservoir, South Australia using the one-dimensional coupled water quality model, GLM-FABM. This required the development of additional 'bolt-on' downscaling approaches to produce projected outputs for wind-speed and cloud cover. The wind speed downscaling approach employed parametric distributions (gamma or Weibull) fitted to observed wind-speed at local stations conditional upon the weather state used in the Task 3 downscaling product and the month of the year. These conditional distributions were then sampled according to the sequence of stochastically generated weather state and month combinations in the Task 3

downscaling. The cloud cover downscaling approach relied upon published methods to estimate cloudiness from the difference in ideal and observed solar radiation.

As this work was performed in parallel to the stream-flow analysis conducted by Westra et al. (2014), the catchment yield data they produced was unable to be incorporated in this study. Consequently, the reservoir water budget was constructed using a series of assumptions and repeating the historical water budget with minor volume adjustments. The parameter set used for biogeochemical and water quality related processes was derived from a well-validated but as yet unpublished application of GLM-FABM to Mount Bold Reservoir developed by Rigosi et al. as part of a study supported by the Water Research Foundation (Project 4382; Rigosi *et al.*, 2015). Reservoir simulations were run for a single realisation of the augmented Task 3 downscaled data for each of 15 Global Circulation Models (GCMs) in 30-year periods (1961-1990; 2011-2040; 2041-2070; 2071-2100); one historical emissions and two projected emission scenarios from the SRES emissions scenarios (representative), as used in the Coupled Model Inter-comparison Project 5 (CMIP5; Taylor *et al.*, 2012).

The resulting meteorological boundary conditions followed seasonally expected patterns and displayed trends derived from the Task 3 downscaling products. Wind-speed, which was an output product of this project, and not directly derived from the Task 3 outputs, showed no trends across time or emissions scenarios. This was as expected, as the transition probabilities between the weather states did not change between the different periods, or emissions scenarios. Superficially this may be considered one weakness of the approach as the data does not reproduce the projected decrease, or stilling, of wind speed at mid-latitudes. The magnitude of this reduction is expected to be small (McVicar *et al.*, 2008) and is probably most relevant in the late century when uncertainties associated with emissions are larger and dominant. Small increases in solar radiation, derived from the Task 3 downscaling products were propagated to result in decreases in cloud cover. Differences in the distributions of cloud cover were produced, mostly in the months of April, September, October and November.

Following simulation with GLM and calculation of ensemble statistics, the projected simulated water quality data demonstrate deteriorating trends in water quality that should be regarded as of concern for reservoir management. However, while the trends can be considered as leading to incrementally worse water quality than the historical period, it must be noted that 1), these assessments are of the direct effects upon water quality; changes in hydrological budget or external nutrient loading were not considered, and 2), the probability characteristics of the multi-day rainfall extremes are known to be under-represented in the NHMM outputs, and it is therefore reasonable to expect that this may also be the case for solar radiation (i.e. heat waves). The projections can therefore be considered to be conservative and represent a best case view of the direct effects of climate change on reservoir quality, i.e. in a situation where average wind speed does not decrease and the probability of heat waves does not change.

The results were broadly consistent with the prevailing understanding of the sensitivity of water quality to warming. Changes in abiotic water quality parameters seem to be predominantly driven by evaporation and the small changes in the reservoir water fluxes made to maintain the validity of the water budget. The worst case increases in surface water temperature resulted in increased growth of cyanobacteria.

Table of Contents

List of Figures

List of Tables

General Introduction

Climate change has been identified as a key challenge for the water industry due to impacts on water availability, energy prices and infrastructure longevity (Brueck *et al.*, 2012; Woodbury *et al.*, 2012). As the product of meteorological effects on physical, chemical and biological processes in landscapes and reservoirs, surface water quality has the potential to be influenced by climate change in many ways (Delpla *et al.*, 2009; Whitehead *et al.*, 2009). The sensitivity of reservoir water quality to the direct effects of climate depend on many factors including trophic state (Rigosi *et al.*, 2014), geographical position, catchment characteristics, morphology and a suite of biotic-abiotic interactions (Blenckner, 2005). A range of modelling activities have proven useful for evaluating climate related impacts on lakes and reservoirs (Jones *et al.*, 2011; Elliott, 2012; Trolle *et al.*, 2014), in combination with empirical studies. A recent review conducted by the authors identified the following risks associated with climate change, in a range of climatic regions: 1) increases in the frequency and severity of cyanobacterial blooms; 2) more frequent episodes of high turbidity; 3) increased frequency or severity of pathogen challenges, 4) elevated concentrations of dissolved organic matter, and 5) increased severity and duration of hypolimnetic deoxygenation. These anticipated risks have contributing factors that operate on a range of temporal scales and can be related to both changes in variability and climatic norms. The contributing factors include, increased rainfall intensity (risks 1, 2 and 3), increased variability in run-off (risks 2, 3 and 4), elevated average temperature (risks 1, 4 and 5) and increased frequency and duration of heatwaves (risks 1 and 5). As such these risks need to be understood and quantified in order to effectively plan adaptive responses.

In order to inform the process of evaluating climate related risks, an advanced understanding of climate processes and good quality downscaled climate projections are required. The Goyder Water Research Institute project '*An agreed set of climate projections for South Australia'* has contributed a significant effort towards understanding climate drivers in South Australia (Cai *et al.*, 2012; Beecham *et al.*, 2014; Cai, Borlace, *et al.*, 2014; Cai, Santoso, *et al.*, 2014) and the production of downscaled climate projections for all the natural resource management regions of South Australia. One such downscaled product from Task 3 of the project applies a non-homogenous hidden Markov model (NHMM) to stochastically downscale rainfall (Fu *et al.*, 2013), and other variables. Briefly, this is achieved by training the NHMM to determine the probability of transition between a series of weather states derived from observed synoptic scale weather patterns. Changes in the transition probabilities can also be derived from the outputs of global circulation models (GCMs) and subsequently used to generate stochastic realisations of statistically consistent (in terms of temporal auto correlation and cross correlation between variables) time series of potential weather data. For more detailed explanation of the methods refer to the Task 3 report for the project. The overall goal of Task 4 of the Goyder WRI C.1.1 project is to evaluate the suitability of the Task 3 outputs for modelling climate change impacts by developing a suite of modelling applications, including models of catchment hydrology, crop growth, groundwater, and drinking water reservoirs.

This report presents the output from the drinking water reservoirs component of Task 4 and is composed of two sections. First, the climate sensitivity of a three dimensional water quality model (Hipsey *et al.*, 2006; Hodges and Dallimore, 2007) is evaluated using a one-at-a-time incremental approach. Second, the downscaling products generated in Task 3 were used to construct a series of simulations of Mount Bold Reservoir using GLM-FABM, a coupled 1D hydrodynamic – water quality model (Hipsey *et al.*, 2013).

Chapter 1. Suitability of a coupled hydrodynamic water quality model to predict changes in water quality from altered meteorological boundary conditions

Abstract:

Downscaled climate scenarios can be used to inform management decisions on investment in infrastructure or alternative water sources within water supply systems. Appropriate models of the system components, such as catchments, rivers, lakes and reservoirs, are required. The climatic sensitivity of the coupled hydrodynamic water quality model ELCOM-CAEDYM was investigated by incrementally altering boundary conditions, to determine its suitability for evaluating climate change impacts. A series of simulations were run with altered boundary condition inputs for the reservoir. Air and inflowing water temperature (TEMP), wind speed (WIND) and reservoir inflow and outflow (FLOW) were altered to investigate the sensitivity of these key drivers over relevant domains. The simulated water quality variables responded in broadly plausible ways to the altered boundary conditions; sensitivity of the simulated cyanobacteria population to increases in temperature was similar to published values. However the negative response of total chlorophyll-*a* suggested by the model was not supported by an empirical analysis of climatic sensitivity. This study demonstrated that ELCOM-CAEDYM is sensitive to climate drivers and may be suitable for use in climate impact studies. It is recommended that the influence of structural and parameter derived uncertainty on the results be evaluated. Important factors in determining phytoplankton growth were identified and the importance of inflowing water quality was emphasised.

Introduction

The Goyder Water Research Institute project C.1.1 was initiated to address a knowledge gap in the current understanding of the potential impacts of climate change on South Australia. The purpose of the project was to gain understanding of climate drivers, downscale global circulation (GCM) model projections of future climate and develop a suite of model applications suitable for use in assessment and adaptation frameworks. Current global circulation model (GCM) projections suggest that Australian average temperatures will increase by 1.0 to 5.0 degrees by 2070 (compared to 1980-1999), rainfall will decrease over southern Australia and the number of hot days and warm nights will increase (CSIRO, 2012). Decreases in autumn and winter wind speed and increases in winter and spring downward solar radiation are also projected, but these projections are subject to large uncertainties (CSIRO, 2007). Recent efforts to downscale GCM outputs to the catchment scale have identified the potential for reduced catchment yields as the result of reduced precipitation, changes in rainfall seasonality and increased temperatures (Charles *et al.*, 2008; Heneker and Cresswell, 2010; Green *et al.*, 2011). Besides issues of water quantity, there are potential impacts of climate change on water quality (Delpla *et al.*, 2009; Whitehead *et al.*, 2009). Reservoirs play a major role in determining the water quality within a given water supply system, as they act as both barriers to (e.g. pathogens) and producers of (e.g. cyanobacteria [toxins, tastes and odours], iron and manganese) water quality hazards (Brookes *et al.*, 2008). Reservoirs integrate the prevailing hydrology, meteorology, biology and biogeochemistry and the resulting quantity and quality of water is a valuable resource that requires sound management to ensure the utility and sustainability of the source water; water quality models are a tool to facilitate this end.

The potential impacts of climate change on water quality have been evaluated using integrated modelling schemes which include water quality models (Mimikou *et al.*, 2000; Arheimer *et al.*, 2005; Thorne and Fenner, 2008; Saloranta *et al.*, 2009; Elliott, 2012). Such schemes use a combination of catchment and lake/reservoir models that use meteorological boundary conditions as inputs. The meteorological conditions are altered to represent projected future climate and the resulting simulations are taken to represent the potential impacts of those changed climatic conditions. Too few of these studies have been conducted to make generalisations about the potential impacts; both positive and negative influences have been identified. Additionally, the differences in model structure and method make it difficult to compare the different studies directly. There are many sources of uncertainty within such a modelling scheme, including the choice of GCM, emissions scenario, downscaling methodology, and the selection of and rigour of application of the hydrological, constituent and lake/reservoir water quality models, including model structure selection and identification of parameters. Each step in the modelling scheme needs to be thoroughly evaluated to ensure the results can be useful.

It is therefore appropriate to adequately test the response of the proposed reservoir water quality model to changes in the environmental variables expected to change in the future. Formalising our understanding of the way that water quality variables respond to climate related model inputs is fundamentally important to understanding the outputs we generate from models (Elliott, 2012). As these models will be used to project the impacts of downscaled climate scenarios, it is important that the response of the water quality models to the boundary conditions is understood. Water quality models vary in their data input requirements and often contain options for the sub-model structures they contain, making it difficult to assume that they will be equally sensitive in any given application. Responses of chemical and biological processes to the changes in physical state generated by changes in meteorological inputs are dynamic and interactive and therefore difficult to resolve without resolving individual sensitivities in an explicit analysis.

The outputs from any model are dependent on the inputs. It follows that uncertainty in the inputs, either the boundary conditions or the model parameters, contributes to the uncertainty of the model results. Quantification of the influence of the inputs on the model outputs is known as sensitivity analysis and has been extensively described in the literature. Complex models with many parameters, boundary conditions and long runtimes have particular challenges associated with the analysis of their sensitivity and uncertainty. Consequently a great deal of effort has gone towards developing screening methods to identify sensitive parameters and evaluate their influence on model output (Saltelli, 2002; Campolongo *et al.*, 2007; Arhonditsis *et al.*, 2008; Makler-Pick *et al.*, 2011). Less often the influence of boundary conditions or input data is evaluated. Generally the error associated with these inputs is considered to be less than the uncertainty associated with model parameters as they are quantities that are generally measured at, or proximal to, the lake or reservoir being modelled, using accurate instrumentation. However the range of meteorological boundary conditions are expected to change in the future (Schlabing *et al.*, 2014) and given the non-linear and non-monotonic nature of ecosystem models, their behaviour in these conditions is uncertain. As suitable observed validation data cannot exist for unobserved future conditions, model behaviour under altered boundary conditions can only be validated against qualitative projected responses of ecosystems. These qualitative responses may be derived from space-for-time approaches, robust ecophysiological conceptual models and response data (Paerl and Paul, 2012) and ensemble model predictions (Trolle *et al.*, 2011).

Therefore, the goal of this work is to answer the question: Does ELCOM-CAEDYM demonstrate appropriate climatic sensitivity to be used as part of a robust integrated modelling scheme? The responsiveness of the ELCOM-CAEDYM model (Hipsey *et al.*, 2006; Hodges and Dallimore, 2007) to changes in meteorological boundary conditions was analysed. A previous application of the model to Happy Valley Reservoir (HVR) was used in conjunction with scenarios with altered environmental forcing of incremental changes in flow, air and water temperature, and wind speed. Responses in water quality variables of primary focus were cyanobacteria and soluble metals; further consideration was given to water temperature and water column stratification due to their important role in determining mixing and the rates of biogeochemical reactions. This work does not constitute a model sensitivity analysis, *sensu stricto*, but evaluates the climatic sensitivity or responsiveness of ELCOM-CAEDYM and compares it to other studies and an empirical climate sensitivity analysis of chlorophyll-*a* in Happy Valley Reservoir.

Materials and Methods

Happy Valley Reservoir

Happy Valley Reservoir (HVR; 35.07 S, 138.57 E) was created by the construction of an earth wall dam between 1892 and 1897. Following a rehabilitation project from 2002 to 2004, it has a capacity of 11,600 ML, a surface area of 178 hectares and average and maximum depths of 6.5 and 18 m, respectively. It is an off stream reservoir and supplies raw water to South Australia's largest water treatment plant, which produces up to 400 ML of filtered water per day, resulting in a hydraulic retention time of 15-30 days. As HVR is isolated from its natural catchment, it is supplied with water from the Onkaparinga River system via an aqueduct from Clarendon Weir, which is in turn supplied from the much larger Mount Bold Reservoir (35.12 S, 138.70 E). Mount Bold Reservoir collects water from the Mount Lofty Ranges and is supplemented with water pumped from the River Murray, as are most of South Australia's reservoirs. Happy Valley Reservoir has experienced a range of water quality challenges in the past, with blue-green algae (cyanobacteria) causing taste and odour problems in recent decades. The use of artificial destratification (mixing) and algaecides are used for management in the reservoir, while granular activated carbon is used in the water treatment process to reduce taste and odour compound concentrations to acceptable levels in the product water. As HVR is supplied with water from an unprotected catchment (i.e. containing various farming activities and human habitation), vigilance against pathogens is required and loads of nutrients are greater than is generally desirable. During the study period, nutrient concentrations were, total phosphorus, 0.05-0.1 mgL^{-1}; total Kjeldahl nitrogen, 0.5-1.0 mgL^{-1}; filterable reactive phosphorus, 0.005-0.03 mgL^{-1}; ammonia, 0.005-0.05 mgL^{-1} and oxidized nitrogen, 0.05-0.5 mgL^{-1}. The seasonal temperature range is generally between 8-10 °C and 25-27 °C; strong persistent stratification is prevented from occurring by the operation of a bubble plume aerator. Due to the importance of Happy Valley Reservoir to Adelaide's water supply, the South Australian Water Corporation has invested heavily in monitoring and research into the processes influencing water quality.

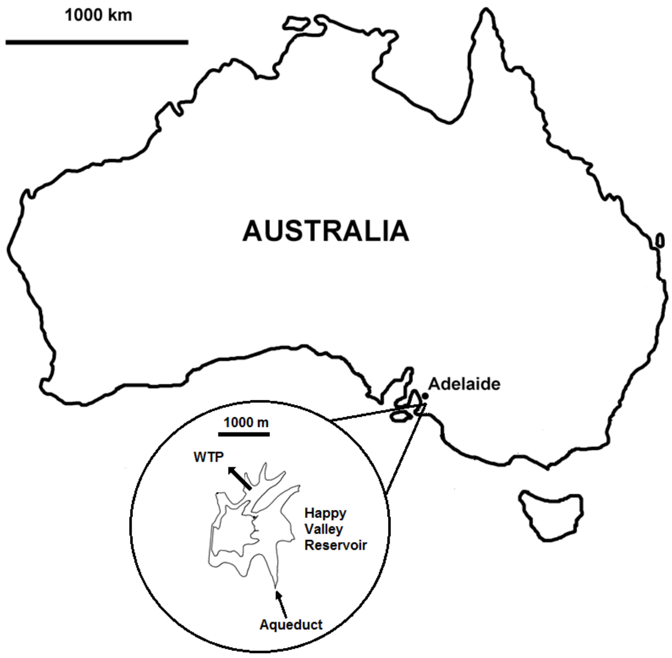

Figure 1. Location of Happy Valley Reservoir. Inset shows 10 m contours of depth and inflow from the aqueduct and the location of the offtake to the water treatment plant (WTP).

Model Description

The Estuary and Lake Computer Model (ELCOM) is a hydrodynamic model that simulates the temporal behaviour of stratified water bodies using environmental inputs such as inflows, outflows and meteorological conditions. The model solves the unsteady, viscous Navier-Stokes equations for incompressible flow using the hydrostatic assumption for pressure. The simulated processes include baroclinic and barotropic responses, rotational effects, tidal forcing, wind stresses, surface thermal forcing, inflows, outflows, and transport of salt, heat and passive scalars (Hodges and Dallimore, 2007). When coupled with the Computational Aquatic Ecosystem DYnamics Model (CAEDYM, Hipsey *et al.*, 2006) water quality model, ELCOM can be used to simulate three-dimensional transport and interactions of flow physics, biology and chemistry. ELCOM uses the Euler-Lagrange method for advection of momentum with a conjugate-gradient solution for the free-surface height. Passive and active scalars (*i.e.*, tracers, salinity and temperature) are advected using a conservative ULTIMATE QUICKEST discretization (See Hodges and Dallimore, 2007 and references within for further details). ELCOM v2.2.2-04 and CAEDYM v3.3.0-01 were used in this study.

The Centre for Water Research was previously engaged to apply ELCOM-CAEDYM to Happy Valley Reservoir (Romero *et al.*, 2005). Upon delivery, the model was considered appropriate for the simulation of water movement, contaminant transport, algal growth and biogeochemical cycling (Romero *et al.*, 2005). ELCOM was applied at three resolutions (25, 50 and 100 m grid sizes); the finest grid to be used for examining short-circuiting and inflow dilution, and the coarser grids for quicker runtimes and running scenarios relating to stratification, algal growth and soluble metal release from sediments (the 100 m grid was used in this study). The hydrodynamic model was validated against temperature sensor data over two periods, 29 June–6 October 2005 and 23 October 2005–8 February 2006. The parameter set for CAEDYM was derived from applications to other Australian reservoirs and some minor calibration of parameters to suit Happy Valley Reservoir. The manual calibration focused on parameters that could not be derived from literature values and included, the density of particulate organic matter, the maximum rates for microbial decomposition of particulate organic phosphorus and nitrogen, the maximum rate of mineralization of dissolved organic phosphorus and nitrogen, the dissolved oxygen ½ saturation constant for nitrification, the rate of denitrification and the phosphorus ½ saturation constant for algal uptake. Some deficiencies in the calibration of the algal growth components of the model remained.

Two algal groups were included in the model structure, representing chlorophytes (green algae) and cyanophytes (blue-green algae). The phytoplankton growth model was parameterized according to literature values, with only a single parameter being manually calibrated for Happy Valley Reservoir (Table 1). Parameters relating to light, temperature, phosphorus uptake and respiratory losses were different between the two phytoplankton groups. All other parameters were shared and derived from literature values. Notably, buoyancy regulation by cyanobacteria was not invoked in the model structure.

For this work, the model was not further calibrated or modified beyond the work of Romero *et al*. (2005) and therefore no performance metrics are presented. The lack of extensive calibration to HVR water quality dynamics means the results of the study can be considered to be a general test of the response sensitivity of ELCOM-CAEDYM to climate drivers and not an investigation of the likely effects of climate change on water quality in Happy Valley Reservoir.

Table 1. Phytoplankton group parameters that differentiate the response to ecophysiological drivers in the ELCOM-CAEDYM model set up.

Parameter	Cyanophyte value	Chlorophyte value	Description (units)	Reference
μ_{GTH}	0.8	1.2	Maximum growth rate (d^{-1})	(USCE, 1995)
ϑ_{Ag}	1.09	1.07	Temperature multiplier for growth (-)	(Coles and Jones, 2000; Krüger and Eloff, 2010)
μ_{RES}	0.09	0.10	Respiration, mortality and excretion (d^{-1})	(Schladow and Hamilton, 1997)
K_P	0.009	0.008	P ½ saturation constant (mg L^{-1})	Calibrated
I_K	130	100	Light ½ saturation constant (μE m^{-2} s^{-1})	(Hamilton and Schladow, 1997)
T_{STD}	24	20	Standard temperature for algal growth (°C)	(Griffin *et al.*, 2001)
T_{OPT}	30	22	Optimum temperature for algal growth (°C)	(Robarts and Zohary, 1987; Griffin *et al.*, 2001)
T_{MAX}	39	35	Maximum temperature for algal growth (°C)	(Griffin *et al.*, 2001)

Scenarios for Analysis of Climatic Sensitivity

A series of twenty four (24) scenarios were defined, synthetic input data files were generated and ELCOM-CAEDYM simulations were run. As stratification, algal growth and soluble metal concentrations were of key interest, the summer period simulation was used. The 100 m grid version of ELCOM was used to minimise the runtime required, as short-circuiting was not a primary concern of the water quality problems being investigated. The input boundary conditions analysed were selected to represent the 'climate drivers' of precipitation, air temperature and wind speed and are represented by the input files as changes in flow, air and water temperature, and wind speed, respectively (these are referred to as INFLOW, WIND and TEMP in the text). The synthetic input files were generated by applying a linear multiplier, for INFLOW and WIND, and an increment in the case of TEMP (Table 2). Temperature was modified in this fashion to facilitate comparison to potential temperature change magnitudes. For comparison, -5 and +5 degrees correspond to multipliers of 0.8 and 1.25, respectively, at 20 degrees Celsius, similar to the average temperature in the reservoir during the simulations. As ELCOM-CAEDYM will fail if changes to the water budget result in violations in the boundary conditions, changes in the inflow and outflow must be balanced, therefore the outflow (consumption at the offtake) was increased by a corresponding amount. The FLOW scenarios could therefore be considered to represent a change in the consumption of water by the water treatment plant (WTP), rather than changes in precipitation, strictly. This may initially seem artificial; however, as HVR is an offline storage and the inflow to the reservoir is fully regulated by a flume at Clarendon Weir, it can be interpreted as representing changes in demand, especially as a summer period was considered.

Table 2. Boundary condition modifications applied in the sensitivity analysis. A scenario was generated for each change in meteorological variable, resulting in twenty four (24) scenarios differing from the base scenario.

Temperature (TEMP) *[increment]*	Precipitation (FLOW) *[multiplier]*	Wind Speed (WIND) *[multiplier]*
-5.0	0.50	0.50
-2.0	0.75	0.75
-1.0	0.90	0.90
-0.5	0.95	0.95
0.5	1.05	1.05
1.0	1.10	1.10
2.0	1.25	1.25
5.0	1.50	1.50

The scenarios were run using the same initial conditions; a 'spin-up' period of 1 week was excluded from all summary calculations to reduce the influence of errors in the initial conditions. As potable water production is the focus of the study, water quality (temperature, suspended solids, chlorophyll, iron and manganese) at the reservoir offtake was analysed, along with 'whole of reservoir' characteristics, such as water temperature and g' (the reduced gravity due to stratification, Hodges and Dallimore, 2007). Changes in water quality were evaluated as changes in the mean concentration, the maximum concentration and the period of the simulation that the concentration was above a threshold value (green algal and cyanobacterial chlorophyll only, 1 and 10 µg/L, respectively). In order to facilitate the interpretation of the phytoplankton dynamics, summaries of the state variables governing the growth of the two species modelled were calculated as means of the time series values.

An Empirical Analysis of the Climatic Sensitivity of Chlorophyll-a to Temperature

Historical records of *chlorophyll-a* and water temperature were collated from the primary reservoir surface monitoring location for the period 1998 to 2013. Monthly medians and anomalies were calculated for water temperature and chlorophyll-*a* concentration. The monthly anomalies were normalised to unity, so as to be able to compare directly to modelling results summarised with a similar method. Linear regressions were fitted to the raw anomalies and normalised values, both for the entire year and for the summer months only.

Results and Discussion

Reservoir Physical Characteristics

The (modelled) physical properties of the Reservoir were altered by the changes in boundary conditions. The degree of stratification, as indicated by average *g',* was altered in all scenarios; increases in wind speed had a strong negative effect on lake stratification (Table 3). Increasing air and inflowing water temperature resulted in increased reservoir stratification, as did increased flow. Water temperature in the reservoir was not strongly influenced by the INFLOW scenarios, however the WIND and TEMP scenarios had strong effects on the mean of the average, minimum and maximum water temperatures observed over the simulations (Table 3). Only small impacts on reservoir volume and level were observed (not shown).

Table 3. Summary of average physical properties for climatic sensitivity analysis of ELCOM-CAEDYM simulations of Happy Valley Reservoir.

Factor	Increment /Multiplier	g' ($/s^2$)	Temp mean (°C)	Temp max (°C)	Temp min (°C)
Original	-	**0.0502**	**20.5**	**21.8**	**16.5**
INFLOW	0.50	0.0481	20.9	22.2	16.6
INFLOW	0.75	0.0490	20.8	22.0	16.6
INFLOW	0.90	0.0496	20.6	21.9	16.5
INFLOW	0.95	0.0498	20.6	21.9	16.5
INFLOW	1.05	0.0503	20.5	21.8	16.5
INFLOW	1.10	0.0505	20.5	21.8	16.6
INFLOW	1.25	0.0510	20.3	21.7	16.6
INFLOW	1.50	0.0513	20.2	21.5	16.6
TEMP	-5.0	0.0454	17.0	18.3	13.4
TEMP	-2.0	0.0481	19.1	20.4	15.9
TEMP	-1.0	0.0490	19.8	21.1	16.2
TEMP	-0.5	0.0495	20.2	21.5	16.4
TEMP	+0.5	0.0505	20.9	22.2	16.7
TEMP	+1.0	0.0511	21.3	22.5	17.0
TEMP	+2.0	0.0524	22.0	23.2	17.3
TEMP	+5.0	0.0571	24.1	25.4	17.5
WIND	0.50	0.0984	22.7	25.9	17.0
WIND	0.75	0.0681	21.5	23.4	17.0
WIND	0.90	0.0560	20.9	22.4	16.7
WIND	0.95	0.0528	20.7	22.1	16.6
WIND	1.05	0.0474	20.4	21.6	16.6

WIND	1.10	0.0452	20.2	21.4	17.2
WIND	1.25	0.0397	19.8	20.8	17.4
WIND	1.50	0.0334	19.3	20.1	17.3

Water Quality

An increase in average modelled cyanobacterial chlorophyll (CyanoChl) was observed with elevated temperature, while simulated chlorophyte chlorophyll (ChloroChl) decreased (Figure 2a). The average concentration of reduced soluble iron (FeII) also increased with temperature while soluble manganese (MnII) was less responsive (Figure 2a). Sensitivity responses were close to linear near the origin (±10%), but some became non-linear at the extremes of the scenarios investigated. Exceedance of the threshold selected for cyanobacterial chlorophyll (CyanoChl) increased approximately linearly with increasing temperature above that of the original scenario, but had little effect below that level (data not shown). The FLOW scenarios had a consistently linear influence on reservoir water quality; increasing average concentrations of chlorophyte (ChloroChl) and cyanobacterial chlorophyll (CyanoChl), MnII and FeII were observed in simulations with reduced flow; only the average concentration of suspended solids (SSOL1) decreased with decreasing flow (Figure 2b). Changes in maximum modelled values behaved similarly as did duration of exceedance for the chlorophyll variables (not shown).

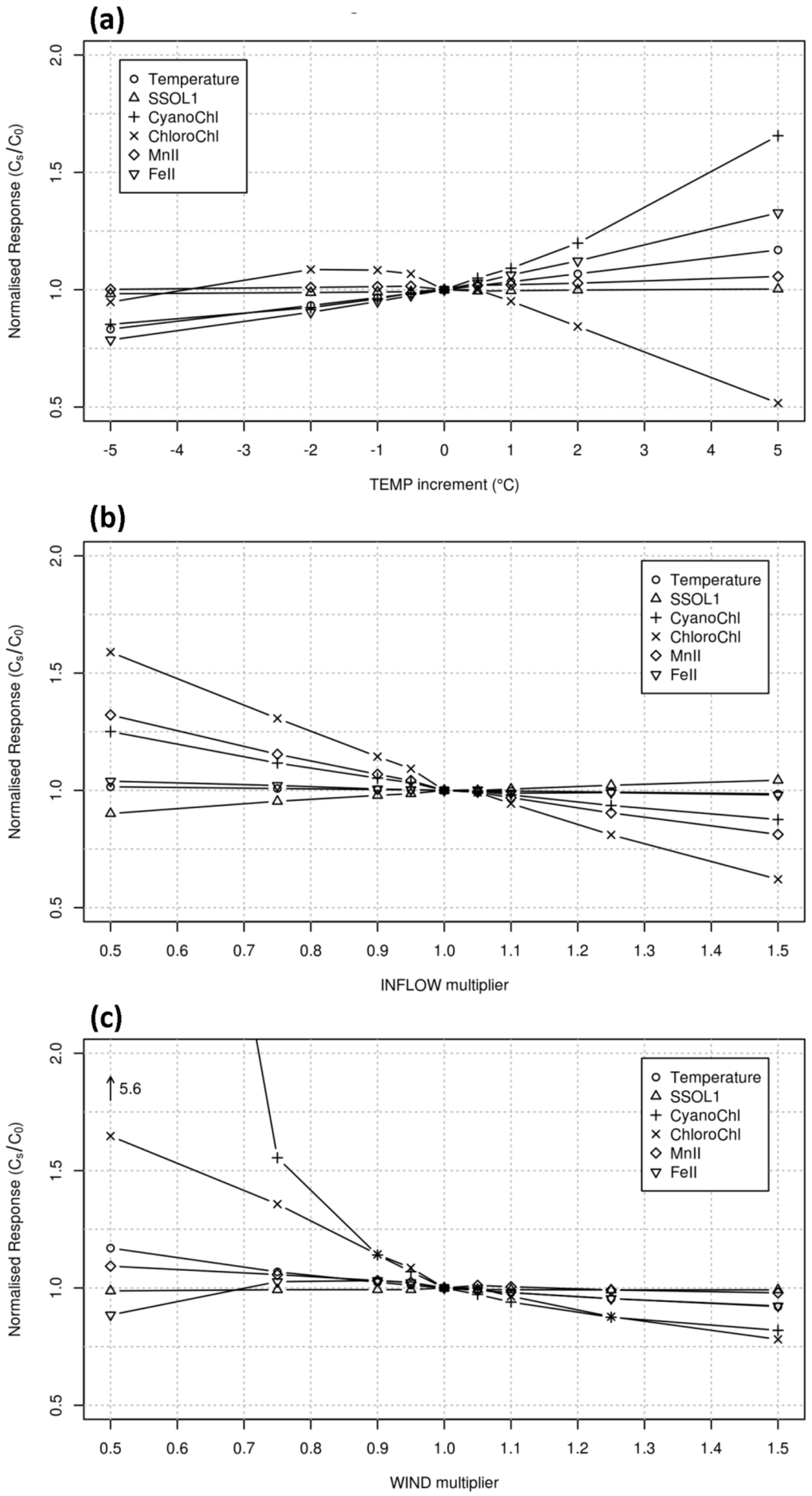

Figure 2. Change in mean modeled water quality values over the summer period in the different sensitivity analysis scenarios where temperature (a**), rate of inflow and outflow (**b**) or wind speed (**c**) were incrementally changed.**

The relationship between WIND and algal growth was obviously non-linear with large increases in the average concentrations of both algal groups with decreasing wind speed (Figure 2C). Cyanobacteria were especially favoured by low wind speeds. Reduction of wind speed from 90% to 75% of today's averages resulted in a large increase in the duration of exceedance by cyanobacteria (not shown). The simulated phytoplankton production rates were low (~0.1 day^{-1}) compared to what they can potentially be (~0.3-0.5 day^{-1}) and probably are in HVR. This was also noted by Romero et al. (2005). The simulated whole lake averages of respiration exceeded that of production in cyanobacteria, indicating that they were limited to growing in a limited volume of the lake where sufficient light was available. Elevated temperatures increased cyanobacterial production rates but these increased production rates were kept in check by elevated respiration. There was very little change in the nutrient (N & P) limitation of phytoplankton, even under the INFLOW scenarios; simulated phytoplankton growth was more limited by light availability (Table 4).

Table 4. Mean cyanobacterial growth characteristics in ELCOM-CAEDYM simulations. The 'Limitation by' values indicate the degree of growth limitation by light, phosphorus and nitrogen. It takes a value from 0 to 1; where 1 is unlimited and 0 is completely limited (no growth)

Scenario	Production (day^{-1})	Respiration (day^{-1})	Limitation by: Light	Phosphorus	Nitrogen
Original	**0.080**	**0.093**	**0.099**	**0.915**	**0.890**
INFLOW by 0.5	0.079	0.096	0.095	0.916	0.883
INFLOW by 1.5	0.081	0.091	0.102	0.916	0.890
TEMP by -5	0.061	0.076	0.101	0.917	0.890
TEMP by +5	0.108	0.115	0.106	0.909	0.884
WIND by 0.5	0.083	0.106	0.086	0.923	0.899
WIND by 1.5	0.075	0.087	0.103	0.917	0.889

Implied Model Climatic Sensitivity

These scenarios demonstrate that ELCOM-CAEDYM is responsive to changes in environmental drivers that are expected to change under future climate. The model tested was not heavily calibrated and therefore the results are able to be generalised. The observed sensitivities are consistent with qualitative expectations on the basis of contemporary understanding of reservoir processes. For example, it is generally accepted that increased water temperatures and stratification may increase the prevalence of cyanobacteria and result in longer periods of decreased dissolved oxygen concentration and higher dissolved metal concentration. Other authors have observed model climatic sensitivities that resulted in increases in the proportion of cyanobacteria by 1 - 7.8% per 1 °C increase in temperature (using the model PROTECH; Elliott *et al.*, 2006). From a review of the literature of the potential impact of climate on phytoplankton communities, Elliott (2012) concluded that projected future climate would result in increased relative abundance of cyanobacteria and changes in the phenology of phytoplankton dynamics but not necessarily an increase in the seasonal amount of phytoplankton biomass. These conclusions are consistent with the responses observed in this study.

Important interactions with nutrient availability exist (Mooij *et al.*, 2007) but this was not investigated here. As an independent factor, nutrient addition (*sensu* INFLOW scenarios) did not have a large effect on the phytoplankton dynamics, presumably because of the lack of nutrient limitation (Table 4). The model tested in this study employed a relatively simple representation of phytoplankton community dynamics; only two main functional groups were represented. Furthermore some physiological mechanisms that facilitate cyanobacterial dominance, despite being available in CAEDYM, were not used in the model application of Romero et al. (Romero *et al.*, 2005). Greater sensitivity and/or more non-linearity may be expected if these mechanisms (e.g. buoyancy regulation) were implemented.

The environmental drivers that were manipulated in the scenarios were not investigated factorially, however they are not completely independent; changes in mean and maximum water temperature occurred in the INFLOW and WIND scenarios (Table 3). This complicates the interpretation of model outputs without extensive comparison of individual simulations; an effort not warranted by the goals of this study. The scenarios were arbitrarily selected to quickly develop a picture of the sensitivity of the model to changed boundary conditions. As such, the important environmental drivers of dilution and nutrient loading are confounded in the multiplication of inflow volumes. Inflow scenarios assumed the same constituent concentrations and therefore the higher flow scenarios had higher nutrient loads. However as chlorophyll concentrations decreased as flow increased, it is apparent that dilution was a more important driver of algal biomass than nutrient load and availability. Despite this, the prediction that phytoplankton growth is rarely limited by nutrient availability may suggest that reducing the external load may be an option for reducing algal growth. The internal load was not investigated as part of this study but given the short water retention time of the reservoir, it is probably of minor importance, compared to the external load. The reduction of nutrient availability represents a potential strategy for adaptation to climate change and the likely negative effects on water quality resulting from increased cyanobacterial growth. Water quality models, such as ELCOM-CAEDYM, can have an important role to play in determining the potential benefit of a nutrient reduction program.

Empirical Reservoir Climatic Sensitivity

Linear regression between water temperature and chlorophyll median monthly anomalies did not resolve slope estimates significantly different from zero (0.105 ± 0.134, Pr(>|t|) = 0.43). The weak positive slope estimate combined with a poor predictive relationship (R^2 = 0.014) demonstrates that surface water temperature did not play an important role in determining total chlorophyll in this period (Figure 3b); it also demonstrates that it was not negatively correlated with water temperature, as implied by the water quality model (Figure 3a). This might suggest that deficiencies in definition of model structure or parameter identification have resulted in a non-behavioral model response (one not consistent with our expectations). These deficiencies could, for example, be found in the parameterization of the temperature response functions for growth, or be the product of the over-simplification of the phytoplankton community. This remains speculative, as this simple comparison cannot resolve the differences between the processes structuring algal growth in the model scenarios as compared to those operating over a longer period and in different years, within the reservoir. It must further be noted that the empirical analysis is limited to (monthly) anomalies less than +2°C and so could not explore the full range of (annual) anomalies as defined by the model scenarios.

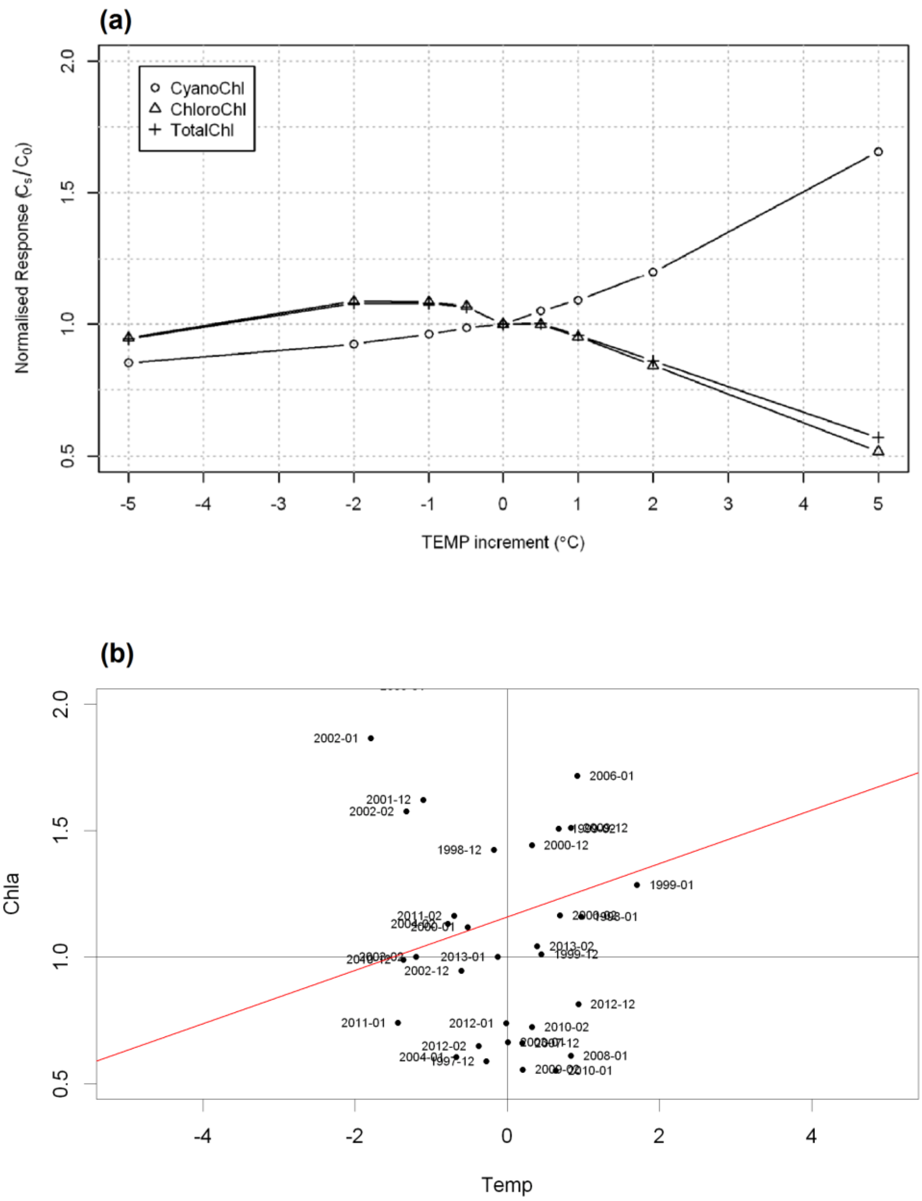

Figure 3. Comparison of (a) model derived climate sensitivity to (b) empirical reservoir climate sensitivity of chlorophyll-*a* to temperature in summer (Dec, Jan, Feb). In panel (b) each point represents the unity normalized anomaly from the monthly median value calculated over the period 1998-2013 and is labelled as yyyy-mm.

4. Conclusions

This study demonstrated that ELCOM-CAEDYM is sensitive to climate drivers and suitable for use in climate impact studies. It further highlighted the important factors in determining phytoplankton growth and that any changes in inflowing water quality will be of major importance to the reservoir water quality dynamics.

Chapter 2. Direct impacts of climate change on water quality in Mount Bold Reservoir using downscaled meteorology.

Introduction

The potential impacts of climate change on water quality can be evaluated using integrated modelling schemes (Mimikou *et al.*, 2000). Such modelling schemes consist of catchment and reservoir models with boundary conditions defined by downscaling or weather generator methods (Schlabing *et al.*, 2005, 2014). A set of downscaling products were generated by Task 3 of the Goyder Water Research Institute Project C.1.1. These downscaling products were used to construct a series of simulations of Mount Bold Reservoir using the General Lake Model – Framework for Aquatic Biogeochemical Models (GLM-FABM), a coupled 1D hydrodynamic – water quality model (Hipsey *et al.*, 2013). Some important meteorological variables required as model boundary conditions/inputs were not available from the Task 3 downscaling, including wind speed, cloud cover and longwave radiation. These variables were therefore imputed from relationships between measured weather variables from a range of relevant data sources as described below. The imputed data is compared to the original dataset compiled for Mount Bold Reservoir for the application of DYRESM-CAEDYM; the input dataset comprises data from observations at Mount Bold Reservoir as well as Happy Valley Reservoir and other sites. The base case model has been validated for this dataset. Therefore the statistical properties of the downscaled data are compared to this three year period to evaluate their consistency and therefore their suitability for implying potential changes in water quality in South Australia's reservoir from climate change. This report presents a preliminary investigation of the impacts and caution must be applied in the interpretation of the results, as many sources of error remain to be characterised.

Methods

The first task required was the development of methods to impute the non-downscaled variables. It is normal practice to base model input data on 'on reservoir' measurements of meteorology in so far as possible. However, available datasets are rarely complete and gap-filling, by imputation or modelling of data, is generally applied when setting up model boundary conditions and forcing variables, in this context, meteorology and inflows to, and withdrawals from a reservoir.

Sources of data

Data was sourced from the NOAA ISD-Lite dataset (ftp.ncdc.noaa.gov/pub/data/noaa/), the Australian Bureau of Meteorology's SILO data base (www.longpaddock.qld.gov.au/silo), weather underground (www.wunderground.com) and SA Water's own data from floating weather stations (i.e. Figure 4).

Wind speed

The method downscaled wind speed consisted of using the weather states of the NHMM, or other weather states defined by the other variables (i.e. wet/dry state), to develop conditional distributions of the required variables. As wind speed at the surface of the reservoir is of primary interest, preferably measured using a floating weather station (Figure 1), there is a limited amount of data available to develop these distributions. The available observed data must be further divided among the conditional weather states. Therefore, generating longer time series of wind speed by linear modelling from other nearby stations was investigated. It was hoped that this extrapolation approach would allow the generation of satisfactory empirical distributions or provide better resolved parameters for parametric distributions.

Data for wind speed from a number of sites were trialled and their suitability evaluated by visualising time series (e.g. Figure 5), autocorrelation properties (Figure 6), frequency distributions (Figure 7) and fitting linear regressions (Figure 8; Figure 9; Figure 11). The most similar statistical properties were found with the physically closest meteorological station (Kuitpo). Regressions were also fitted to monthly subsets of the data in order to investigate if any seasonality was influencing the regression performance. This additional complexity did result in slightly lower residual error and a marginal improvement in the distribution of the residuals (Figure 10; Figure 12). Simulated data from the models developed were subjected to Kolmorgorov-Smirnov (K-S) tests to test the reproduction of distribution properties; the wind speed predictions from Kent Town appear similar but the null hypothesis, that the samples come from the same distribution, was rejected (Figure 13). The wind speed distributions generated from the Kuitpo model, however, were able to be considered to be the same as the observations at Mt Bold (Figure 14). Despite having the best statistical performance, the Kuitpo station had a much shorter period of observations than the Kent Town station. Consequently, the monthly models were used to predict an extended range of wind speed data from both the Kuitpo and Kent Town stations. The longer period of wind speed data generally allowed resolution of conditional distributions of wind speed by NHMM weather state (Figure 15), however some less frequent weather states remain poorly resolved. Some months seem to have weather states that have different distributions, May and September, for example. Changes in the frequency of weather states may therefore result in changes in wind speed distribution.

Two parametric distributions, Gamma and Weibull, were fitted to wind speed conditional on month and NHMM weather state (these distributions are generally considered to fit wind speed data well) using *fitdistr* from the *MASS* package (Venables and Ripley, 2002). The best of the two distributions was selected on the basis of the log likelihood calculated during the distribution fitting. A representative example was selected (Figure 16) which demonstrates the differential performance of the distributions within different weather states and one of the more poorly resolved 'rare' weather states (Figure 16, NHMM state = 4). The parameters estimated during the fitting process were subsequently used to stochastically generate wind speed for a given month and weather state.

Figure 4. Floating weather station at Mt Bold Reservoir. Featuring ultrasonic wind speed and direction, global and long wave radiation sensors, air temperature and humidity and water temperature at multiple depths.

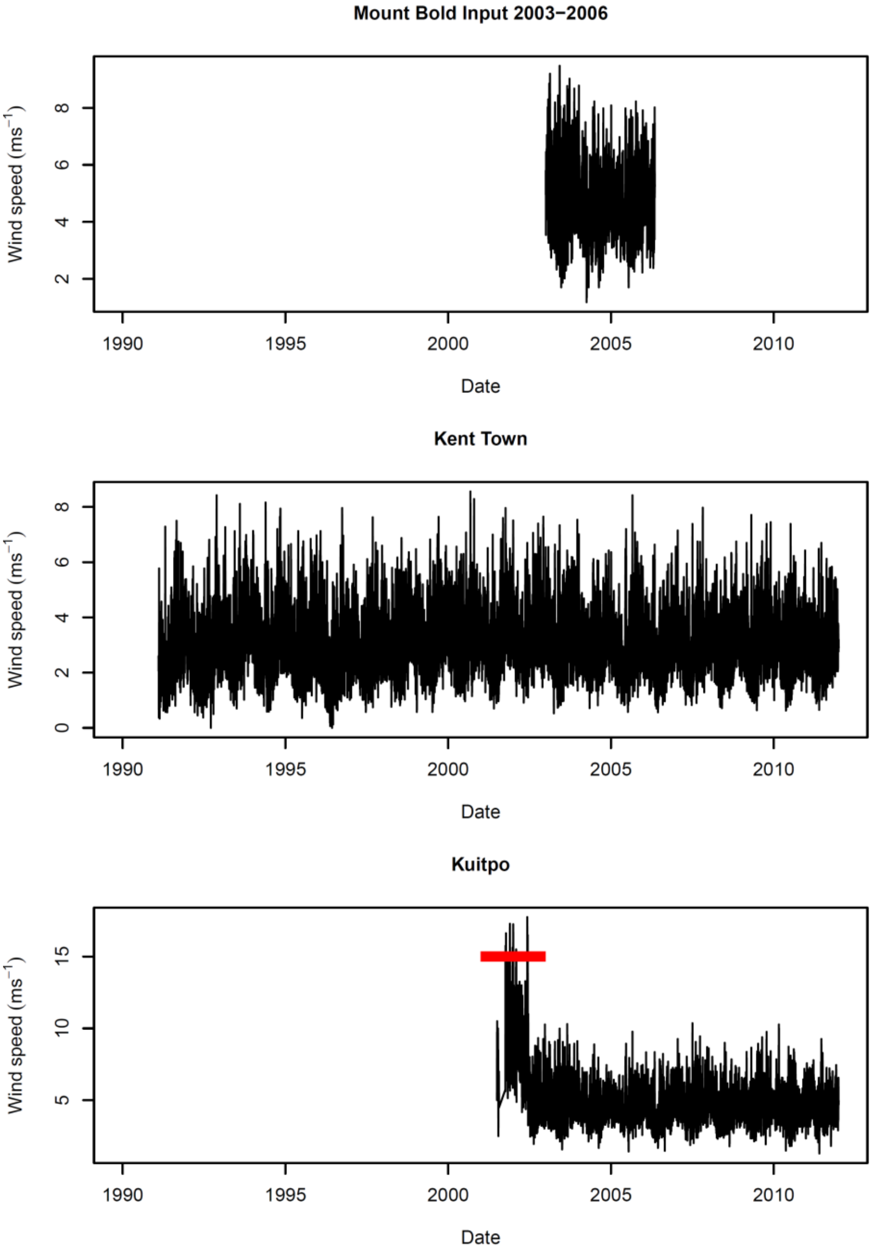

Figure 5. Time series of daily average wind speed measured at Mount Bold, Kent Town and Kuitpo. The data downloaded from the NOAA ISD-Lite database was found to contain erroneous data (marked by the red bar in the bottom panel) which was excluded from subsequent analyses.

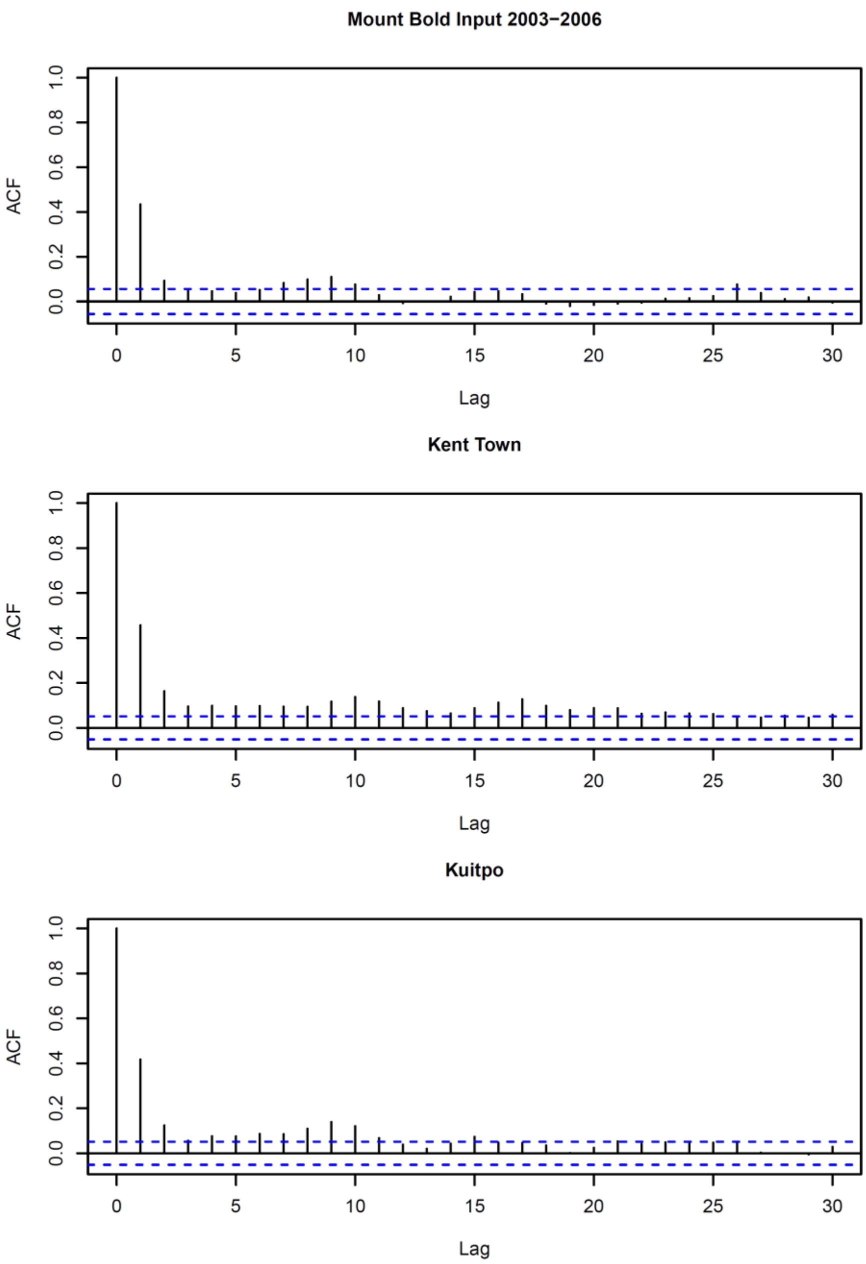

Figure 6. Autocorrelation function (ACF) of time series of wind speed over 2003-2006.

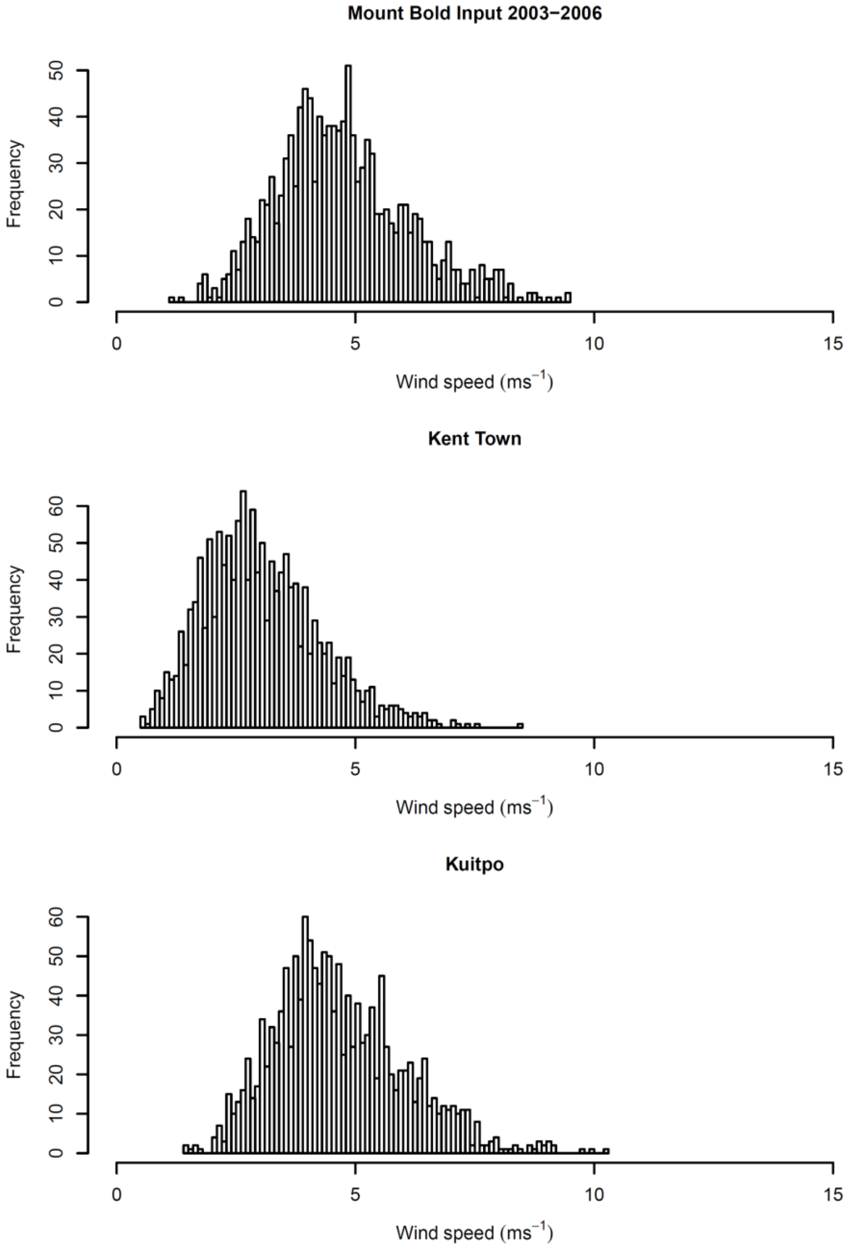

Figure 7. Histograms of daily wind speed observed at Mount Bold, Kent Town and Kuitpo.

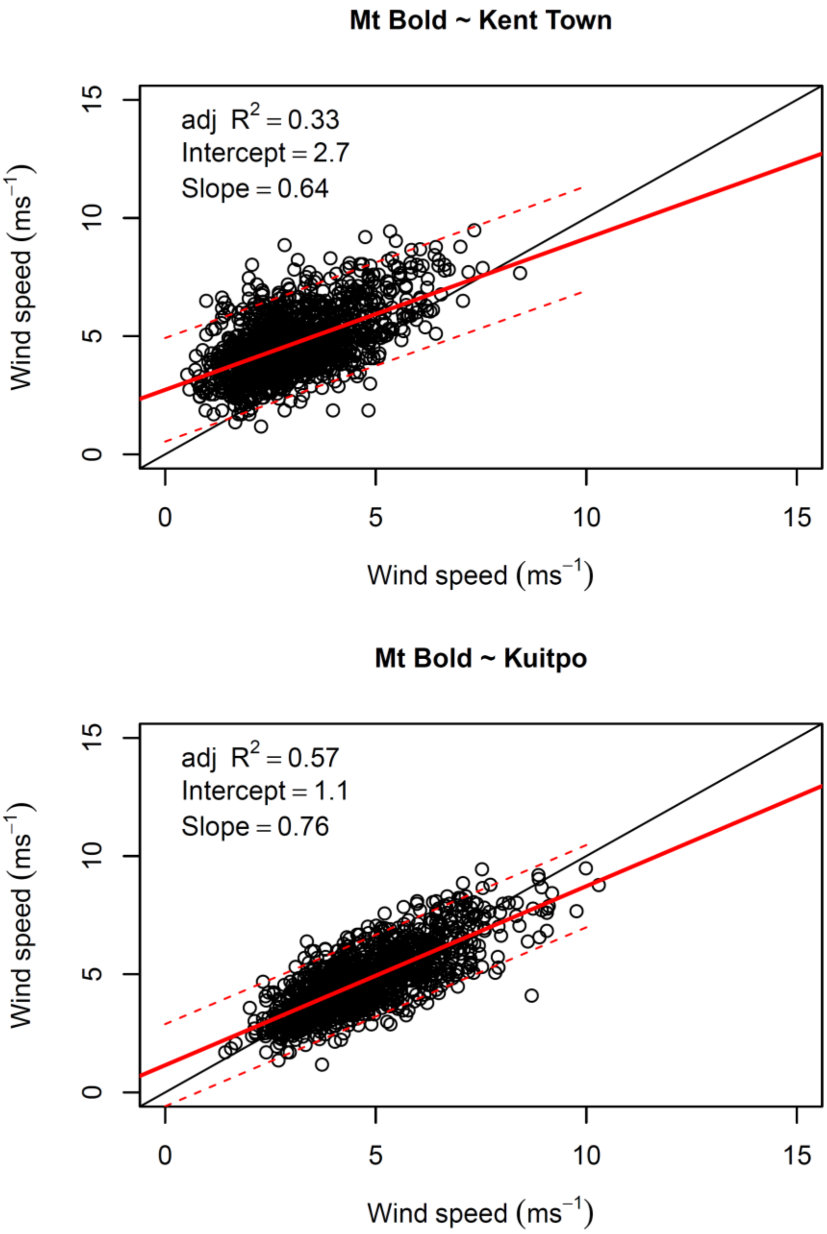

Figure 8. Daily average wind speed at Mount Bold Predicted by observed daily average wind speed at other observation stations. These regression fits are subsequently described as 'lumped' fits. The black line is the 1:1 line while the red line is the fitted line.

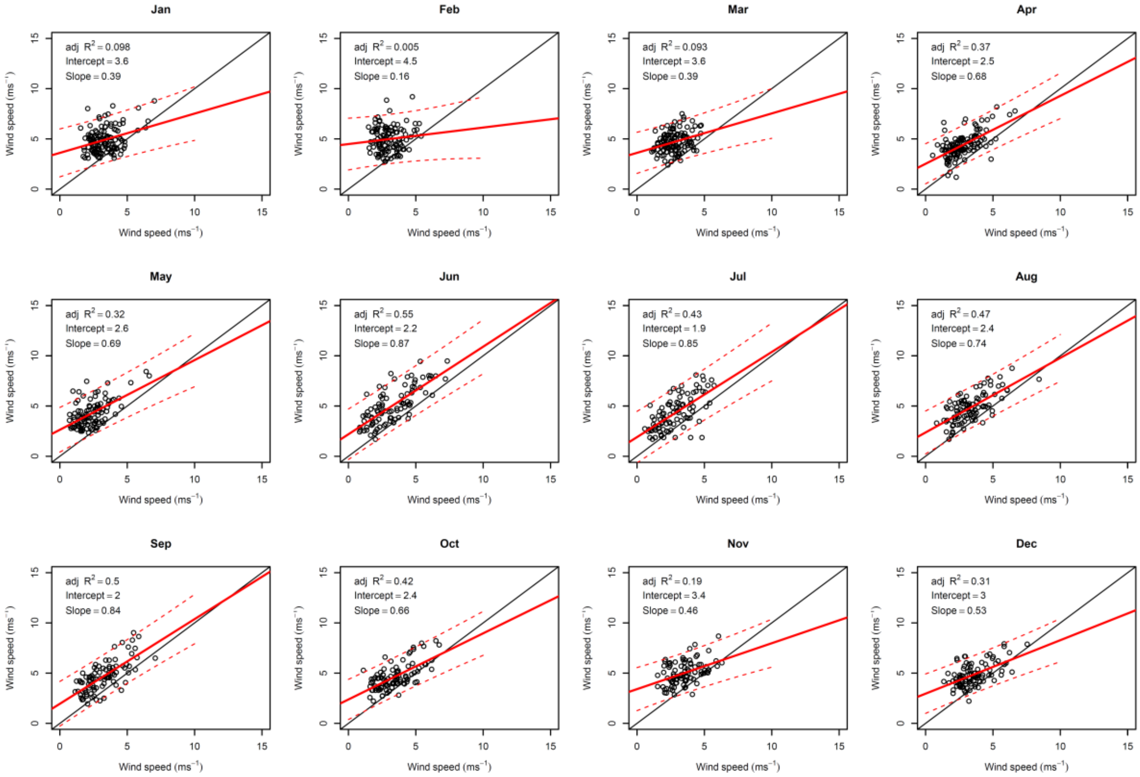

Figure 9. Daily average windspeed at Mount Bold predicted by daily observed wind speed at Kent Town (#); the regression was applied conditionally by month and the fits used to generate subsequent 'monthly' fits. The black line is the 1:1 line while the red line is the fitted line.

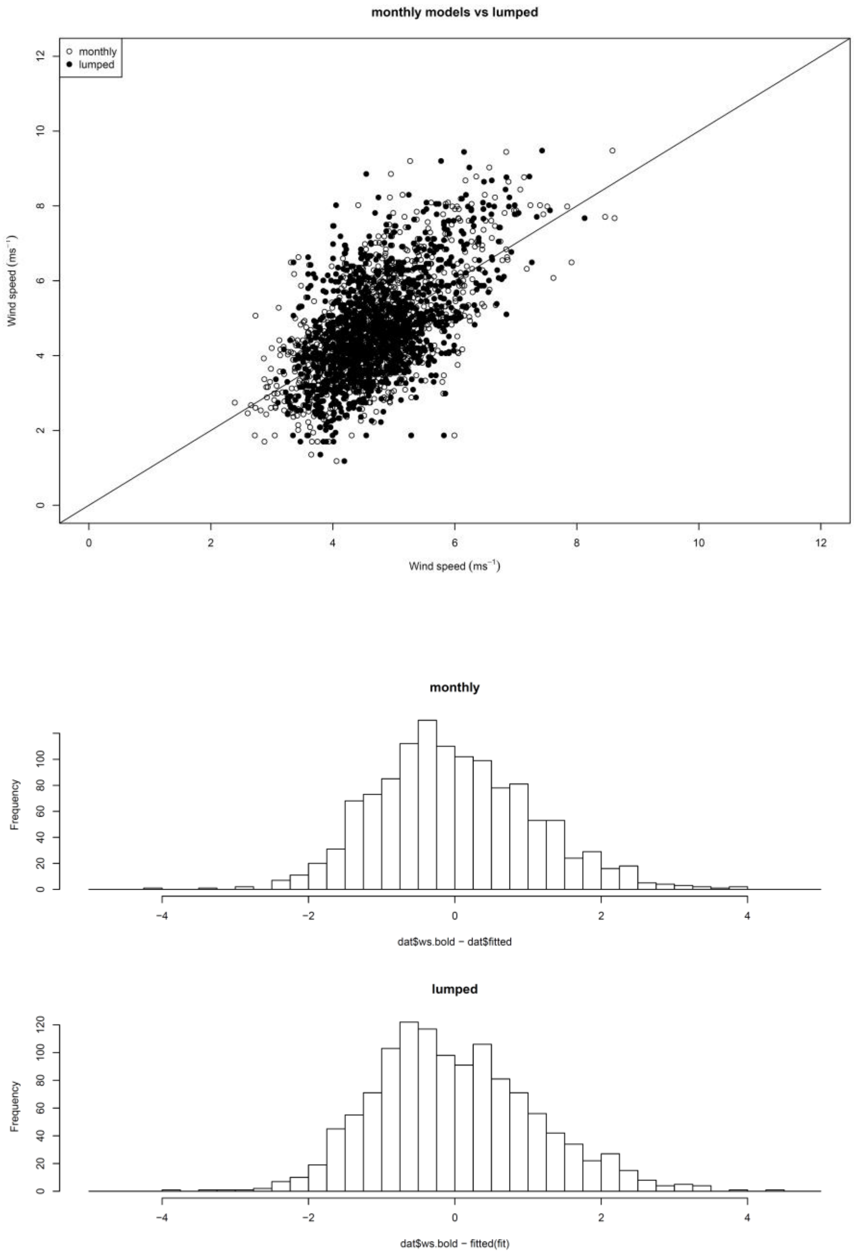

Figure 10. Lumped vs monthly model fit comparison for Kent Town. Top panel: Observed vs predicted wind-speed at Mount Bold Reservoir. Bottom panels: histograms of residuals.

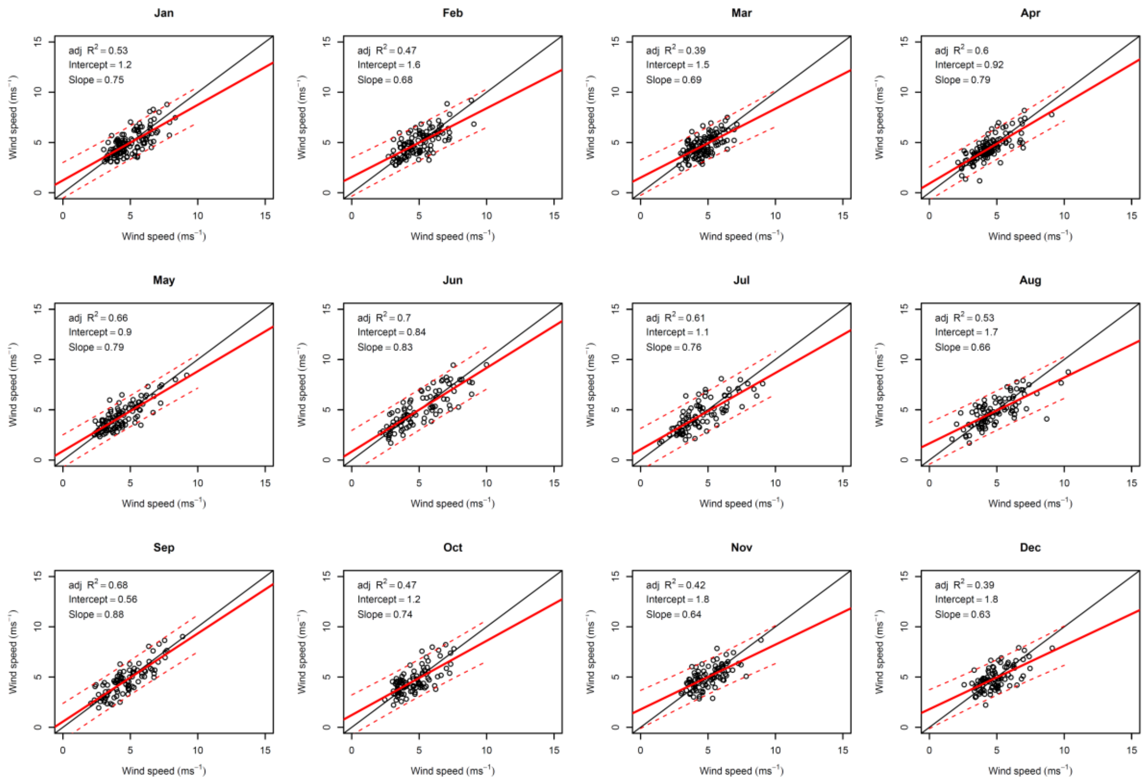

Figure 11. . Daily average wind-speed at Mount Bold predicted by daily observed wind-speed at Kuitpo (#); the regression was applied conditionally by month and the fits used to generate subsequent 'monthly' fits. The black line is the 1:1 line while the red line is the fitted line.

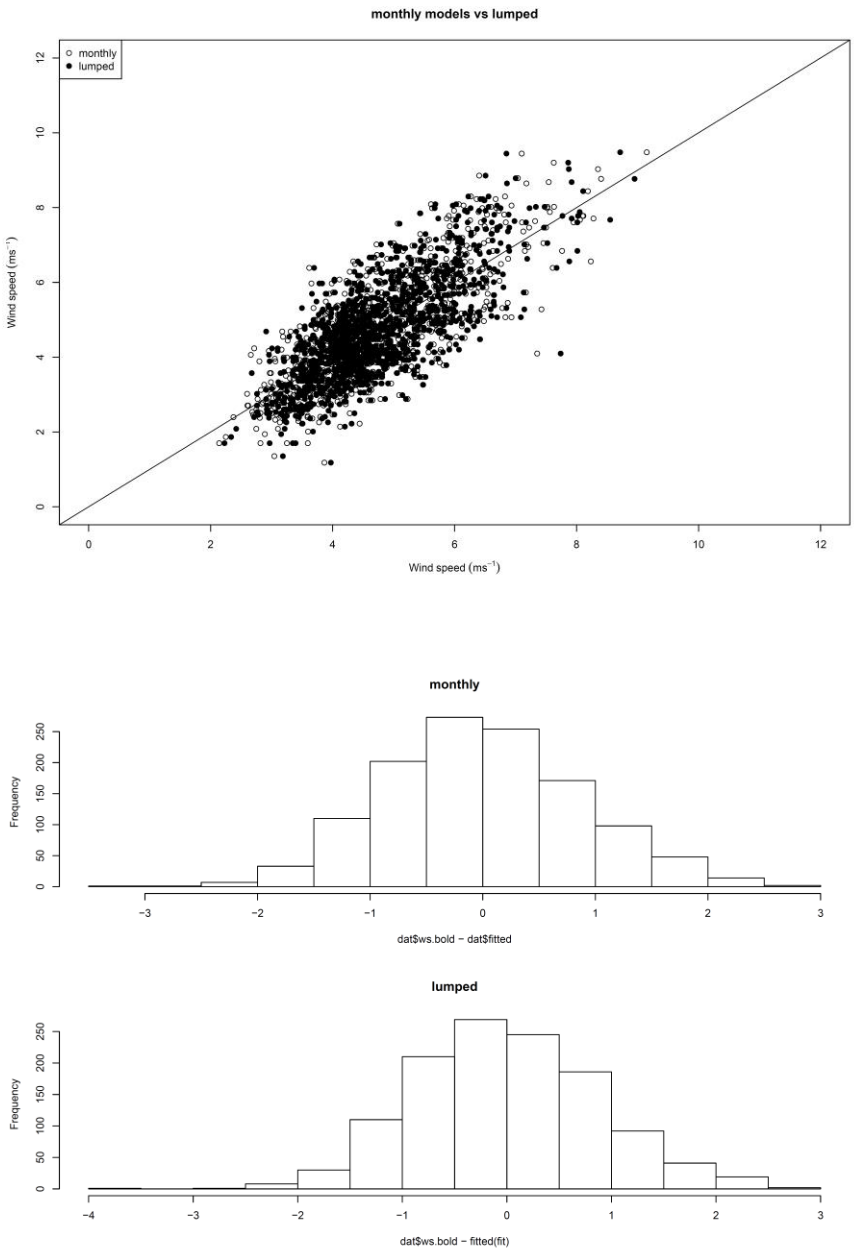

Figure 12. Lumped vs monthly model fit comparison for Kent Town. Top panel: Observed vs predicted wind-speed at Mount Bold Reservoir. Bottom panels: histograms of residuals.

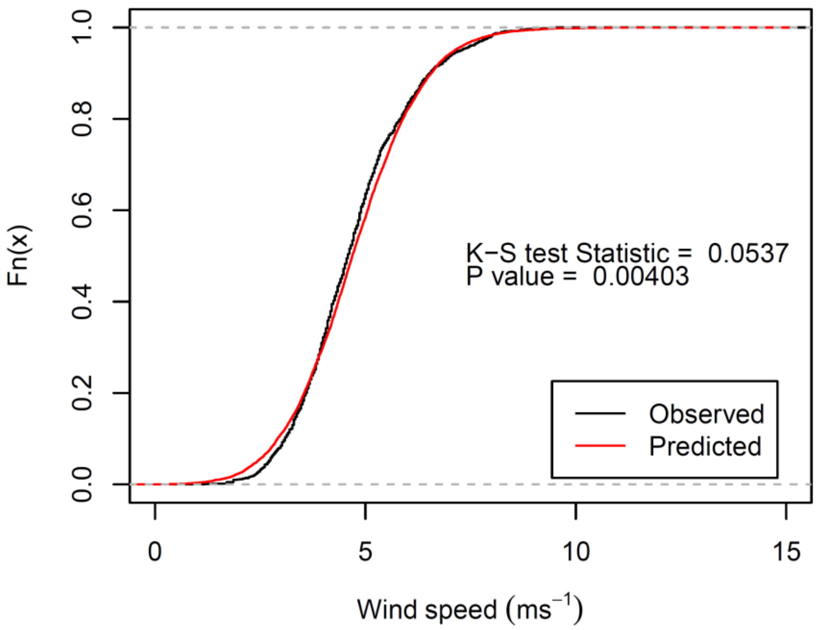

Figure 13. Kent town empirical cumulative distribution function (ECDF) of prediction and Kolmogorov-Smirnoff (K-S) test statistics. The p-value indicates that the null hypothesis that the samples come from the same distribution is rejected and we must conclude that the distributions are different.

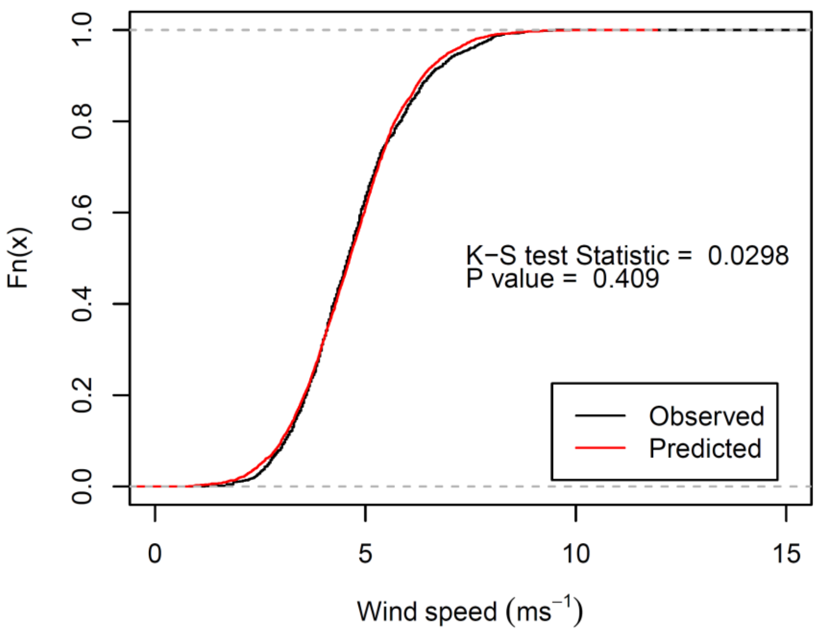

Figure 14. Kuitpo empirical cumulative distribution function (ECDF) of prediction and Kolmogorov-Smirnoff (K-S) test statistics. The p-value indicates that the null hypothesis that the samples come from the same distribution is not able to be rejected and therefore we cannot conclude that the distributions are different.

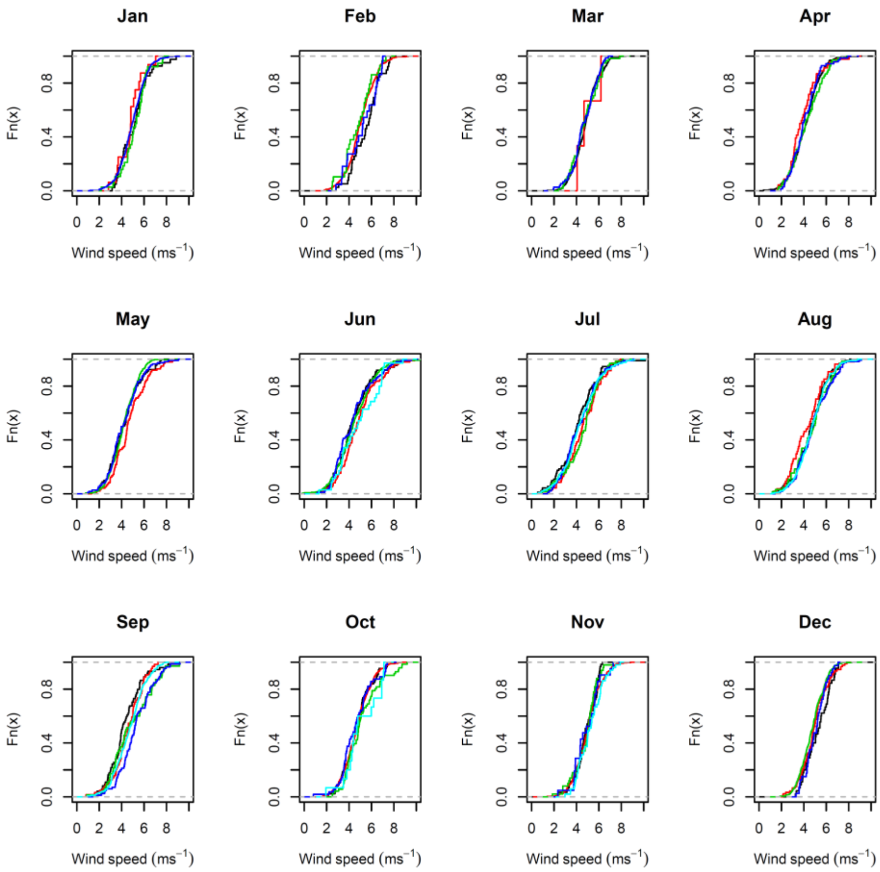

Figure 15. ECDFs of windspeed conditional on weather state in each month as derived by comparison of the 'Set 9' NHMM states (for Kuitpo) and wind-speed predicted for Mt Bold Reservoir from models developed between Kuitpo and Kent Town observations. Different lines represent different monthly weather states which are arbitrary as compared to other months.

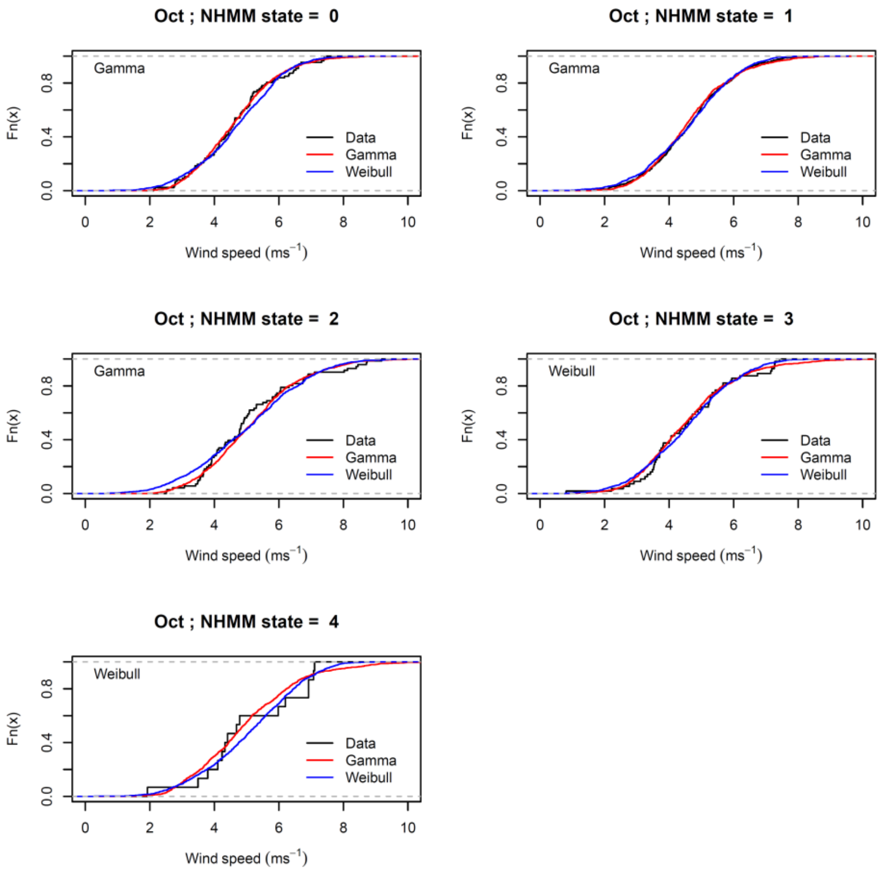

Figure 16. Example of wind speed distribution fits conditional on month and NHMM weather state. Gamma and Weibull parametric distributions were fitted and the best selected according to maximum log likelihood.

Solar radiation, cloud cover and longwave radiation

Clear sky shortwave

Long term SILO data and the Task 3 downscaling products contain the shortwave radiation variable, which allows the development of a function to estimate cloud cover. An estimate of cloudiness is used to estimate the longwave radiation balance in many lake models, when measured data is unavailable. First, the observed or downscaled or modelled radiation (E_o) is compared to the clear sky solar radiation (E_c) for that location. The clear sky radiation function (Appendix 1: clearSkyShortWave) was determined from solar geometry calculations and an optimisation to the solar pyranometer measurements made at Happy Valley Reservoir from 2007-02-18 to 2012-10-09. The optimisation algorithm fitted the atmospheric attenuation coefficients of the Hottel (1976) model using a subset of observation days visually evaluated to be cloud free (i.e. smooth curves with high peaks). The function was fitted using a contracted Nelder-Mead direct search minimisation of the sum of absolute differences between the daily maximum observed solar radiation and that estimated by the clear sky radiation function (Appendix 1). The fitting process resulted in a satisfactory fit however some residual curvature remained in the observed vs modelled relationship (Figure 17). This is likely the result of topographic effects on the morning and evening radiation intensity. The days selected for parameter estimation were subsequently validated against cloud cover observations at Mount Barker, the closest BOM site with cloud cover observations (Figure 18).

The function was then vectorized (made to accept vectors as arguments; Appendix 1: clearSkyShortWave.v) and incorporated into a function to calculate average short wave radiation for any given date (Appendix 1: AveSolarRadiation.v).

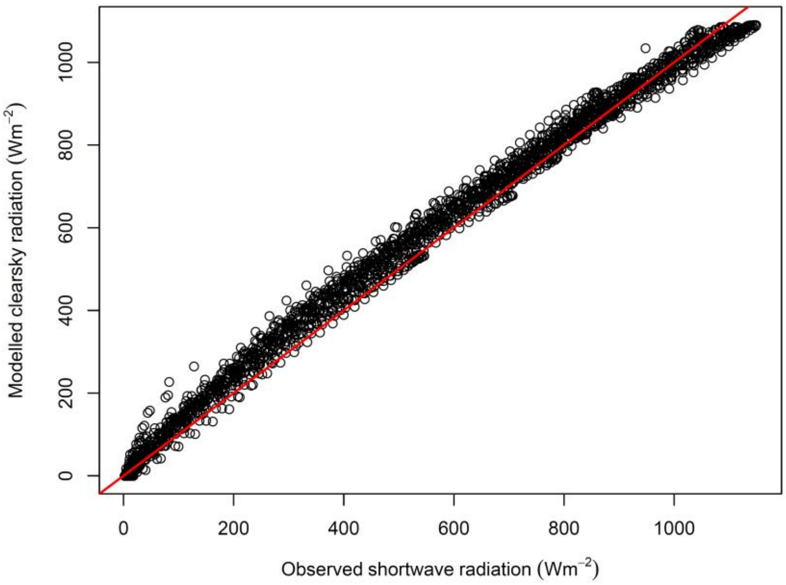

Figure 17. Results of fitting clear sky radiation model. Red line is the 1:1 line.

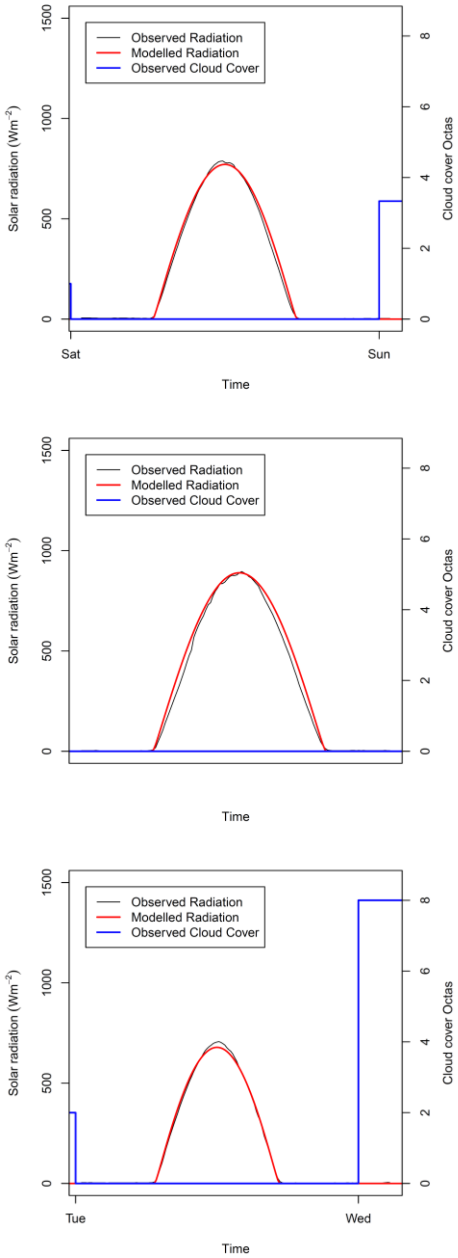

Figure 18. Examples of daily trajectory of observed and modelled radiation at Happy Valley Reservoir.

Downscaling cloud cover – a novel method

A method to impute cloud cover was developed with the proportion of ideal radiation observed (E_p):

$$E_p = \left(\frac{E_o}{E_c}\right)$$

E_p was related to proportional cloud cover (C_p; cloud cover in Octas/8) via a scaling function:

$$C_p = \begin{cases} \frac{E_c}{P_n}, & if\ E_p < \frac{E_c}{P_n} \\ E_cP_x, & if\ E_p > E_cP_x \\ 1 - P_g^{\left(\frac{E_o - \left(\frac{E_c}{P_n}\right)}{P_g{}^{Sx}}\right)} & \end{cases}$$

Where:

P_n = A fitted parameter representing the proportion of E_c below which C_p = 1

P_x = A fitted parameter representing the proportion of E_c above which C_p = 0

P_g = A fitted parameter that defines the non-linearity of the distribution of C_p between 0 and 1.

And:

$$S_x = (E_cP_s) - \left(\frac{E_c}{P_m}\right)$$

This function (Appendix 1: cloudCoverFromSRdev) effectively scales E_p between minimum and maximum values with a non-linear distribution determined by the parameter P_g. The parameters P_n, P_x and P_g were fitted by minimising the sums of squares of differences in the sample quantiles between the observed and predicted proportional cloud cover time series. Therefore, the model was fitted to reproduce the statistical properties of the cloud cover observations as opposed to directly predicting cloud cover from radiation. To investigate the generality of the parameters, the parameters were estimated for cloud cover observations for 3 sites, over the simulation period and the full station record (Table 5). Ideally, parameters would represent both the observations over the period of the established reservoir model simulation period and the longer term cloud observations. Examining the longer term datasets shows that reproduction of cloud cover is not drastically different when predicted from the longer term distribution of cloud cover. The parameterisation for the Mount Bold GLM simulation period was considered for use and compared to the method described in the following section (Appendix 1: cloudCoverFromSR.MtBoldGLM).

Table 5. Parameters estimated for cloud cover prediction function from quantile fitting and performance metrics when compared to cloud observations at Mount Barker (closest station with overlapping observations).

Location	Period	P_n	P_x	P_g	RE	Slope	R^2adj
MtBold GLM	2003-01-01 - 2006-05-09	4.45	1.05	1.01	0.24	0.951	0.720
Kent Town	2003-01-01 - 2006-05-09	4.41	1.05	1.01	0.216	0.932	0.723
Mount Barker	2003-01-01 - 2006-05-09	4.80	1.06	1.02	0.182	0.831	0.736
Adelaide Airport	2003-01-01 - 2006-05-09	2.10	1.08	1.01	0.288	0.894	0.732
Kent Town	1954-12-31 - 2011-12-31	4.41	1.05	1.01	0.225	0.905	0.727
Mount Barker	1990-02-01 - 2011-12-31	4.49	1.07	1.02	0.271	0.825	0.737
Adelaide Airport	1955-02-15 - 2011-12-31	4.69	1.08	1.01	0.213	0.895	0.730

Downscaling cloud cover – published methods

A number of alternative methods were compared to the method above, namely the linear method of Bristow and Campbell (1984):

$$C_p = 1 - \left(\frac{T - T_{min}}{T_{max} - T_{min}}\right)$$

And that of Black (1956):

$$C_p = \begin{cases} \dfrac{0.34 - \sqrt{0.34^2 + 4 \times 0.458(0.803 - T)}}{-2 \times 0.458} & if\ T \leq 0.803 \\ 0\ if\ T > 0.803 \end{cases}$$

Where *T* is atmospheric transmissivity, and *Tmin* and *Tmax* are the threshold parameters, namely the transmissivity at which complete cloud cover occurs and that at which the sky is considered cloud free, respectively (Figure 19)

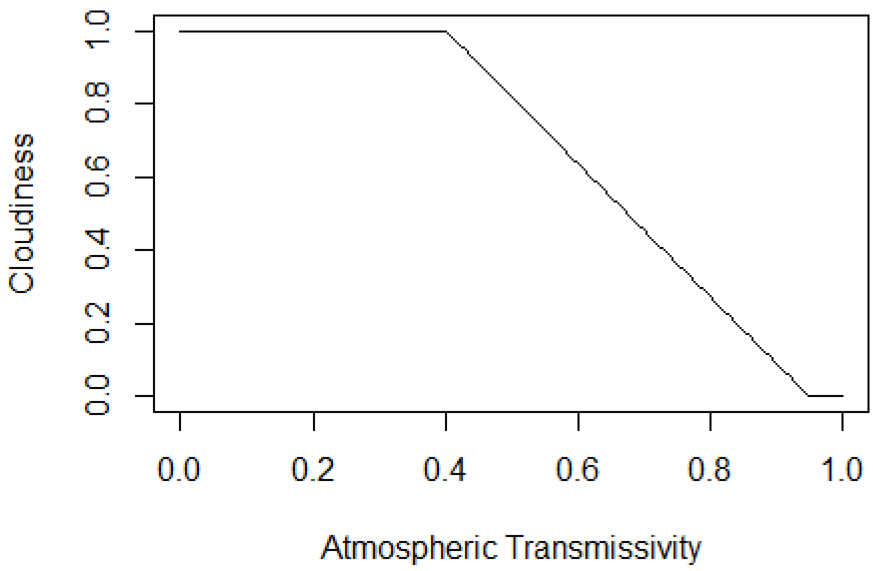

Figure 19. Form of the Bristow and Campbell (1984) linear atmospheric transmissivity and cloudiness function.

Calibration of the functions was conducted by minimising differences in the distributions (sample quantiles) of the modelled and observed cloud cover time series, as per the novel function described above. Ultimately these simpler empirical equations were demonstrated to produce more plausible output distributions than the novel equation. The function of Bristow and Campbell was adopted for the downscaling performed for this report.

Reservoir water budget

The hydraulic management of Mount Bold Reservoir is conducted in response to rainfall and run-off, evaporation, flood mitigation, customer demand and environmental flows. The system is provided with water from the Murray-Darling Basin via the Mannum-Adelaide pipeline that discharges into the Onkaparinga River at Hahndorf. As such, the hydraulics are partially decoupled from the climate system and determined primarily by operational management. Mount Bold Reservoir supplies Happy Valley Reservoir via the Onkaparinga River, Clarendon Weir, and an underground tunnel. Subsequently, the water is treated at Happy Valley Water Filtration Plant which supplies a significant proportion (~50%) of metropolitan Adelaide's water supply. Optimising the response of such a system to climate drivers is a significant body of work and was beyond the scope of this study (see Maheepala *et al.*, 2014). However, given the significance of the Onkaparinga-Happy Valley system it is likely that it will continue to operate within similar hydraulic parameters into the future and an assumption of operation based on recent years will be acceptable in the first instance.

Flow from catchment

The boundary conditions for the inflows from the catchment in the model scenarios were generated by repeating observed time series of flow and adjusting them to prevent model errors relating to reservoir water capacity. This was performed for the following reasons:

1. Stream flow projections were not available from the other project partners

2. An assessment of the direct impacts of the downscaled datasets upon reservoir water quality is a fundamental component of an integrated assessment.

Demand and inter-basin transfers

Demand from the system, and therefore release from the reservoir to the Onkaparinga River downstream, was assumed to be the same as historical observations. The following assumptions about the system lead to the conclusion that total volumetric yield of the reservoir is unlikely to increase in the future:

1. The local catchment yield is fully allocated.
2. Allocations from the Murray-Darling Basin are unlikely to increase.
3. No major expansion in capacity is planned for the Happy Valley water filtration plant.
4. Increases in demand for the greater Adelaide region will be satisfied by augmentation of supply to other parts of the SA Water network.

Mount Bold Reservoir is therefore likely to have similar operating rules going forward and the hydrologic budget of the simulations was established as such. The hydrological regime of the reservoir was kept as close to that for the years defining the base simulation as possible. However, changes to the hydrological inputs associated with changes in direct rainfall inputs and evaporative losses and the differences in inflow and outflow between the years of the base simulation needed to be made to avoid violating the GLM model requirements for water budgeting.

Water quality concentrations

Concentrations of water quality constituents in catchment derived inflows were assumed to remain the same as per the observed time series used for the base scenario. This is consistent with the assumptions made relating to inflow volumes.

Table 6. Ranges of water quality in reservoir inflow boundary conditions.

	Minimum (mM / mg/L)	Mean (mM / mg/L)	Maximum (mM / mg/L)
Dissolved oxygen	273 / 8.5	320 / 10	375 / 11.7
Reactive silica	178 / 3.0	350 / 5.8	5623 / 93.7
Nitrogen as Ammonia	0.0 / 0.0	346 / 24.7*	10929 / 780*
Nitrogen as Nitrate	0.0 / 0.0	14.1 / 1.0	82.9 / 5.9
Filterable reactive phosphorus	0.161 / 0.005	0.968 / 0.031	3.29 / 0.106
Particulate organic nitrogen	2.86 / 0.204	27.6 / 1.97	98.6 / 7.04
Dissolved organic nitrogen	2.86 / 0.204	27.6 / 1.97	98.6 / 7.04
Particulate organic phosphorus	0.065 / 0.002	2.95 / 0.095	21.3 / 0.69
Dissolved organic phosphorus	0.065 / 0.002	2.95 / 0.095	21.3 / 0.69
Particulate organic carbon	28.3 / 2.36	63.6 / 5.30	102 / 8.49
Dissolved organic carbon	255 / 21.23	572 / 47.6	915 / 76.2

* product of transient peak ammonia episode

Construction and running of scenarios

A set of folders containing model configuration files was first constructed using scripted "for- loops" and the following file operations as described in Figure 20.

1. Copy base files required (shared parameter configurations etc: *aed_geochem_pars.dat, aed_pathogen_pars.nml, aed_phyto_pars.nml, aed_zoop_pars.nml, fabm.nml*)
2. Update the base glm.nml file with appropriate file references and simulation period details
3. Format the downscaled meteorological data to the appropriate format and combine with the wind speed, cloud cover and longwave radiation data downscaling developed in this study.
4. Construct and correct the inflow and outflow data.
5. Run the simulations using glm.exe
6. Compute summary statistics for variables across time period, GCM, emissions scenario, month. The following summary statistics were calculated: quantiles corresponding to probability = 0.01, 0.25, 0.5, 0.75 and 0.99 corresponding to the 1st, 25th, 50th (median), 75th and 99th percentile.

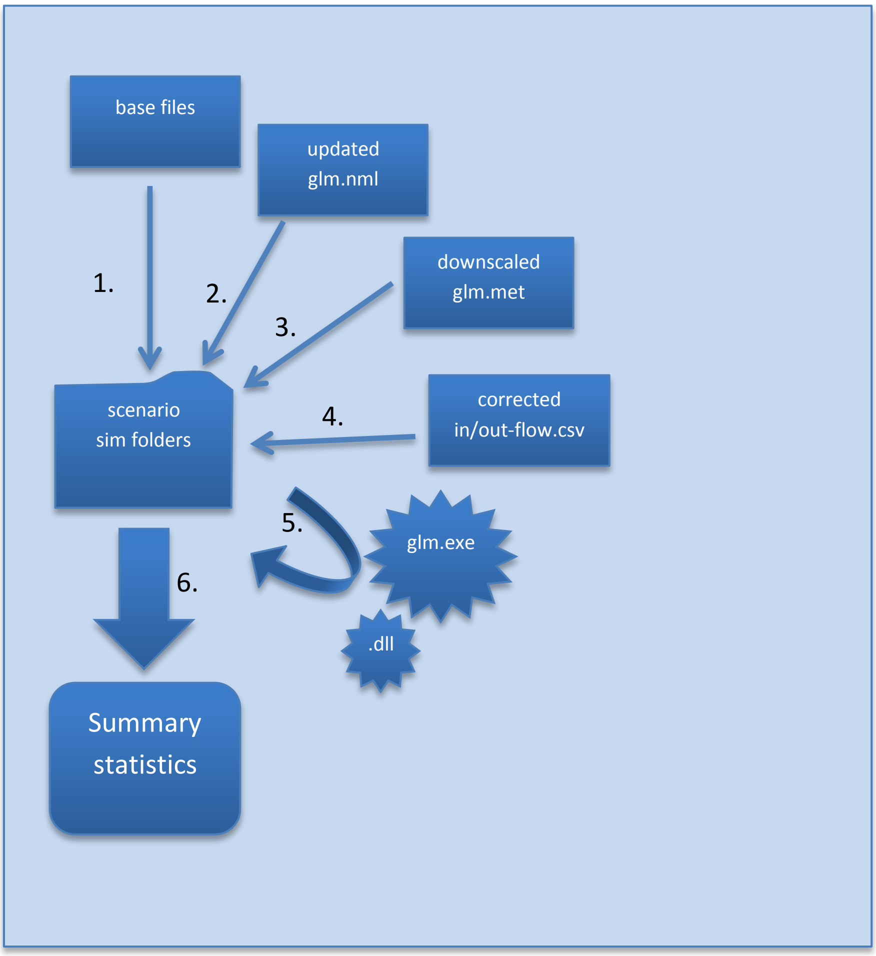

Figure 20. Schematic of scenario construction, simulation and summary.

Statistical analysis of results

Besides presenting the ensemble changes in water quality variables, the data was further explored using principal component analysis (Husson *et al.*, 2015) and multiple linear regression with relative importance assessment (Grömping, 2006). Principal component analysis was used to evaluate the complexity of the relationships (correlations) within the model results and to evaluate the changes in these relationships, focussing on comparing the historical period and the most severe climate change scenario. Multiple linear regression was used to specifically investigate the reasons for the projected changes in abundance of the cyanobacterial functional group. The relative importance of the different regressors was evaluated using the *lmg* algorithm implemented in the *relaimpo* package in 'R' (R Development Core Team, 2011). Briefly, this process involves partitioning of the goodness-of-fit statistic, R^2, by comparing regression models with terms incrementally and hierarchically removed; this then allows the evaluation of the relative importance of those regressors, according to their contribution to the goodness-of-fit of the overall model.

Results

The figures in this section generally have the following structure. Except in a few cases, the data are presented as box and whisker plots where the box represents the interquartile range (25th to 75th percentile) and the whiskers represent the 1st to 99th percentile range. The line inside the box represents the median of the data observed (simulated). In the cases that a bar plot with error bars is presented, the main bar represents the median and the error bars represent the inter-quartile range.

Summary of Meteorological and Hydrological Inputs

Inputs of solar radiation followed generally expected seasonal patterns with the highest insolation in December and January (Figure 21). Very little difference between the historical and future periods was observed; slight increases in future periods, compared to historical, were apparent in the spring (Sep-Nov) and in the month of April. These increases in solar radiation, which are derived from the Task 3 downscaling product are propagated by the downscaling performed in this study to result in changes in cloud cover (Figure 23) and down welling longwave radiation (Figure 22). Small differences in the distributions of cloud cover was observed, mostly in the months of April, September, October and November, consistent with changes in shortwave radiation. However some further differences in the distributions of cloud cover, not apparent in the distributions of solar radiation data can be observed, i.e. slight decreases in cloud cover in the future in January and February (Figure 23).

Increases in air temperature were a characteristic of the projection boundary layer in all seasons (Figure 24), consistent with the trends and variability projected by the downscaled GCMs. Relative humidity was projected to decrease into the future and with higher emissions (Figure 25). Reductions were slight in winter and more pronounced in autumn.

Wind-speed, which was the product of this work, as opposed to directly derived from the Task 3 outputs, showed no trends across time or emissions scenarios (Figure 26). This is as expected as the transition probabilities between the weather states did not change between the different periods, or emissions scenarios. The consistency of the distributions demonstrates that this important variable was consistently stochastically sampled across time and emission scenario. The trends in near surface wind speed projected by GCMs and the 'stilling' phenomenon observed in recent decades, while small on an annual scale (-0.009 m s^{-1} a^{-1} McVicar et al. 2008), may ultimately amount to a significant quantity at the timescale of climate projections (McVicar *et al.*, 2012). The potential implications for the projections made from these boundary conditions will be discussed later.

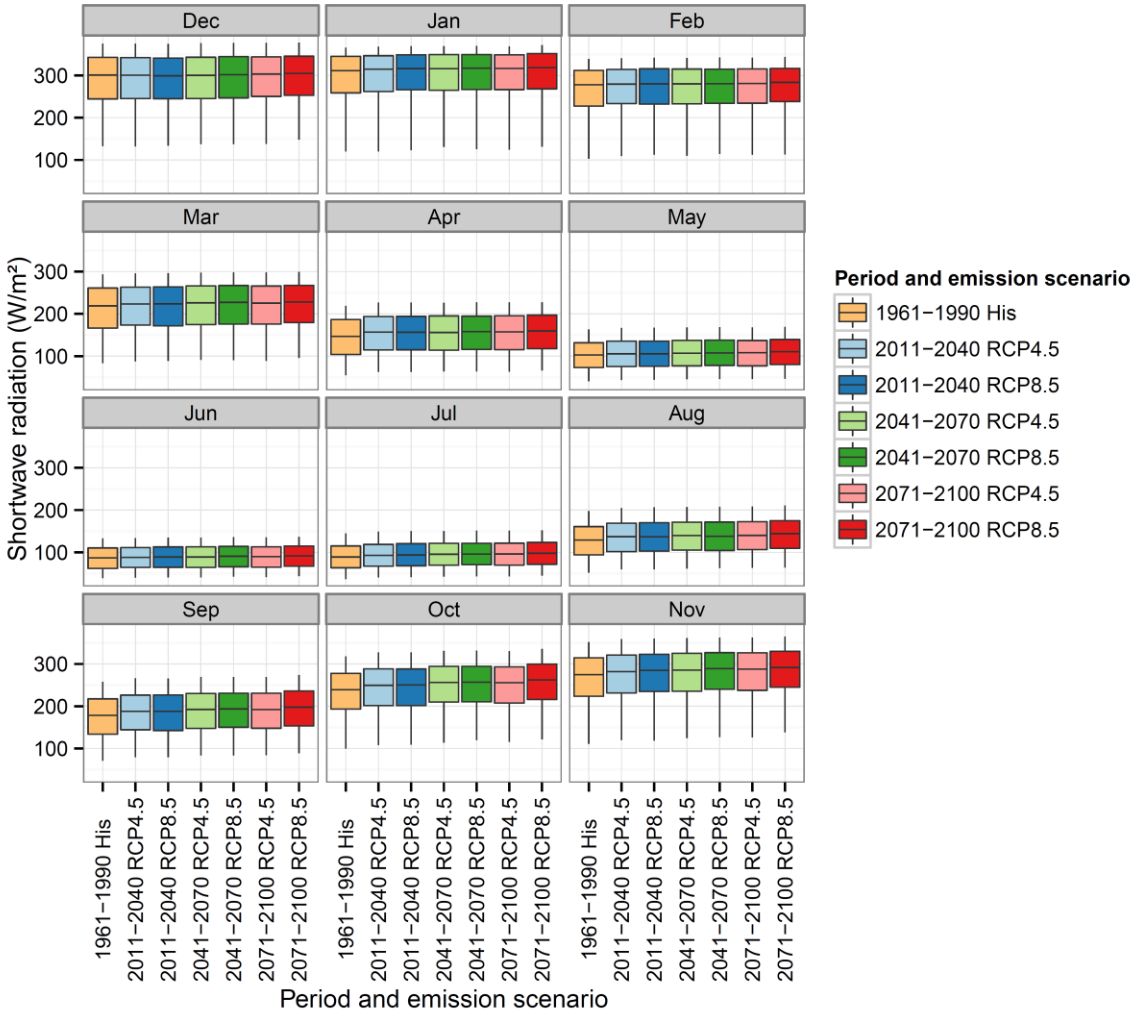

Figure 21. Shortwave radiation in the downscaled meteorological boundary conditions.

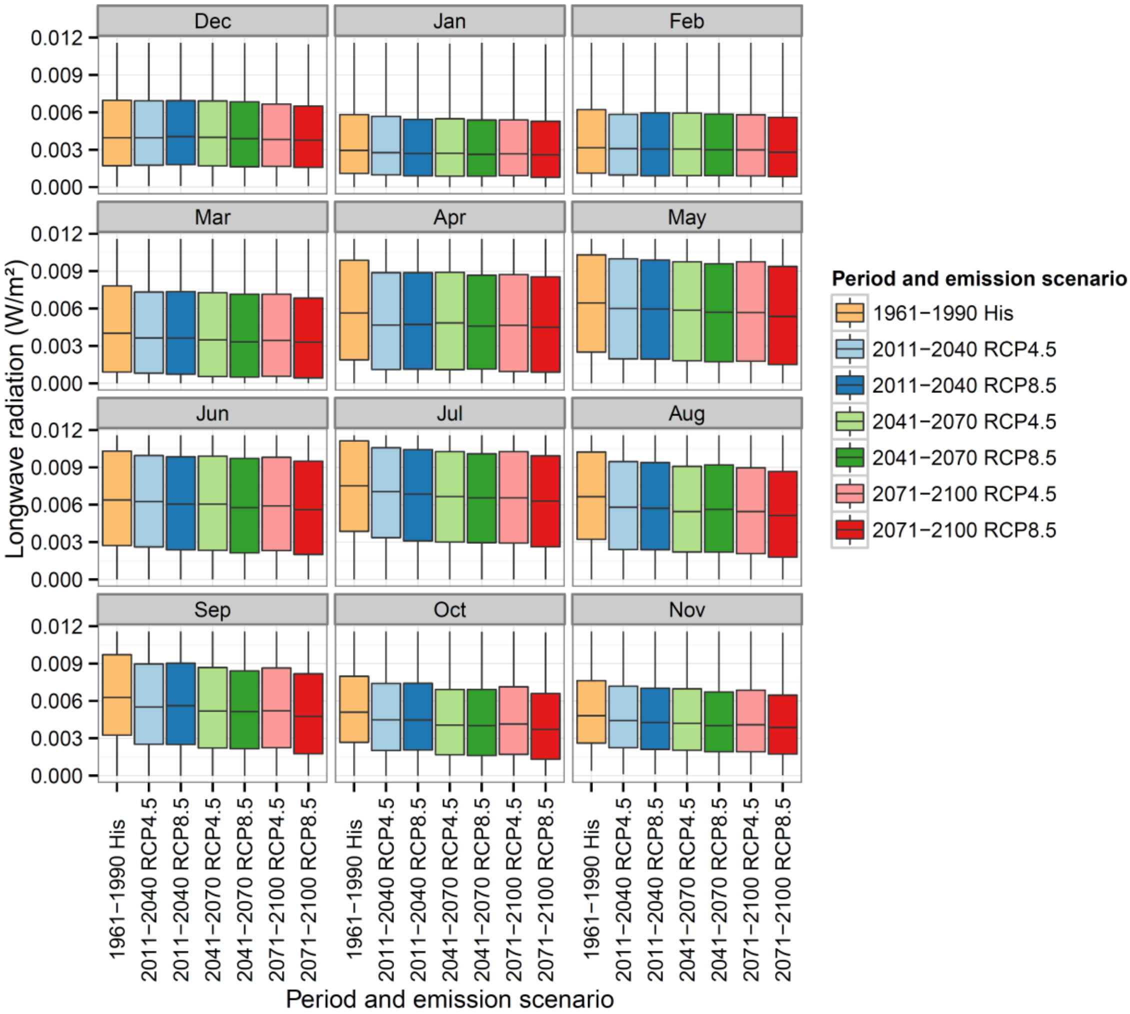

Figure 22. Longwave radiation in the downscaled meteorological boundary conditions.

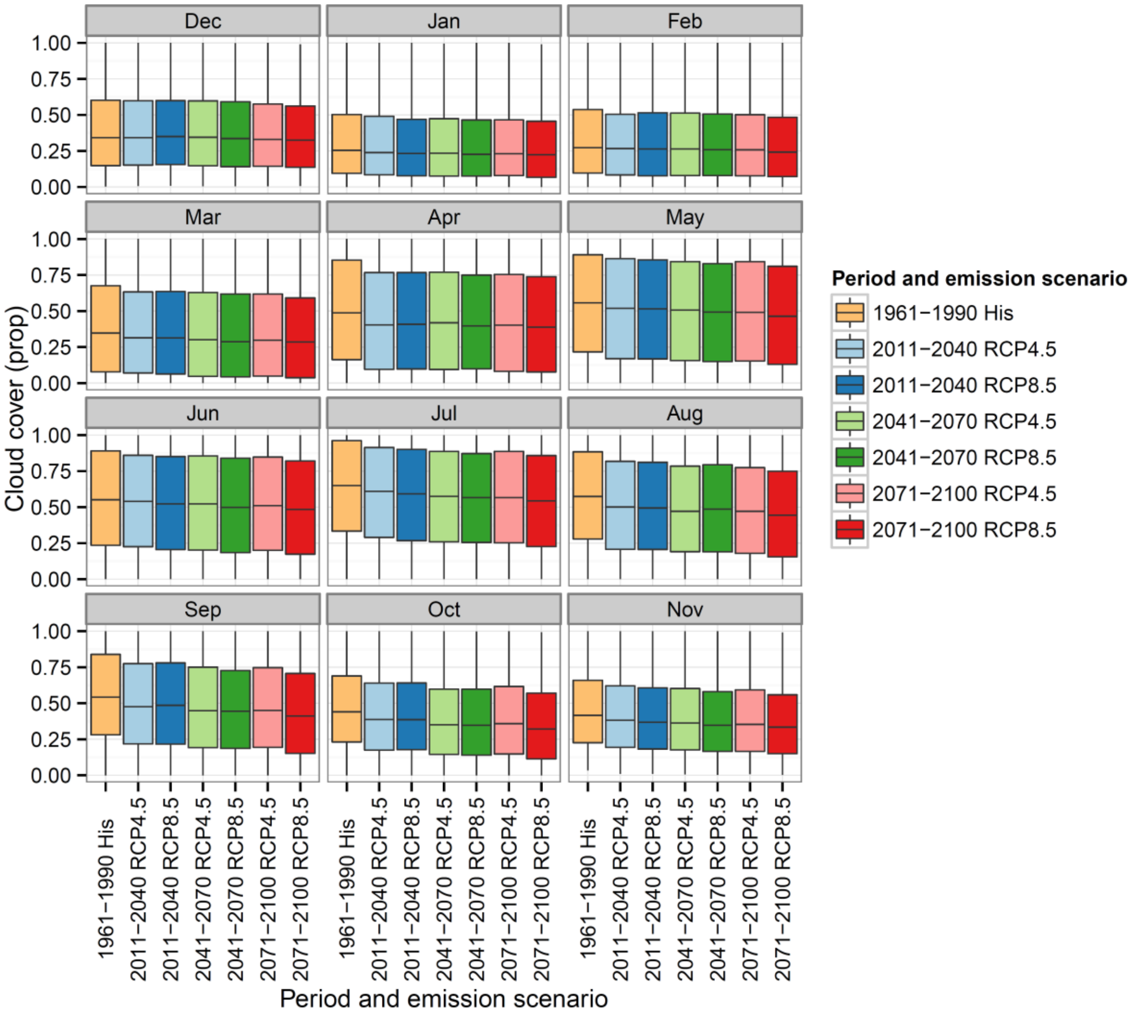

Figure 23. Cloud cover in the downscaled meteorological boundary conditions.

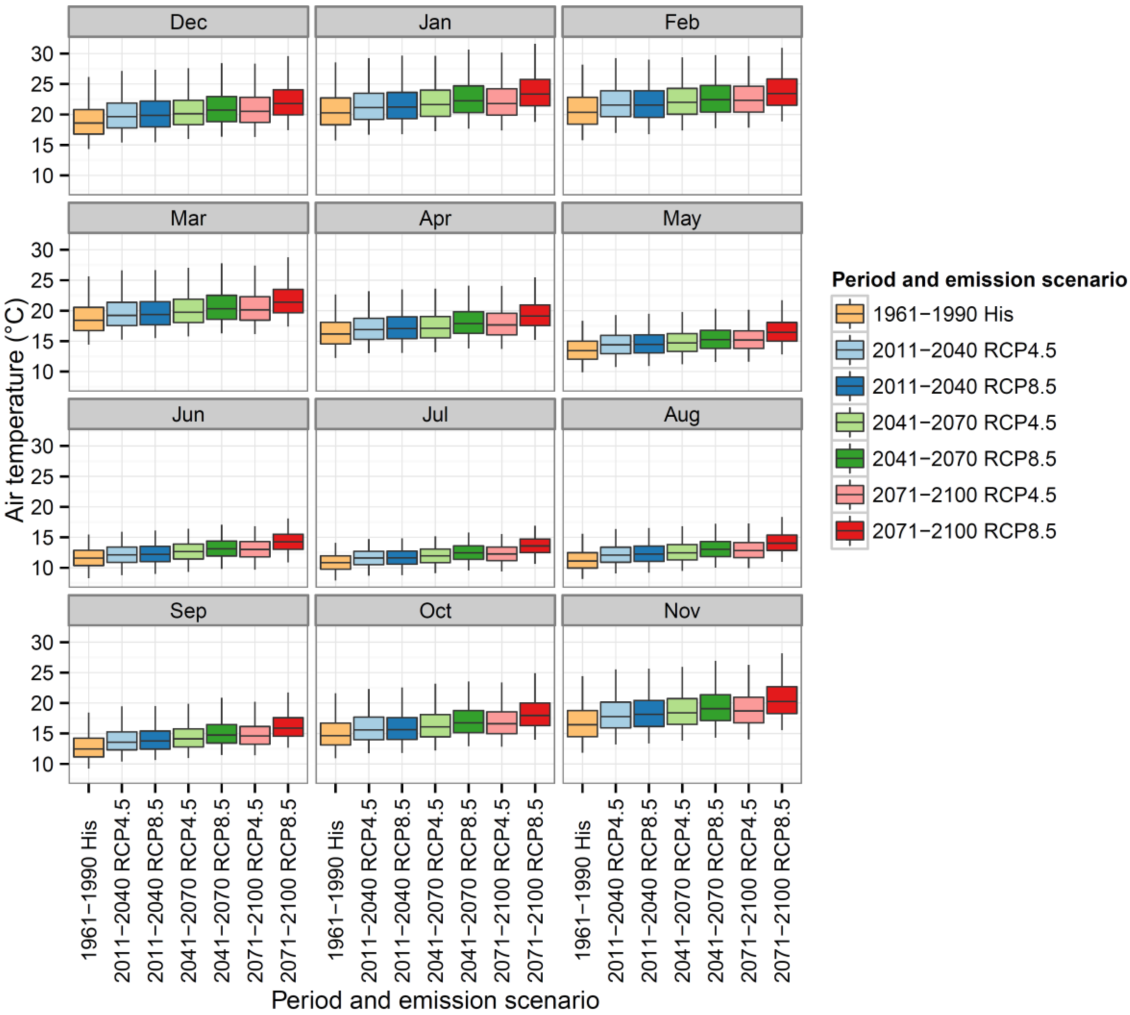

Figure 24. Air temperature in the downscaled meteorological boundary conditions.

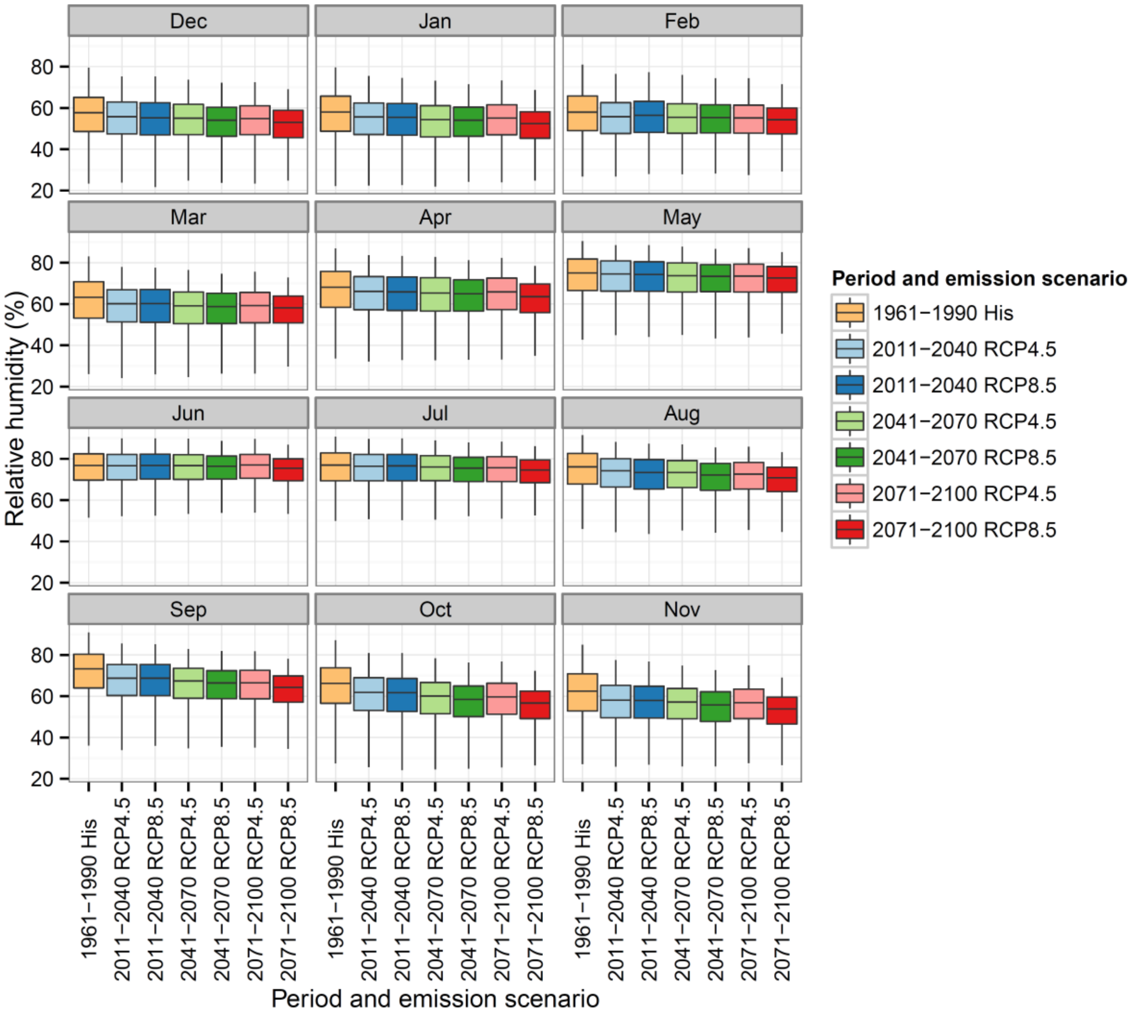

Figure 25. Relative humidity in the downscaled meteorological boundary conditions.

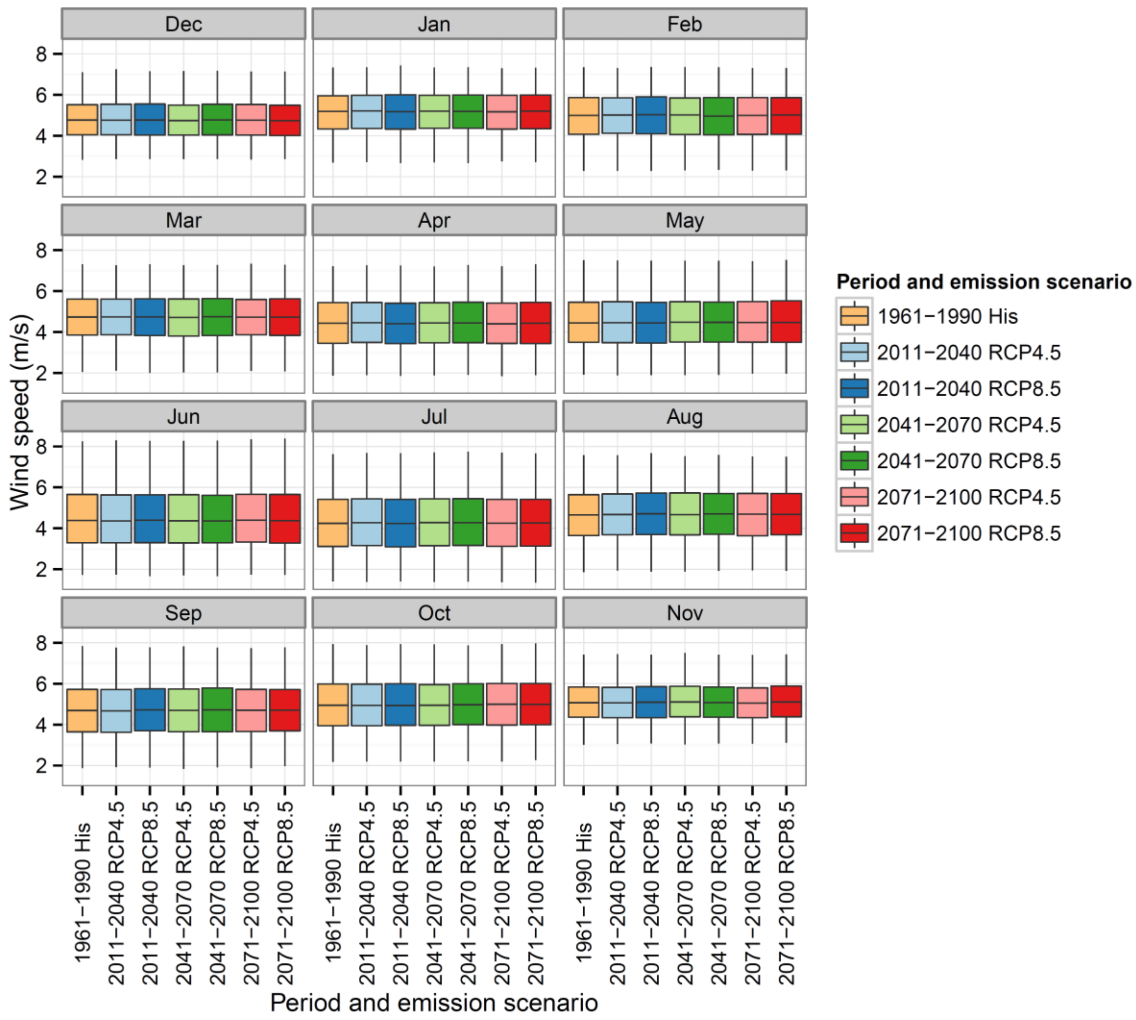

Figure 26. Wind speed in the downscaled meteorological boundary conditions.

Water temperature, stratification and surface energy balance

Surface water temperature increased with the progression of time and with greater greenhouse gas emissions. Very little difference was observed between the two emissions scenarios in near future periods (2011-2040), as opposed to much greater differences at the end of the century when the greatest difference between these representative concentration pathways occurs (Figure 27). The minimum water column temperature, which occurs in the hypoliminon, was projected to increase in all seasons (Figure 28) and showed notable variation in seasonal pattern; in Jan-Mar, the occurrence of rare mixing events probably contributed to the high marginal values observed. Lake Number (see Etemad-Shahidi and Imberger, 2006; Read *et al.*, 2011), which describes the probability that diapycnal mixing will occur (upwelling or internal wave generated mesoscale mixing, with lower numbers suggesting a higher probability of such events) was highly variable (only the interquartile range could be shown, Figure 29). Changes in daily shortwave heat flux (Figure 30) closely matched the shortwave radiation shown in Figure 21 (these quantities are related by the lake surface area and the reflectance of the lake surface due to roughness). Latent heat flux, the energy lost due to evaporation from the reservoir surface, was greater in the future projection scenarios and greater in scenarios with greater radiative forcing. The largest differences in latent heat flux between scenarios was in the spring (Figure 31). The sensible heat flux, which is the loss of heat due to convection (driven by the temperature difference between the water surface and the atmosphere), increased only slightly with future projection period and with increased radiative forcing (Figure 33). Daily net longwave heat flux decreased slightly, meaning the reservoir was losing less heat, predominantly in spring and winter (Figure 33). Daily volumetric evaporation from the lake surface increased in all months, ranging from relatively small increases in median values in winter months (i.e. 1.4 - 6.7% in July) to the greatest increases occurring in spring (i.e., 13.4 – 33.8% in October; Figure 34)

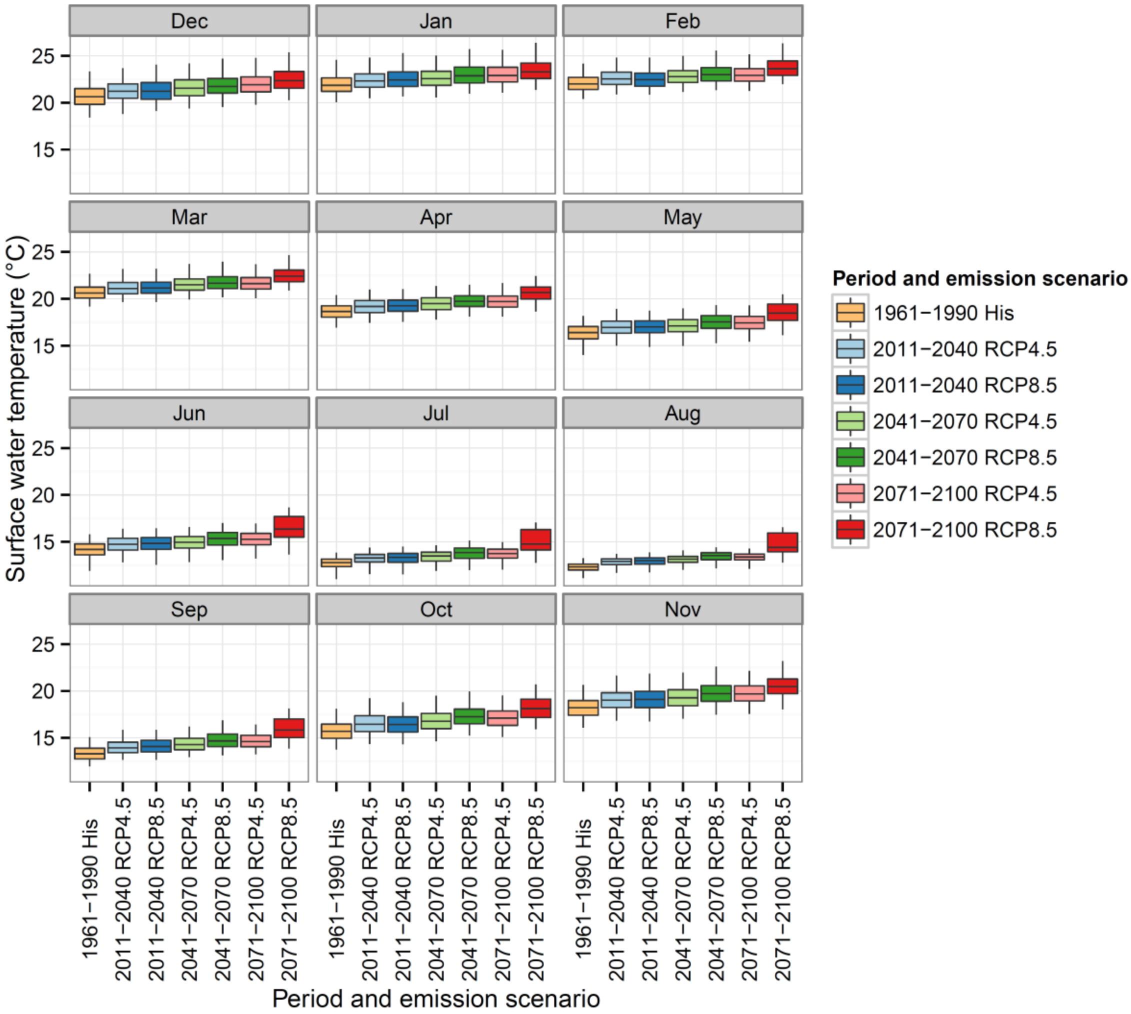

Figure 27. Surface water temperature in reservoir simulations with boundary conditions derived from downscaled climate data (SA Climate Ready).

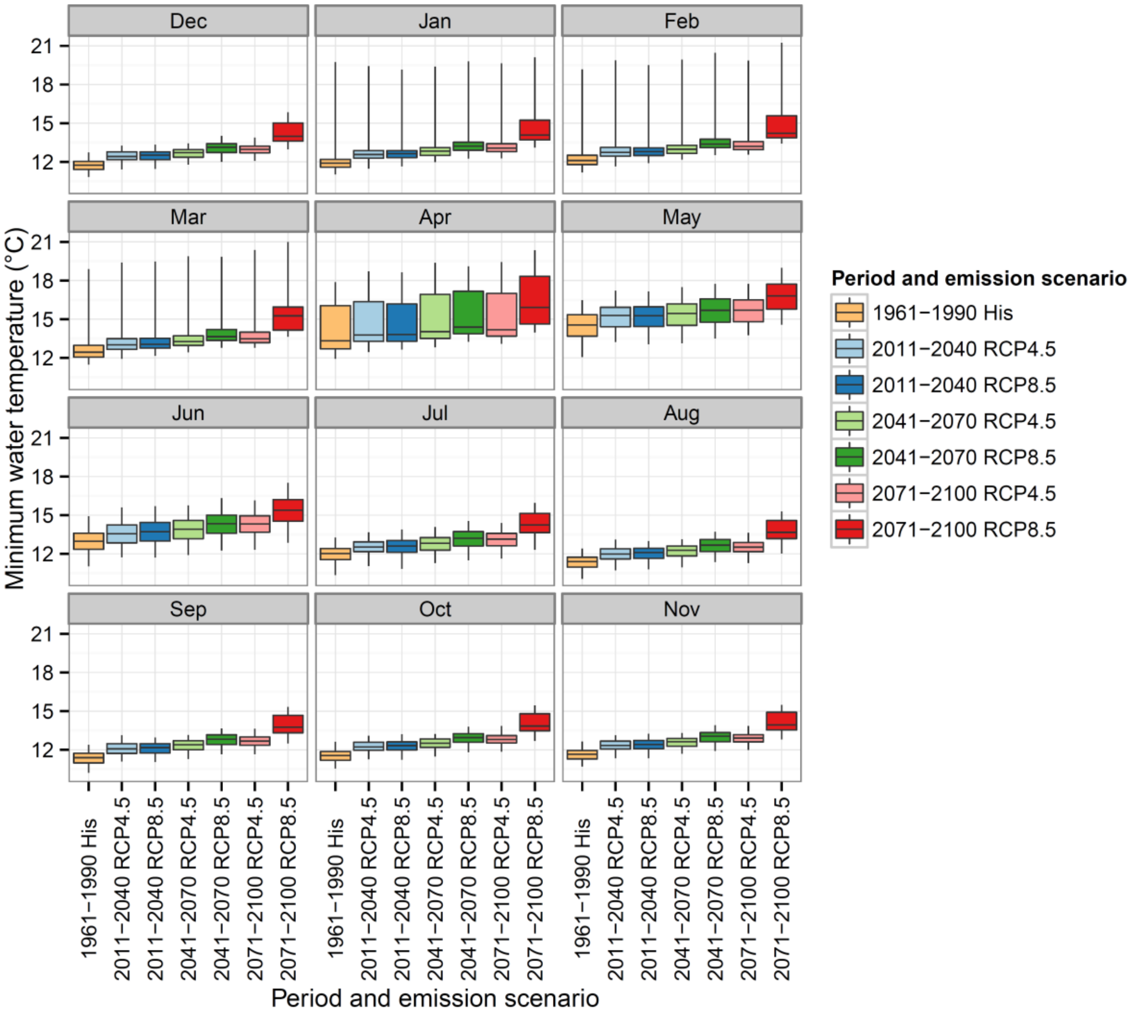

Figure 28. Minimum water temperature in reservoir simulations with boundary conditions derived from downscaled climate data (SA Climate Ready).

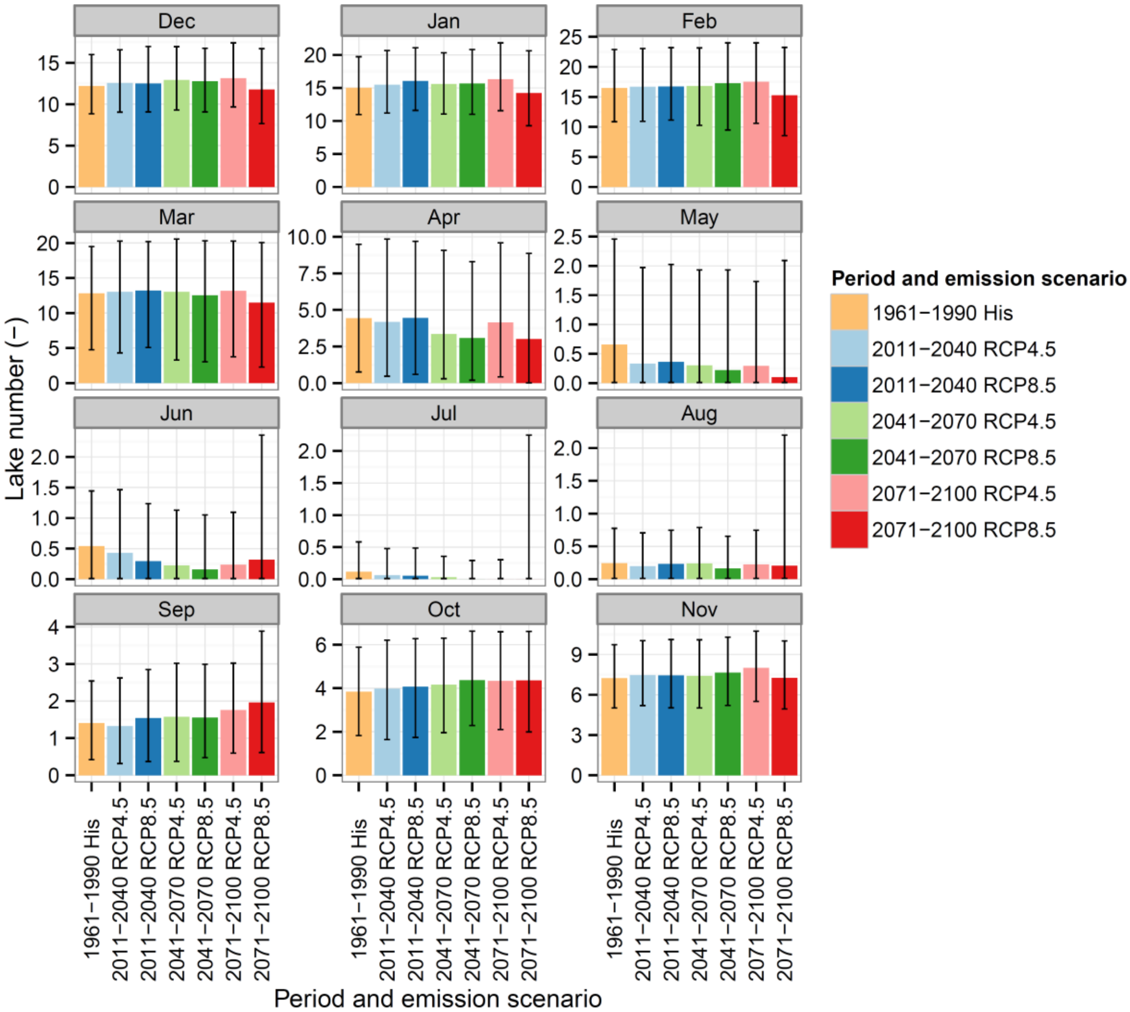

Figure 29. Lake Number in reservoir simulations with boundary conditions derived from downscaled climate data (SA Climate Ready).

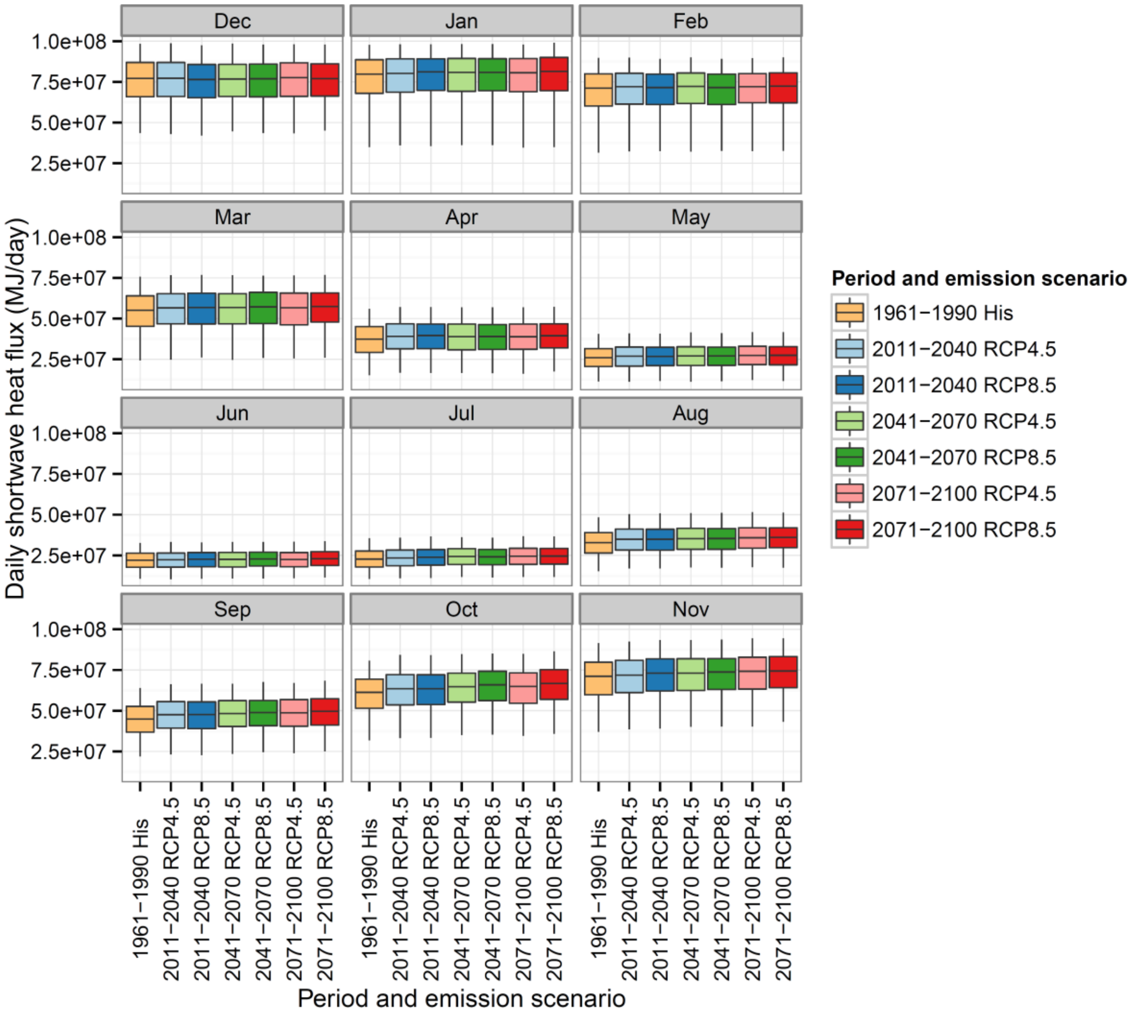

Figure 30. Daily shortwave heat flux in reservoir simulations with boundary conditions derived from downscaled climate data (SA Climate Ready).

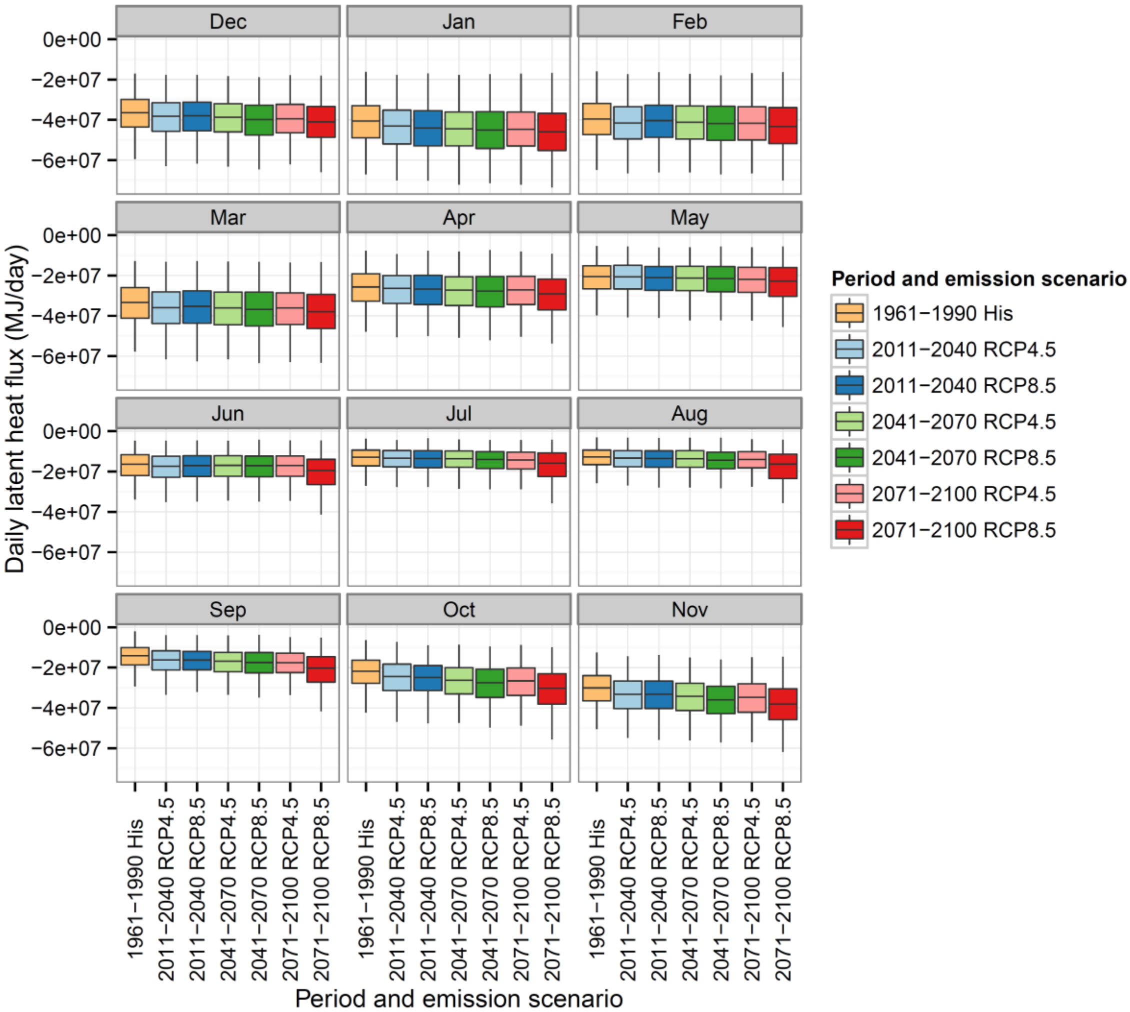

Figure 31. Daily latent heat flux in reservoir simulations with boundary conditions derived from downscaled climate data (SA Climate Ready).

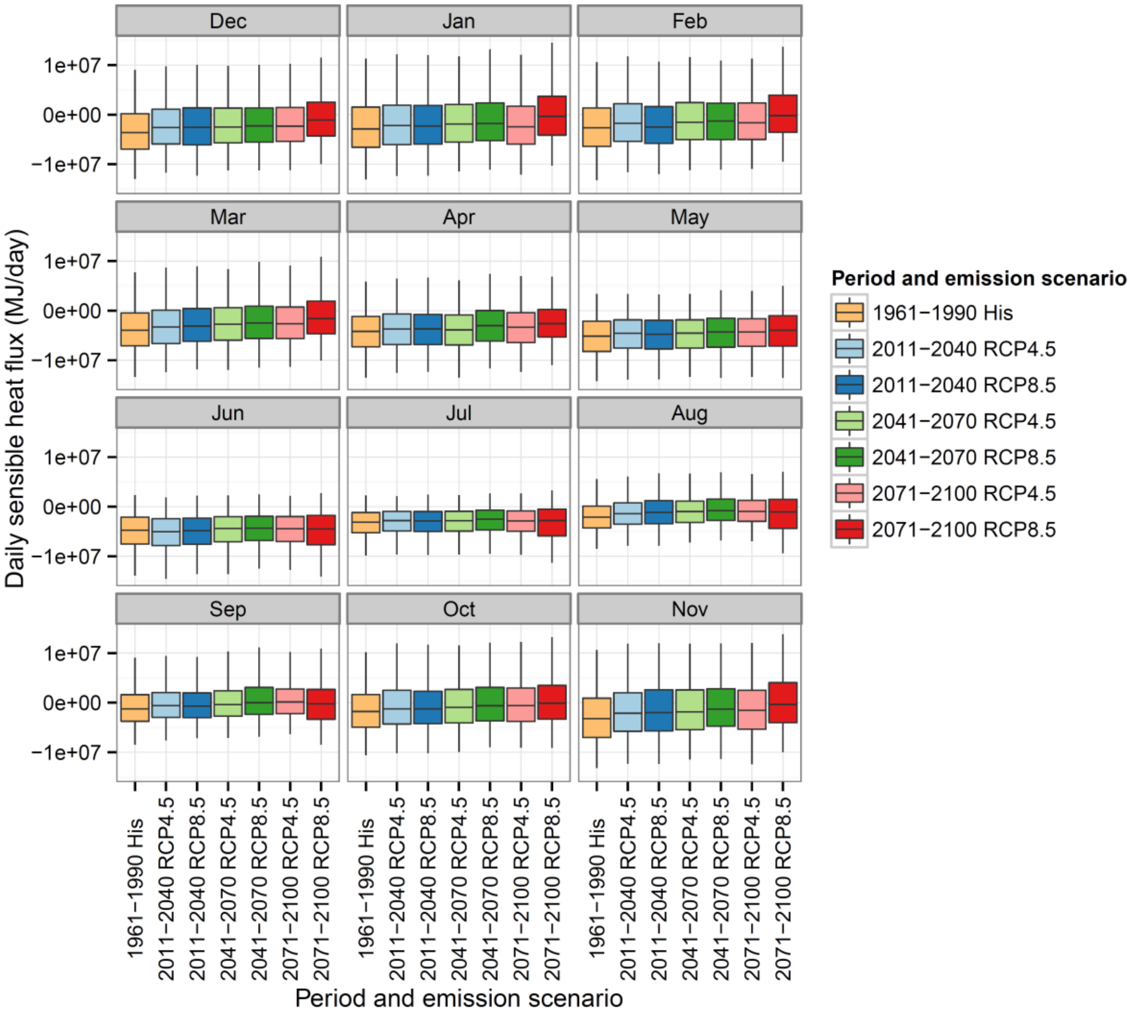

Figure 32. Daily sensible heat flux in reservoir simulations with boundary conditions derived from downscaled climate data (SA Climate Ready).

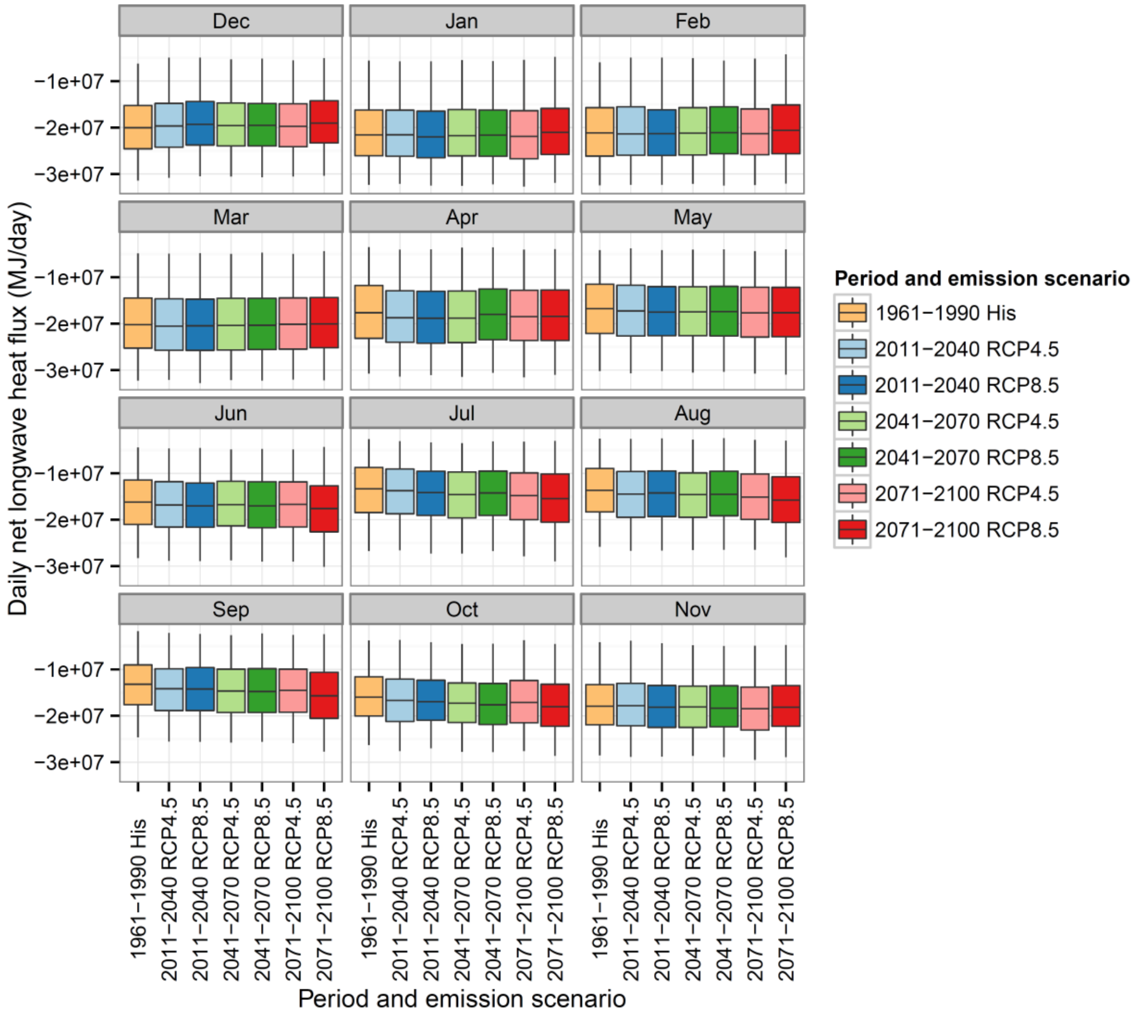

Figure 33. Daily net longwave heat flux in reservoir simulations with boundary conditions derived from downscaled climate data (SA Climate Ready)

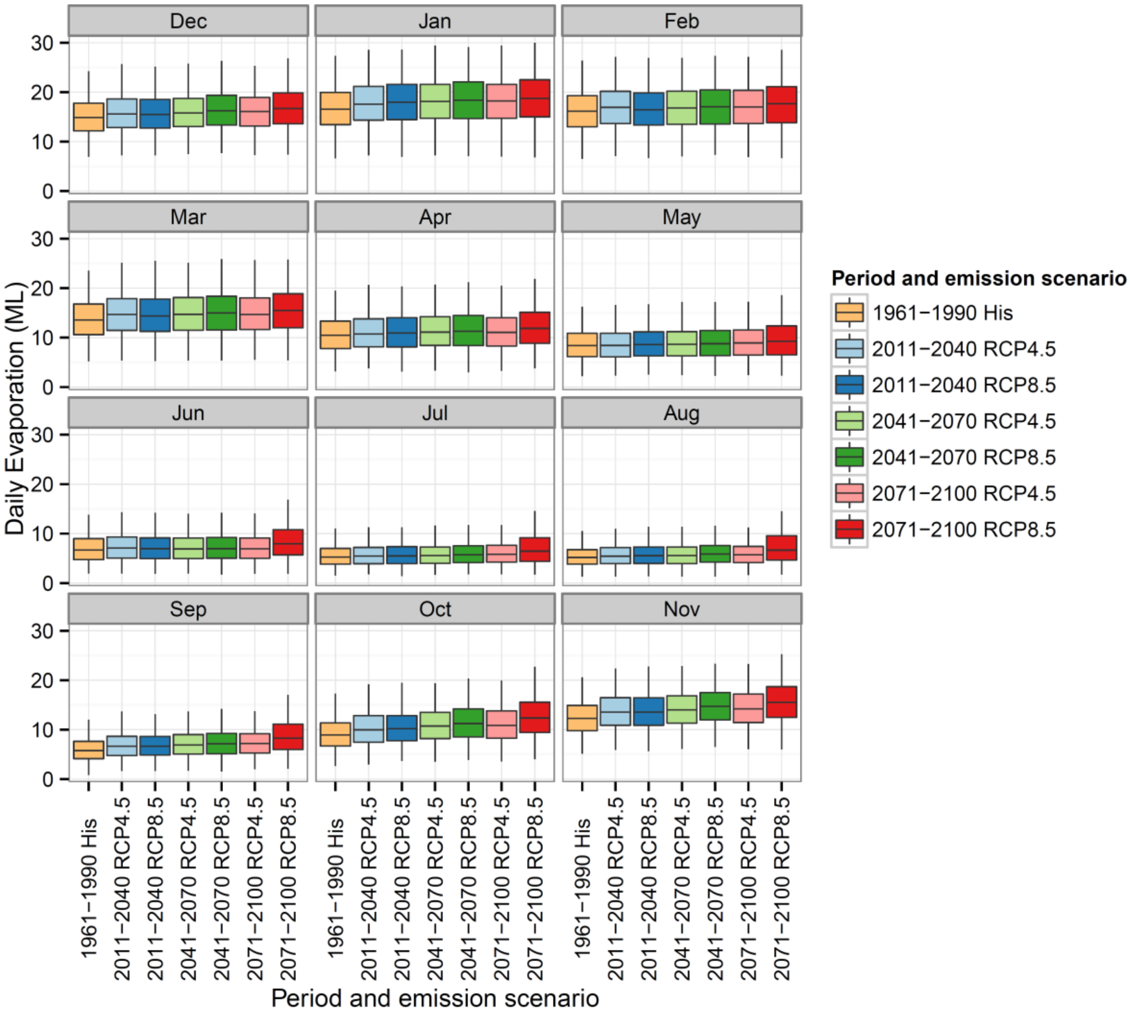

Figure 34. Daily volumetric evaporation in reservoir simulations with boundary conditions derived from downscaled climate data (SA Climate Ready)

Abiotic water quality parameters

The increases in salinity projected by these scenarios was in all cases less than 3%. This small increase is generated by the increase in evaporation from the water surface. Near term (2011-2040) increases over the historical period were similar to 0.5 to 1.0 % increases depending on emission scenarios (Figure 35). In the short-term, decreases in dissolved oxygen concentrations, similar to a 1.7 – 4.2 % decrease (winter) to 4.5 – 7.9% decrease (summer) is projected. By the end of the century, these reductions in dissolved oxygen concentration are projected to be similar to 3.6 – 5.7 % (winter) and 10 – 16% (summer) (Figure 36). While dissolved inorganic carbon increased by similar percentages to salinity (Figure 37), pH did not change in the scenarios (not shown). Changes in filterable reactive phosphorus concentrations were inconsistent and generally less than 3% (Figure 38). There was little impact on the concentrations of dissolved organic nutrients; dissolved organic nitrogen and dissolved organic phosphorus showed no differences over time periods or emissions scenarios (not shown). Nitrate and Ammonium concentrations changed with time period and emission scenario. By the end of the century, reductions in median nitrate concentration were in the ranges of 1.6 – 15 % and 2.8 – 24 % for the RCP4.5 and RCP8.5 scenarios, respectively (Figure 39). Ammonium concentrations increased in the summer and autumn but were stable in winter (Figure 40). Dissolved organic carbon concentration varied by less than 3% in all scenarios (not shown). Median particulate organic carbon increased by between 15 and 35% by the end of the century, depending on the month and scenario (Figure 41).

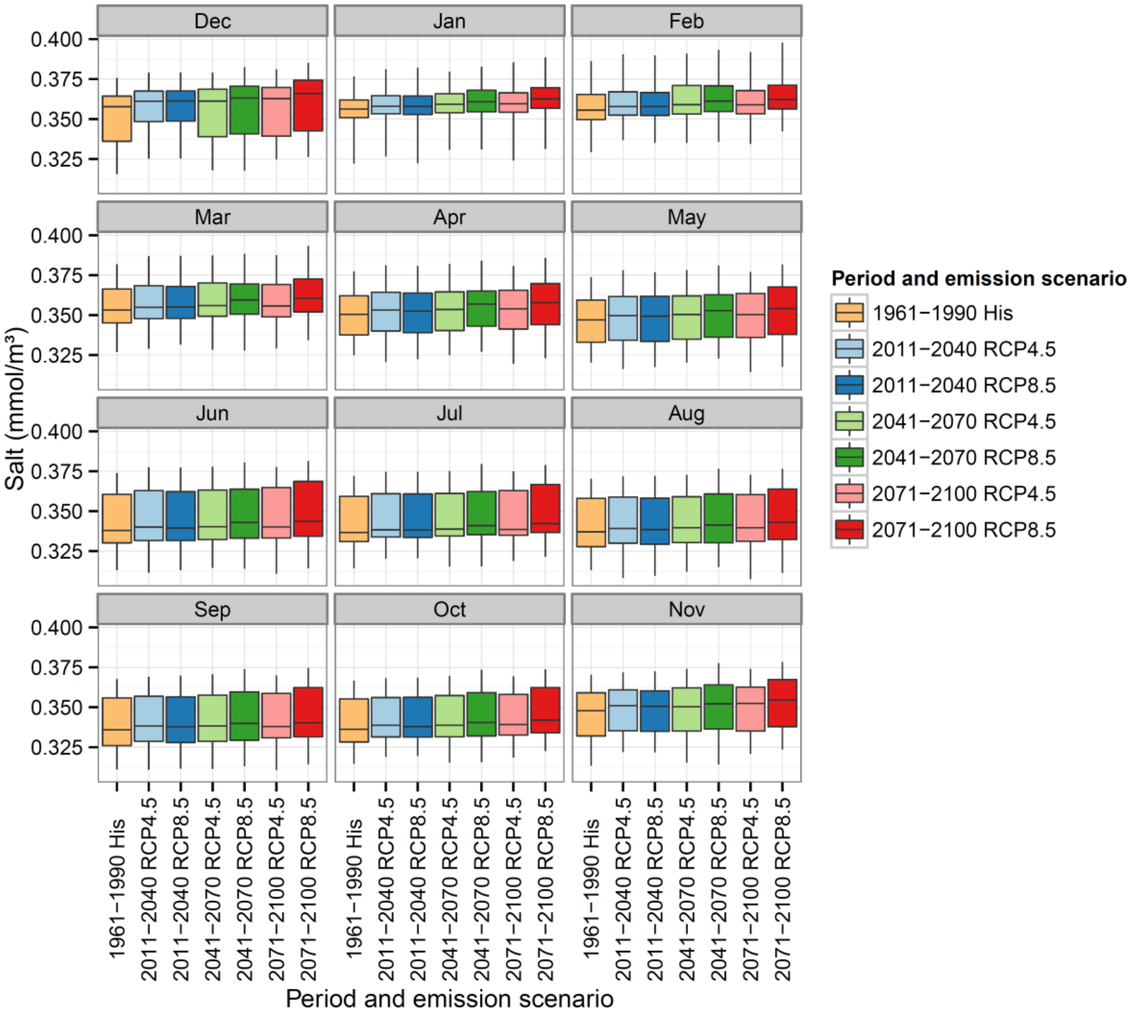

Figure 35. Salt concentration in reservoir simulations with boundary conditions derived from downscaled climate data (SA Climate Ready)

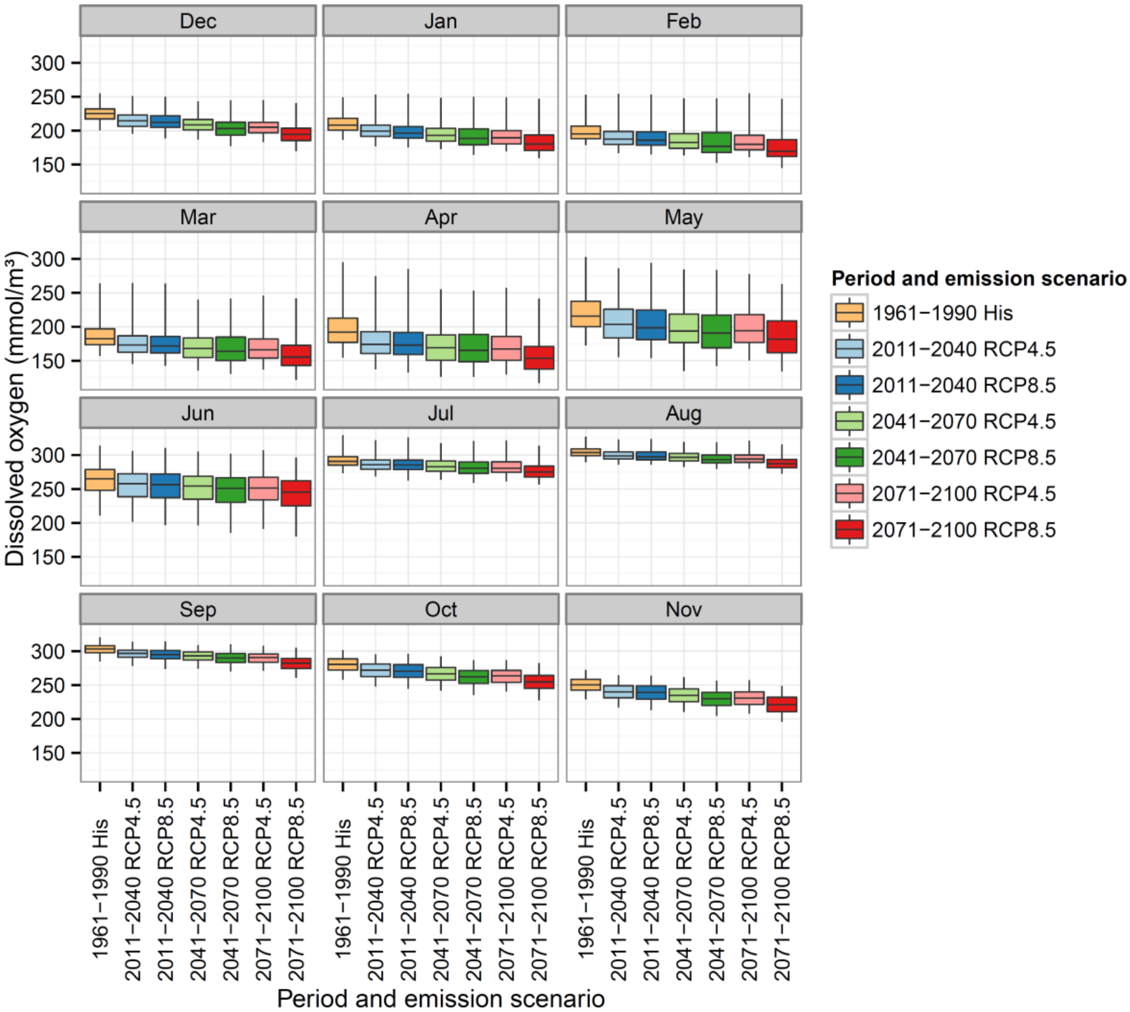

Figure 36. Dissolved oxygen concentration in reservoir simulations with boundary conditions derived from downscaled climate data (SA Climate Ready)

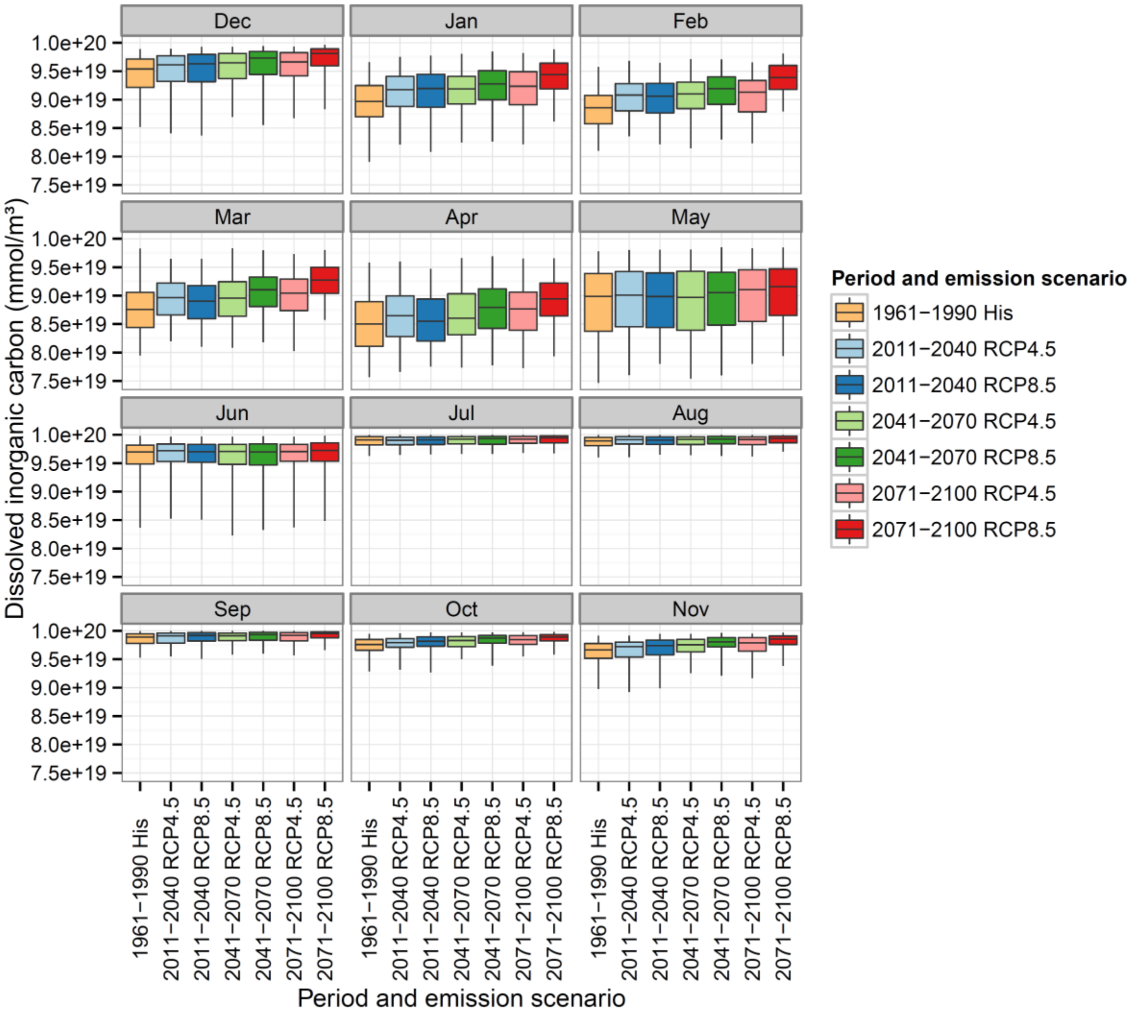

Figure 37. Dissolved inorganic carbon concentration in reservoir simulations with boundary conditions derived from downscaled climate data (SA Climate Ready)

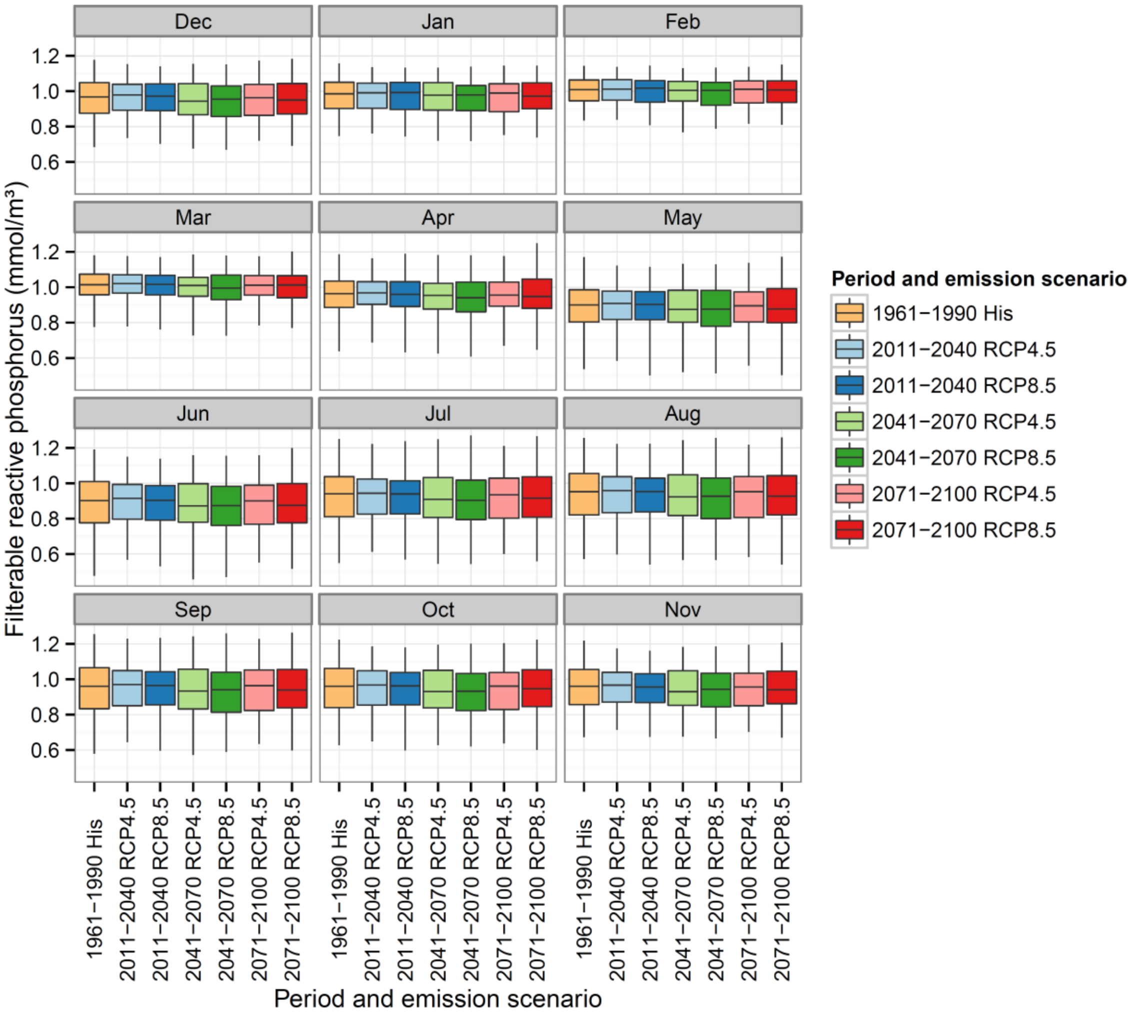

Figure 38. Filterable reactive phosphorus concentration in reservoir simulations with boundary conditions derived from downscaled climate data (SA Climate Ready)

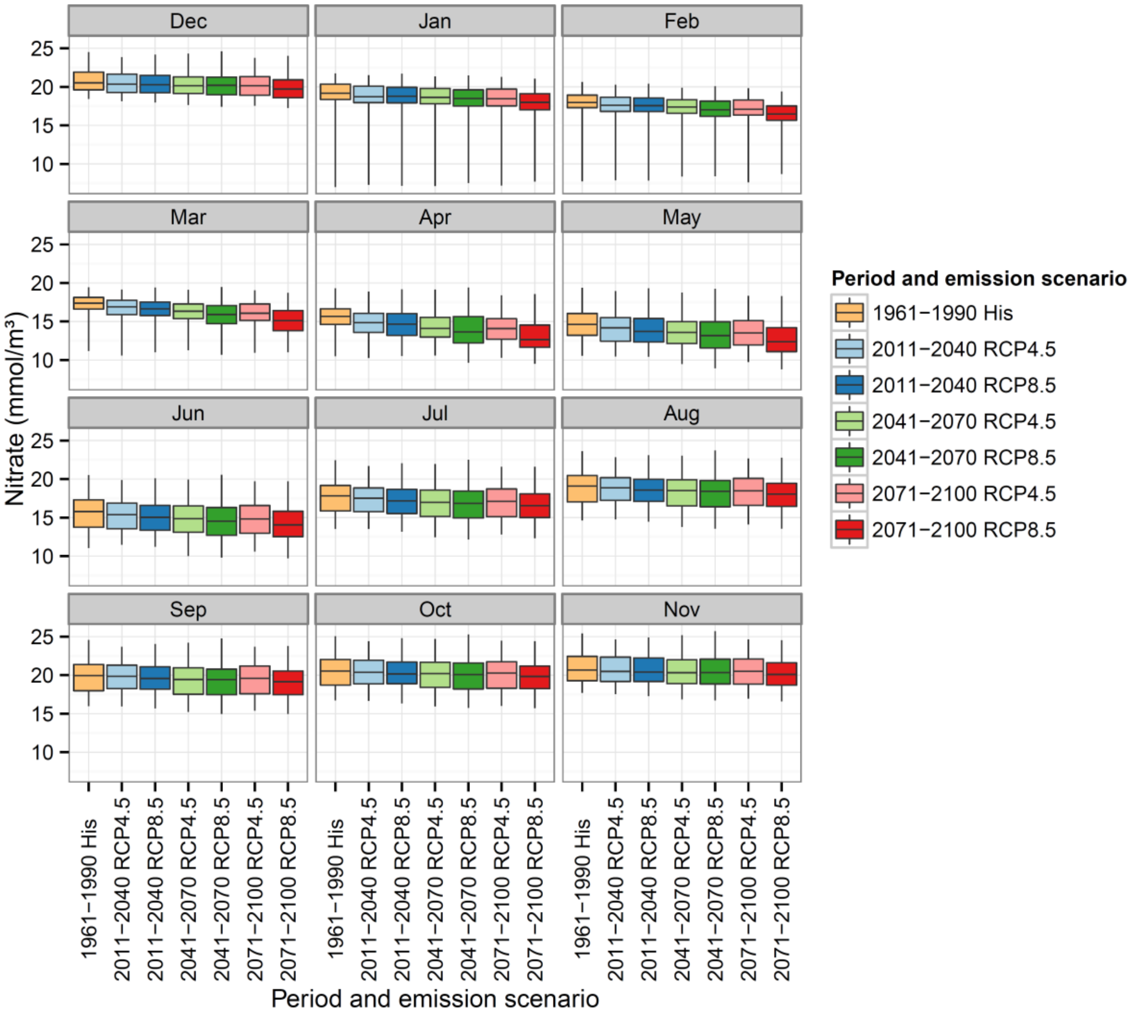

Figure 39. Nitrate concentration in reservoir simulations with boundary conditions derived from downscaled climate data (SA Climate Ready)

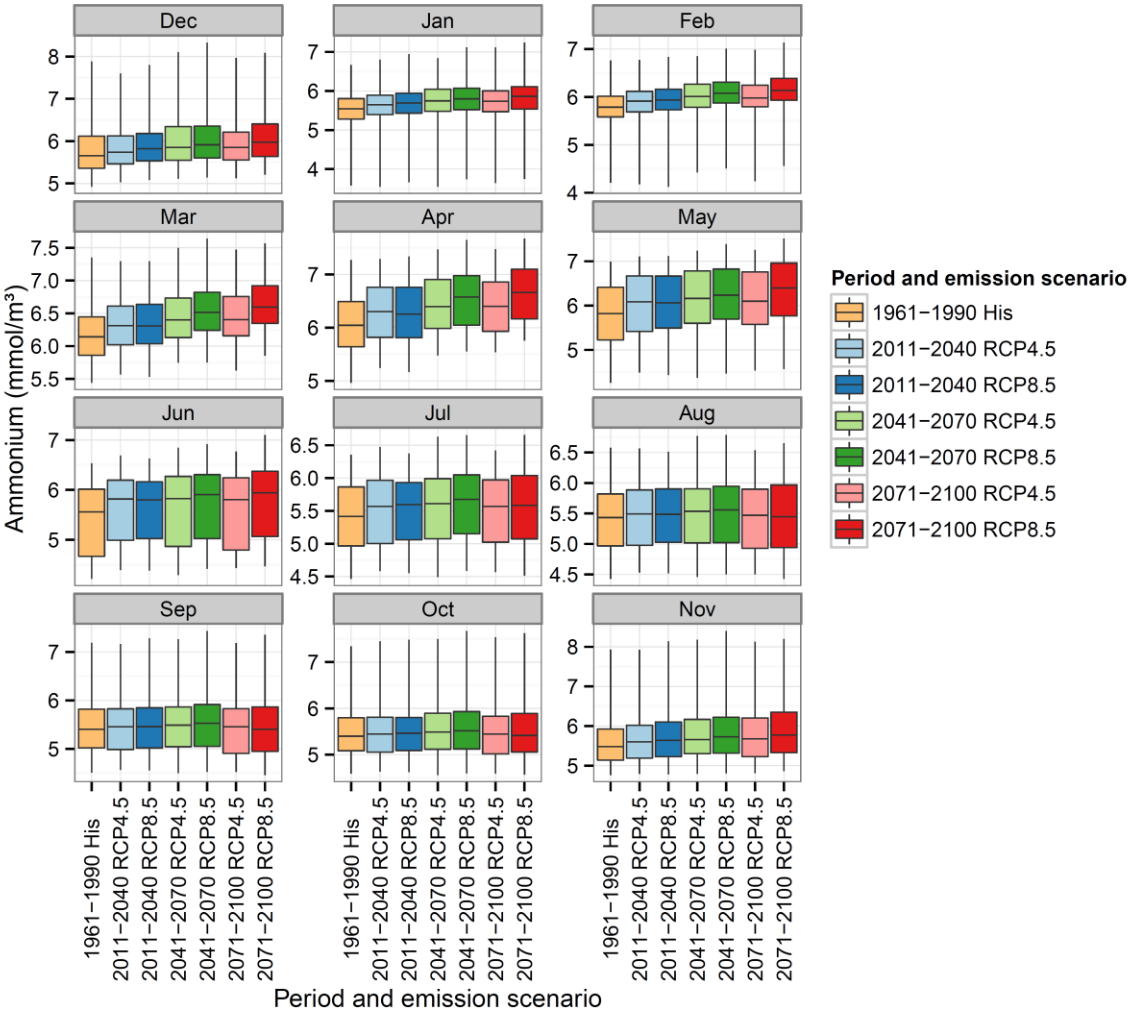

Figure 40. Ammonium concentration in reservoir simulations with boundary conditions derived from downscaled climate data (SA Climate Ready)

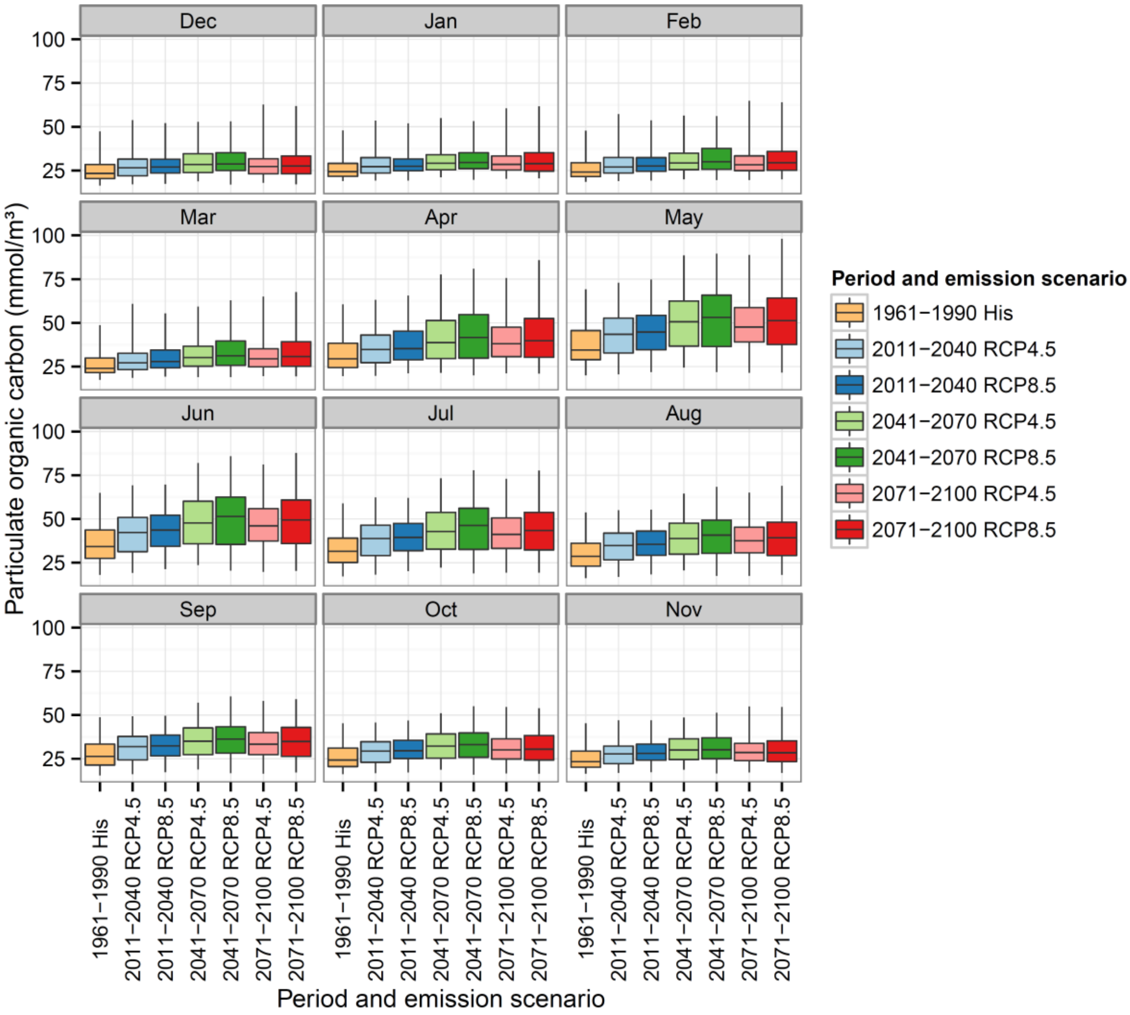

Figure 41. Particulate organic carbon concentration in reservoir simulations with boundary conditions derived from downscaled climate data (SA Climate Ready)

Phytoplankton variables

Green algae were very unsuccessful in future climate scenarios, with 50 – 500% reductions in median biomass projected in the near term and 100 – 1000% reductions by the end of the century (Figure 42). Diatom abundance was also negatively affected by future climate (Figure 43). The functional group parameterised to represent the cyanobacteria *Microcystis* was more successful in the future climate scenarios, with increases in median biomass of between 50 and 75% in the near term and 68 – 82% by the end of the century (Figure 44). The Yellow-Brown algae, or cryptophytes (for example the genera *Cryptomonas* and *Croomonas*) remained competitive in the spring, they increased in median biomass by a few percent in September and October in the future scenarios. However throughout the rest of the year they performed worse, with reductions of up to 215% (Figure 45). The functional group representing dinoflagellates similar to *Peridinium* was more successful in the future between September and January; however a decline in their performance was observed in the months between March and July (Figure 46). In terms of biomass, green algae and cyanobacteria dominated the modelled community; under projected future conditions the green algae were out-competed by the cyanobacteria. The total phytoplankton biomass, calculated as the sum of the median biomass (as carbon) of all the modelled phytoplankton groups increased by up to 53% in the highest emissions scenario and latest climatic period (2071-2100). Interestingly, the projected change in total phytoplankton biomass between the historical period and the earliest projection period (2011-2040) ranged from -7% (April) to +28% (November), with most months in the range +10 – +25%.

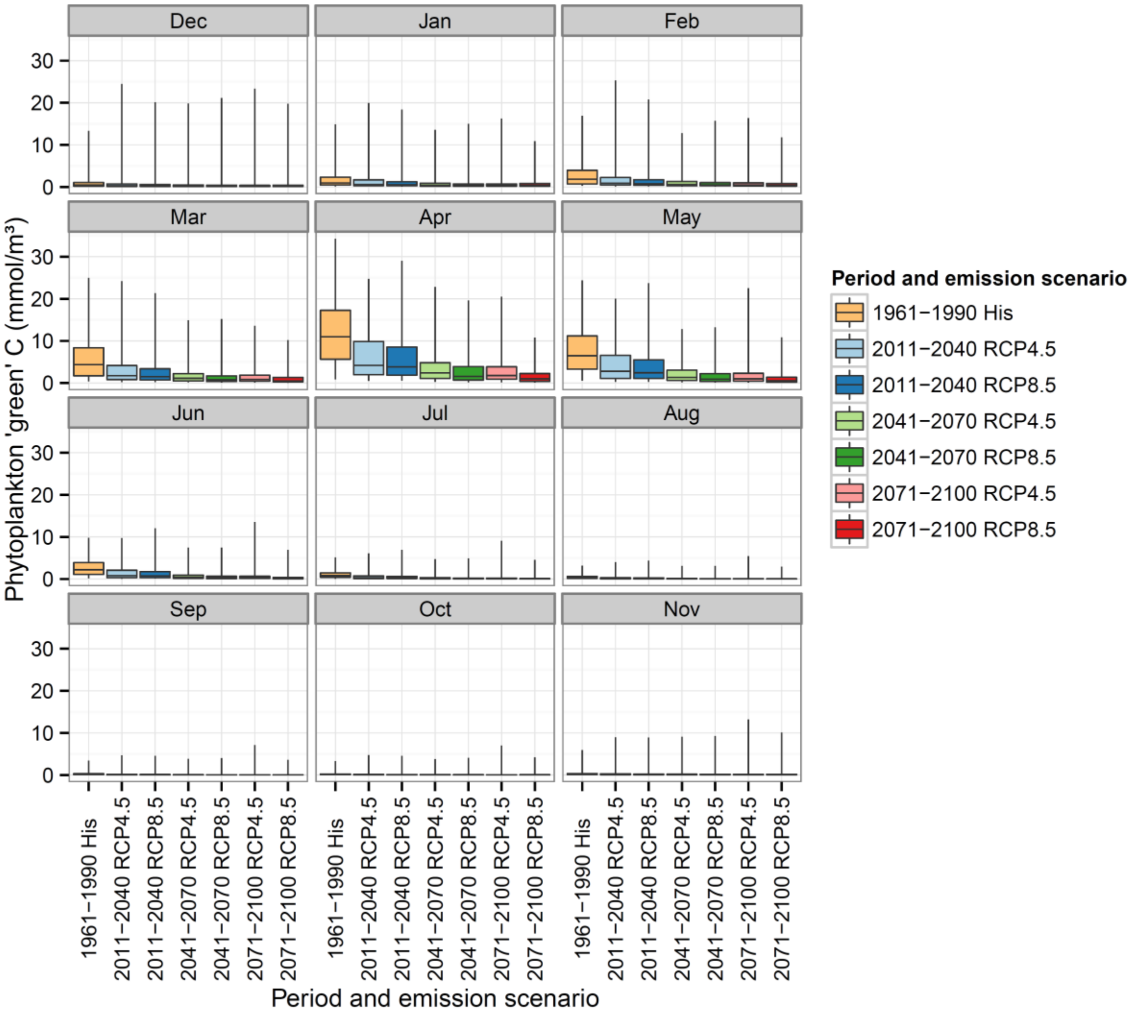

Figure 42. Concentration of carbon within phytoplankton functional group representing Chlorophytes (green algae) in reservoir simulations with boundary conditions derived from downscaled climate data (SA Climate Ready)

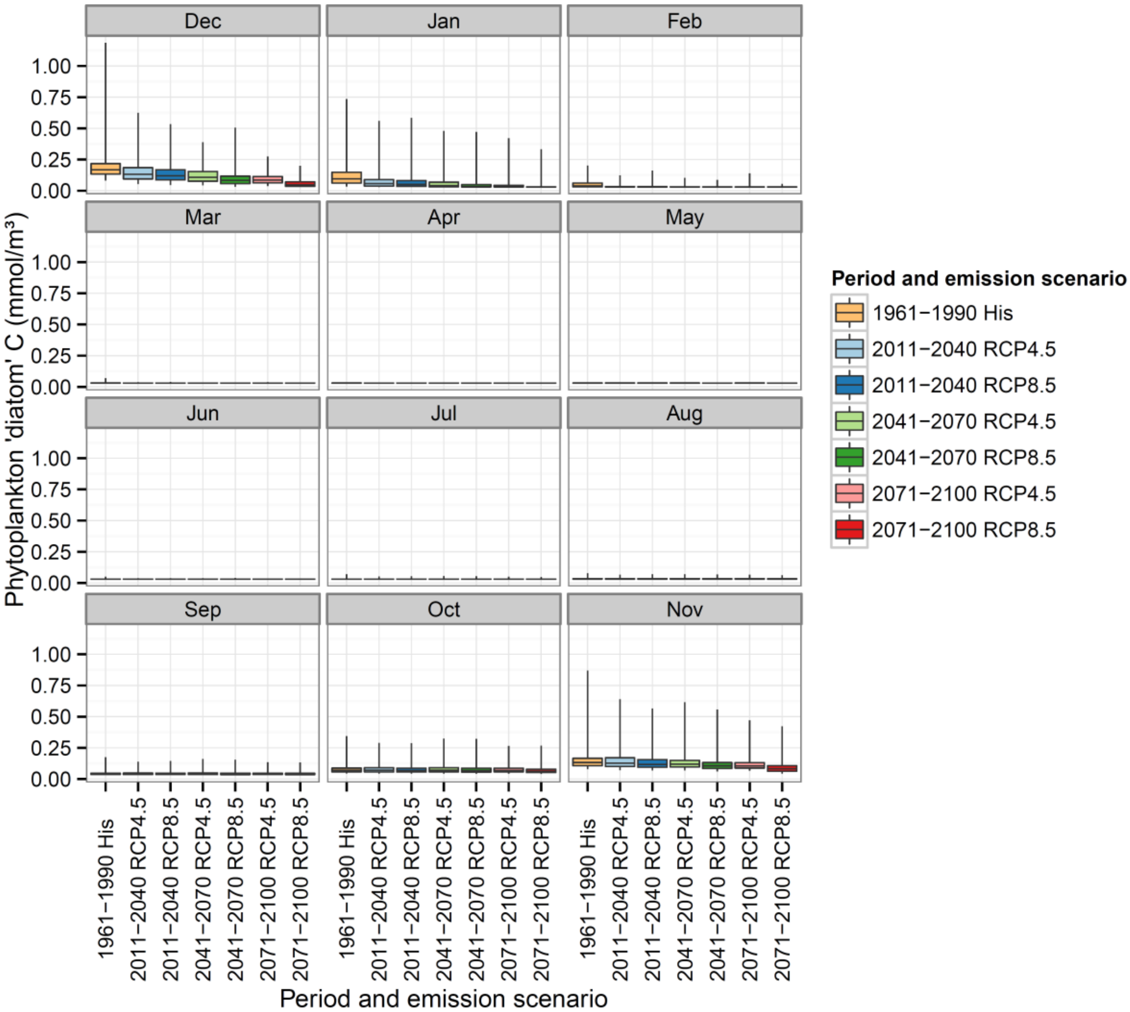

Figure 43. Concentration of carbon within phytoplankton functional group representing Bacillariophytes (diatoms) in reservoir simulations with boundary conditions derived from downscaled climate data (SA Climate Ready)

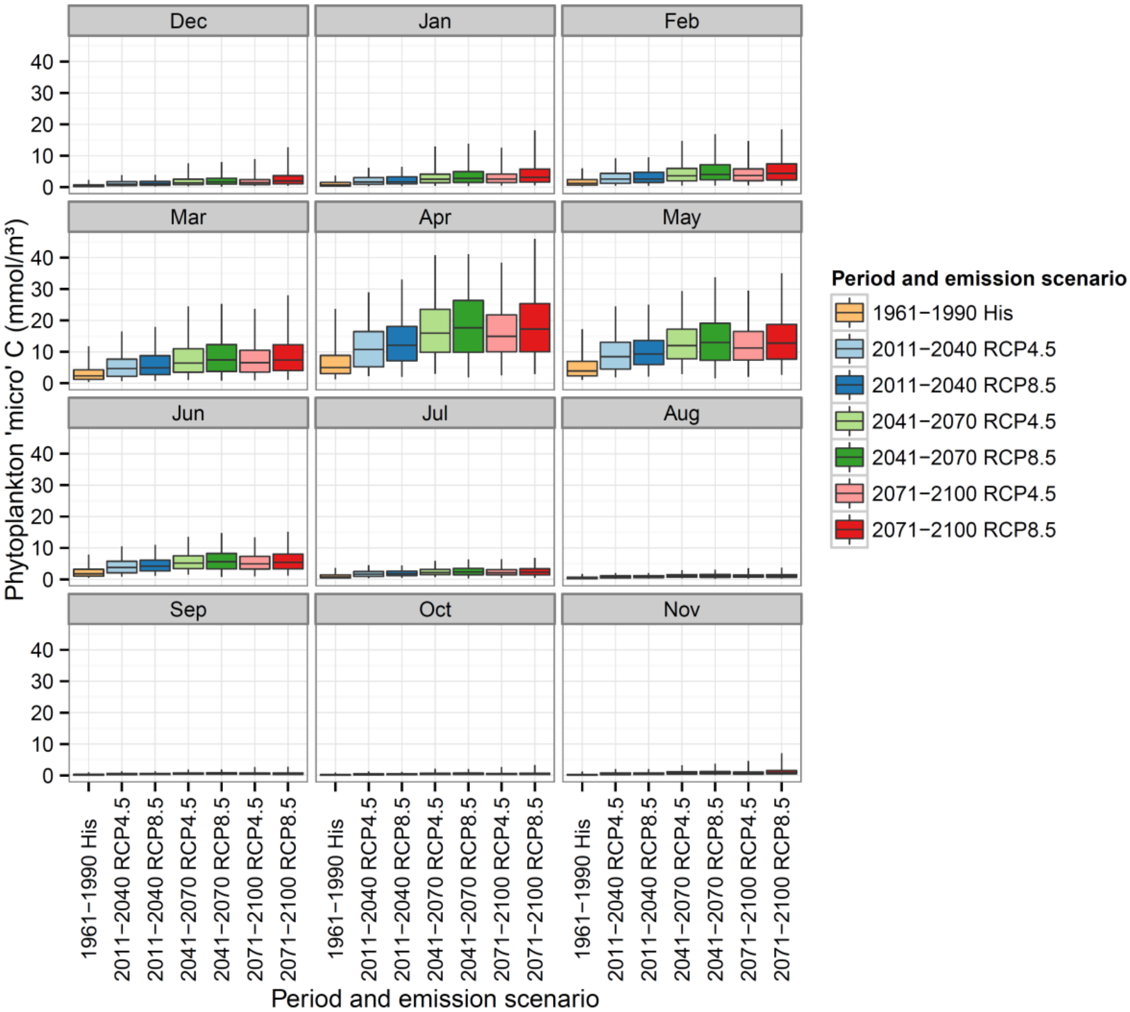

Figure 44. Concentration of carbon within phytoplankton functional group representing cyanobacteria (*Microcystis*-like cyanobacteria) in reservoir simulations with boundary conditions derived from downscaled climate data (SA Climate Ready)

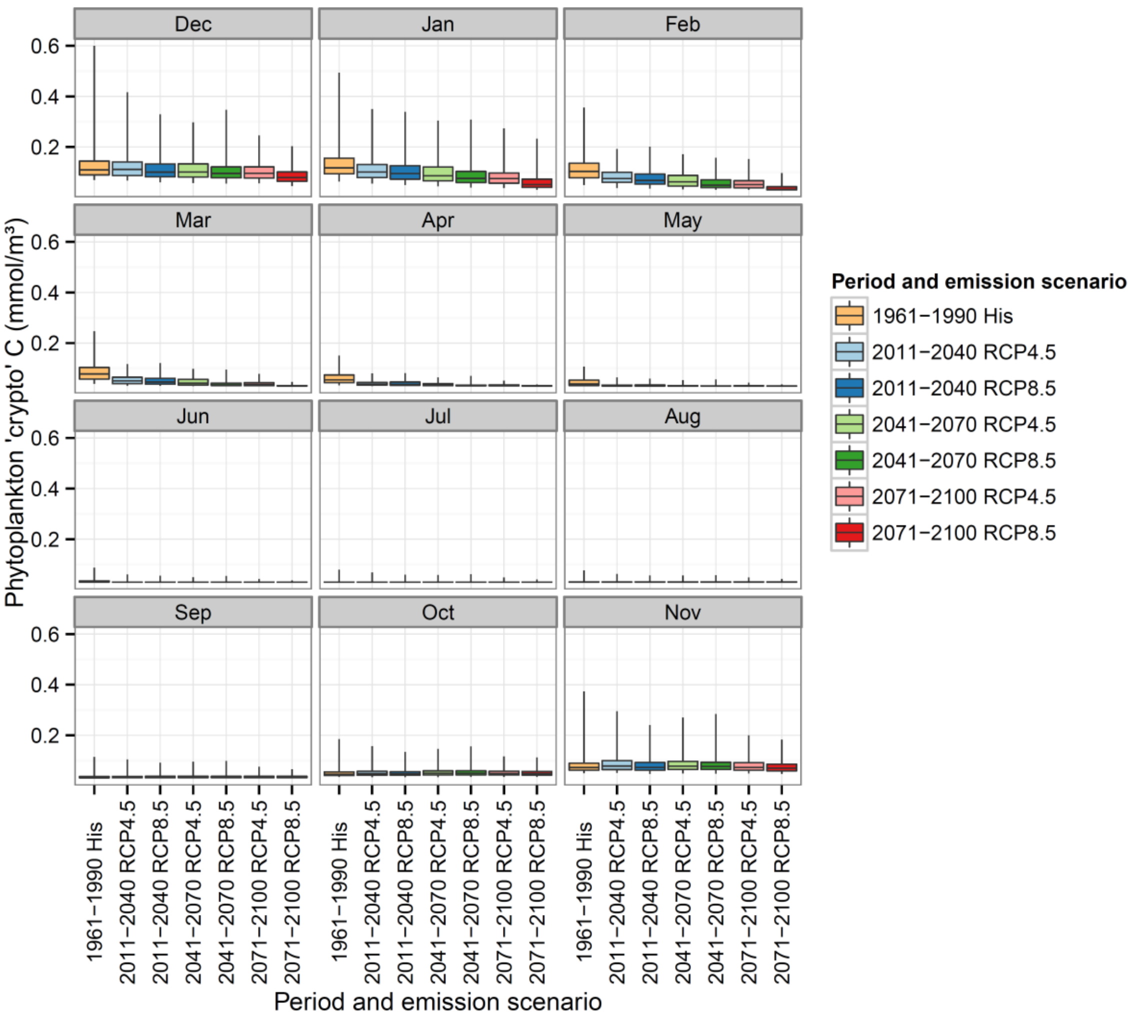

Figure 45. Concentration of carbon within phytoplankton functional group representing Cryptophytes (crypto; yellow-brown algae) in reservoir simulations with boundary conditions derived from downscaled climate data (SA Climate Ready)

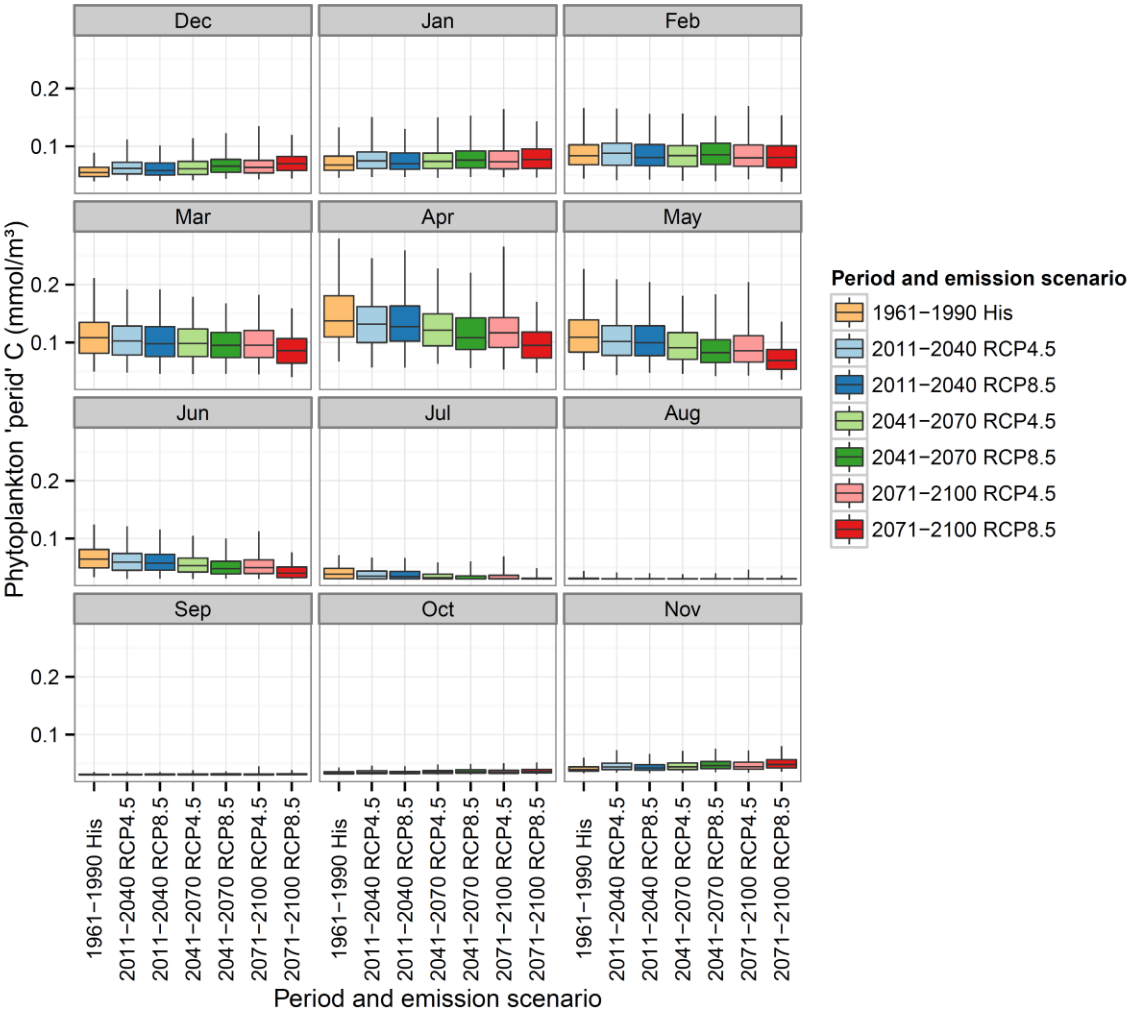

Figure 46. Concentration of carbon within phytoplankton functional group representing Dinoflagellates (perid; Peridinium-like dinoflagellates) in reservoir simulations with boundary conditions derived from downscaled climate data (SA Climate Ready)

Statistical analyses of simulated outputs

Multivariate correlation of algal groups from meteorological and environmental variables

Following pre-processing, where the data was centred, scaled and transformed by the Yeo-Johnson method (Yeo and Johnson, 2000) as implemented in the *caret* package in *R* (Kuhn *et al.*, 2016). The analysed variables were reduced to avoid those with extremely high, or extremely low correlations (< -0.9 or > 0.9) due to simple physical or semantic reasons, i.e. maximum temperature and surface temperature or lake level and surface area. These correlations, and those of the other variables, can be seen in Figure 47. A principal components analysis was conducted using the *FactoMineR* package (Lê *et al.*, 2008). An example of a scree plot for the analysis is shown, demonstrating that almost all the variation can be described by two principal components (Figure 48). In both the historical and future period analysed (1961-1990 Historical and 2071-2100 RCP8.5), the first two principal components accounted for more than 90% of the variance in the data (see axis labels in Figure 49 and Figure 50); therefore only these two dimensions are presented in the vector plots. The vector plots represent the correlation of the algal groups (black arrows) with each other and the 5 most important quantitative supplementary variables (blue arrows). There are broad similarities between the vector plots for the two periods, suggesting similar processes are at play. In the future, the *micro* group vector has moved a little further away from the *green* and *perid* vectors, indicating some separation in the conditions in which these groups are occurring. As it is difficult to conclude much about the processes responsible for this, a multiple linear regression was applied to investigate the role of the environmental variables in determining the success of *micro*.

Multiple linear regression of cyanobacterial abundance

Multiple linear regression was applied to Yeo-Johnson transformed variables. In the first instance, the most parsimonious linear model (the simplest model that appropriately fits the data) was identified using a step-wise model selection algorithm based on Akaike's An Information Criterion (AIC) as implemented in the *MASS* package (Venables and Ripley, 2002). The factors of the model selected are presented in the left-most column of Table 7 and are rank ordered according to their relative importance as determined for the historical period, using the methods defined in (Grömping, 2006). Month of the year was by far the most important predictor of the amount of *micro* (49.1%), followed by *Nitrate* (14.9%) and *Surface Temperature* (13.3%). Smaller amounts (< 10%) were attributable to Ammonium, Lake Number, Salt (salinity) and the interactions between the other factors. As the period into the future progresses, and with higher emissions scenarios in the same time period, the month of the year and Nitrate concentration become progressively less important for determining the occurrence of *micro*, while Surface Temperature and Ammonium become progressively more important.

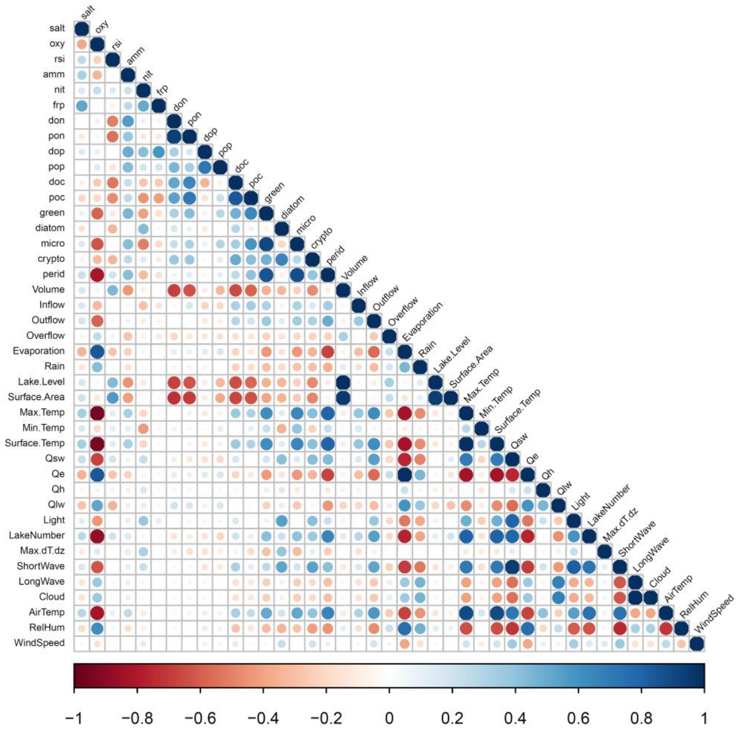

Figure 47. Correlation plot for weekly GLM-FABM outputs from historical projection period

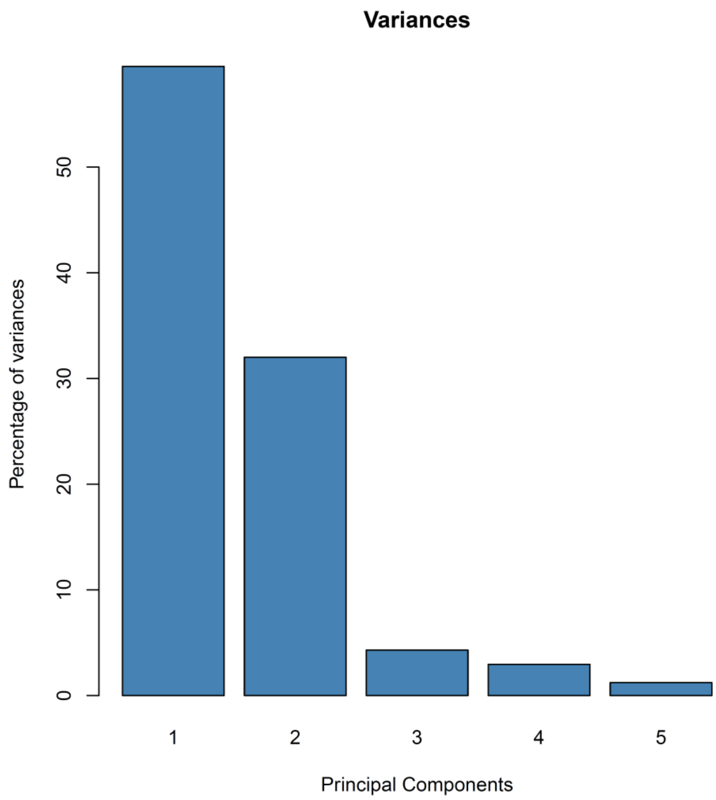

Figure 48. Scree plot of variance attributable to the principal components in the historical period.

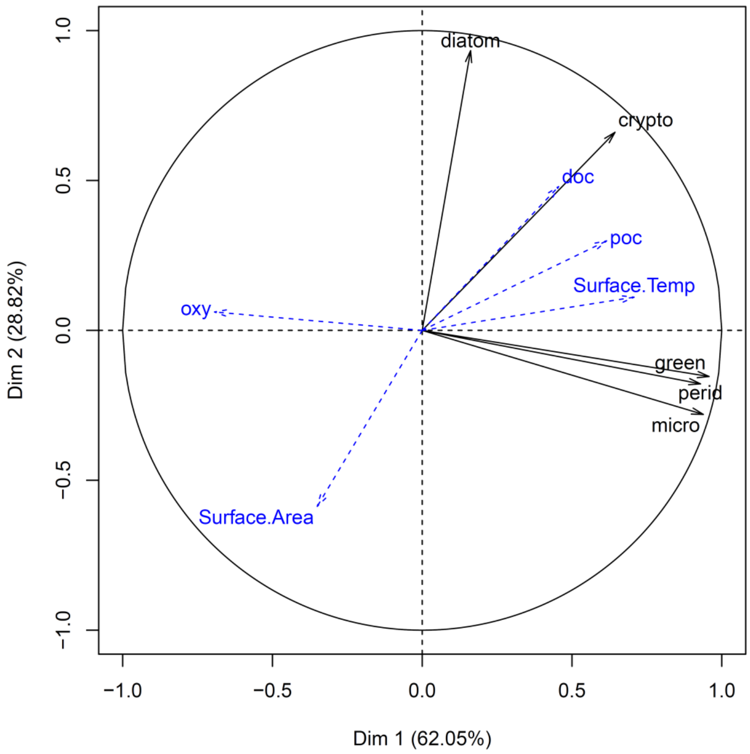

Figure 49. Vector plot of PCA analysis of historical period

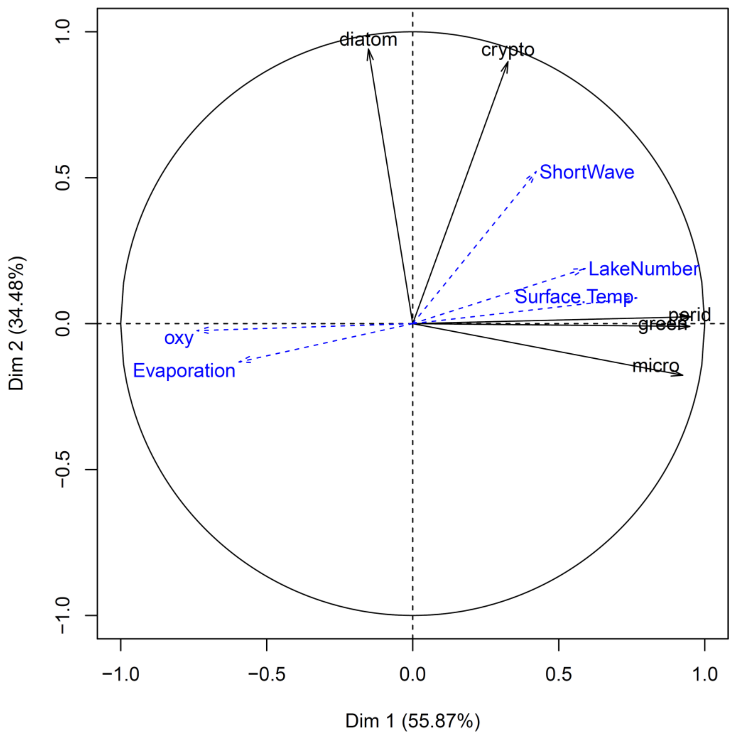

Figure 50. Vector plot of PCA analysis of 2017-2100 RCP 8.5 projections

Table 7. Results of the multiple linear regression analysis with relative importance assessment of model factors and interactions.

Period	1961-1990	2011-2040	2011-2040	2071-2100	2071-2100
Emission scenario	his	r45	r85	r45	r85
Month	49.1%	48.3%	47.5%	47.8%	42.0%
Nitrate	14.9%	13.5%	13.3%	12.5%	12.0%
Surface Temp	13.3%	14.3%	14.4%	15.1%	16.8%
Ammonium	6.7%	8.2%	8.4%	10.1%	14.9%
Lake Number	5.4%	5.9%	5.7%	5.3%	5.9%
Month:Nitrate	3.3%	2.7%	3.0%	1.8%	1.3%
Month:Salt	2.7%	2.5%	2.4%	2.7%	2.6%
Month:Ammonium	1.6%	1.8%	2.0%	1.6%	1.9%
Salt	1.5%	1.6%	1.8%	1.9%	1.6%
Month:Surface Temp	0.7%	0.6%	0.7%	0.6%	0.6%
Month:Lake Number	0.7%	0.7%	0.8%	0.6%	0.5%

Discussion

The main purpose of this study was to demonstrate the suitability of the Goyder Task 3 downscaling dataset for use in modelling the impacts of projected climate change on reservoir water quality. To achieve this required additional downscaling of wind and cloud cover. Potential methods were developed, but there remains the opportunity for more rigorous testing of the methods applied and the use of alternative methods, which may, for example refer to the original GCM outputs. At least, it would be appropriate to further test the sensitivity of the results to some of the key functions and their parameters. This would not be a trivial undertaking and has not been attempted at this stage. A strategy to examine the sensitivity on a subset of model runs would be suggested; running such an analysis on the full set of scenarios would be prohibitive (for example a single set of runs results in 52 GB of model outputs). Only a single realisation of the 100 stochastic realisations was used; it would also be appropriate to test the robustness of the results by comparing a number of realisations for a given scenario.

While this model analysis may provide useful guidance on climate change impacts, it relies upon a number of assumptions that must be considered during interpretation:

1. These responses represent those of a relatively simple phytoplankton community and there is the possibility for changes in community structure that cannot be modelled with a deterministic functional group model as implemented. However the responses generated are likely to represent the physiological reality that conditions are shifting to favour cyanobacteria in the future, as demonstrated by many empirical and model-based studies.
2. No impacts of changes in evapotranspiration or precipitation on the catchment hydrology were considered. This work was performed in parallel to the hydrological modelling and as such this was beyond the scope of the work.
3. Following on from this, no impact of climate change effects on the constituents of water flowing from the catchment was considered (i.e. nutrients, turbidity).
4. No changes in the annual regime of water demand, pumping and patterns of operational reservoir level were considered.

Model parameterisation remains a source of considerable uncertainty, as in any model with many parameters, some degree of irreducible uncertainty of the parameter values remains, resulting in equifinality of model performance (Arhonditsis *et al.*, 2008; Luo *et al.*, 2009). Therefore, despite the best efforts to properly calibrate the base scenario, and however valid it may appear during the validation period, it has been applied here in a deterministic way, with one single set of parameters. The uncertainty in the projected results derived from parameter uncertainty has not been evaluated. A further concern exists that the model parameters may not be valid outside the range of the data presented to the goodness-of-fit function used during calibration and validation. Such issues may mean that when the model was run with decadal scale meteorological boundary conditions, the seasonal course of phytoplankton succession was not as expected. An example of this was that the model outputs of the peak concentrations of cyanobacteria were observed in autumn (April and May), rather than in the summer, as generally expected.

It appears that the changes in cyanobacterial cell numbers in these scenarios were driven predominantly by the increase in water temperature, rather than increases in stratification. This may warrant further investigation, as the ecological mechanisms that favour the growth of cyanobacteria under conditions of stratification are well understood. For example, buoyancy regulation by gasvacuolated cyanobacteria was not applied via the model parameterisation, nor was the occurrence of nitrogen fixation, however the latter is unlikely to provide much advantage in this nitrogen replete reservoir. While the external load to the reservoir was kept relatively stable in the scenarios that were simulated, there was a small decrease in the concentration of reactive nitrogen, as well as a change in the speciation of the reactive nitrogen. As the *micro* group had a lower half-saturation coefficient for nitrogen uptake, this seems to have provided them with a slight advantage for the acquisition of nitrogen and resulted in the identification of the importance of nitrate and ammonium in the multiple linear regression analysis.

Relatively large increases in *Microcystis* occurred on a percentage basis. However if these values are converted to cell numbers using cell carbon quota values (Reynolds, 1984), the projected worst case concentration did not exceed the Australian Alert Level 3 guideline value of 65,000 cell/mL for *Microcystis aeruginosa* (Newcombe *et al.*, 2010).

References

Arheimer, B., Andréasson, J., Fogelberg, S., Johnsson, H., Pers, C.B., and Persson, K. (2005) Climate change impact on water quality: model results from southern Sweden. *Ambio* **34**: 559–66.

Arhonditsis, G.B., Perhar, G., Zhang, W., Massos, E., Shi, M., and Das, A. (2008) Addressing equifinality and uncertainty in eutrophication models. *Water Resour. Res.* **44**: n/a–n/a.

Beecham, S. (2015) Development of an agreed set of climate projections for South Australia Final Report. Goyder Institute for Water Research, Technical Report Series No. 15/3, Adelaide, South Australia.

Beecham, S., Rashid, M., and Chowdhury, R.K. (2014) Statistical downscaling of multi-site daily rainfall in a South Australian catchment using a Generalized Linear Model. *Int. J. Climatol.* **34**: 3654–3670.

Black, J.N. (1956) The distribution of solar radiation over the Earth's surface. *Arch. für Meteorol. Geophys. und Bioklimatologie Ser. B* **7**: 165–189.

Blenckner, T. (2005) A conceptual model of climate-related effects on lake ecosystems. *Hydrobiologia* **533**: 1–14.

Bristow, K.L. and Campbell, G.S. (1984) On the relationship between incoming solar radiation and daily maximum and minimum temperature. *Agric. For. Meteorol.* **31**: 159–166.

Brookes, J.D., Burch, M.D., Hipsey, M.R., Linden, L.G., Antenucci, J., Steffensen, D., et al. (2008) A practical guide to reservoir management Cooperative Research Centre for Water Quality and Treatment, Adelaide, Australia.

Brueck, T., O'Berry, D., Blankenship, L., and Brink, P. (2012) Forecasting the Future: Progress, Change, and Predictions for the Water Sector Water Research Foundation, Denver, Colorado, USA.

Cai, W., Borlace, S., Lengaigne, M., van Rensch, P., Collins, M., Vecchi, G., et al. (2014) Increasing frequency of extreme El Niño events due to greenhouse warming. *Nat. Clim. Chang.* **4**: 111–116.

Cai, W., Cowan, T., and Thatcher, M. (2012) Rainfall reductions over Southern Hemisphere semi-arid regions: the role of subtropical dry zone expansion. *Sci. Rep.* **2**: 702.

Cai, W., Santoso, A., Wang, G., Weller, E., Wu, L., Ashok, K., et al. (2014) Increased frequency of extreme Indian Ocean Dipole events due to greenhouse warming. *Nature* **510**: 254–8.

Campolongo, F., Cariboni, J., and Saltelli, A. (2007) An effective screening design for sensitivity analysis of large models. *Environ. Model. Softw.* **22**: 1509–1518.

Charles, S.P., Heneker, T., and Bates, B.C. (2008) Stochastically downscaled rainfall projections and modelled hydrological response for the Mount Lofty Ranges, South Australia. In, Lambert,M., Daniell,T., and Leonard,M. (eds), *Water Down Under*. Engineers Australia, Adelaide Australia, pp. 428–438.

Coles, J.F. and Jones, R.C. (2000) Effect of temperature on photosynthesis-light response and growth of four phytoplankton species isolated from a tidal freshwater river. *J. Phycol.* **36**: 7–16.

CSIRO (2007) Climate Change in Australia CSIRO, Canberra, Australia.

CSIRO (2012) State of the Climate 2012 CSIRO and Bureau of Meteorology.

Delpla, I., Jung, A.-V., Baures, E., Clement, M., and Thomas, O. (2009) Impacts of climate change on surface water quality in relation to drinking water production. *Environ. Int.* **35**: 1225–1233.

Elliott, J.A. (2012) Is the future blue-green? A review of the current model predictions of how climate change could affect pelagic freshwater cyanobacteria. *Water Res.* **46**: 1364–1371.

Elliott, J.A., Jones, I.D., and Thackeray, S.J. (2006) Testing the Sensitivity of Phytoplankton Communities to Changes in Water Temperature and Nutrient Load, in a Temperate Lake. *Hydrobiologia* **559**: 401–411.

Etemad-Shahidi, A. and Imberger, J. (2006) Diapycnal mixing in the thermocline of lakes: Estimations by different methods. *Environ. Fluid Mech.* **6**: 227–240.

Fu, G., Charles, S.P., and Kirshner, S. (2013) Daily rainfall projections from general circulation models with a downscaling nonhomogeneous hidden Markov model (NHMM) for south-eastern Australia. *Hydrol. Process.* **27**: 3663–3673.

Green, G., Gibbs, M., and Wood, C. (2011) Impacts of Climate Change on Water Resources, Phase 3 Volume 1: Northern and Yorke Natural Resources Management Region DFW Technical Report 2011/03.

Griffin, S.L., Herzfeld, M., and Hamilton, D.P. (2001) Modelling the impact of zooplankton grazing on phytoplankton biomass during a dinoflagellate bloom in the Swan River Estuary, Western Australia. *Ecol. Eng.* **16**: 373–394.

Grömping, U. (2006) Relative importance for linear regression in R: the package relaimpo. *J. Stat. Softw.* **17**: 139–147.

Hamilton, D.P. and Schladow, S.G. (1997) Prediction of water quality in lakes and reservoirs . Part I - Model description. **96**: 91–110.

Heneker, T. and Cresswell, D. (2010) Potential Impact on Water Resource Availability in the Mount Lofty Ranges due to Climate Change Adelaide.

Hipsey, M.R., Bruce, L.C., and Hamilton, D.P. (2013) General Lake Model v1.3.2 University of Western Australia.

Hipsey, M.R., Romero, J.R., Antenucci, J.P., and Hamilton, D.P. (2006) Computational aquatic ecosystem dynamics model, CAEDYM v2.3, User Manual Centre for Water Research, University of Western Australia.

Hodges, B. and Dallimore, C. (2007) Estuary, Lake and Coastal Ocean Model, ELCOM v2.2, User Manual Centre for Water Research, University of Western Australia.

Hottel, H.C. (1976) A simple model for estimating the transmittance of direct solar radiation through clear atmospheres. *Sol. Energy* **18**: 129.

Husson, F., Josse, J., Le, S., and Mazet, J. (2015) FactoMineR: Multivariate Exploratory Data Analysis and Data Mining R package version 1.31.4.

Jones, I.D., Page, T., Alex Elliott, J., Thackeray, S.J., and Louise Heathwaite, a. (2011) Increases in lake phytoplankton biomass caused by future climate-driven changes to seasonal river flow. *Glob. Chang. Biol.* **17**: 1809–1820.

Krüger, G.H.J. and Eloff, J.N. (2010) The influence of light intensity on the growth of different Microcystis isolates. *J. Limnol. Soc. South. Africa* **3**: 21–25.

Kuhn, M., Wing, J., Weston, S., Williams, A., Keefer, C., Engelhardt, A., et al. (2016) caret: Classification and Regression Training.

Lê, S., Josse, J., and Husson, F. (2008) {FactoMineR}: A Package for Multivariate Analysis. *J. Stat. Softw.* **25**: 1–18.

Van der Linden, L., Daly, R.I., and Burch, M.D. (2015) Suitability of a coupled hydrodynamic water quality model to predict changes in water quality from altered meteorological boundary conditions. *Water (MDPI)* **7**: 348–361.

Luo, Y., Weng, E., Wu, X., and Gao, C. (2009) Parameter identifiability, constraint, and equifinality in data assimilation with ecosystem models. *Ecol. Appl.* **19**: 571–574.

Maheepala, S., Dandy, G., Marchi, A., Mirza, F., Wu, W., Daly, R., et al. (2014) A Decision Support Framework for identifying optimal water supply portfolios : Metropolitan Adelaide Case Study Volume 1 : Main Report Goyder Institute for Water Research, Technical Report Series No. 14/17, Adelaide, South Australia.

Makler-Pick, V., Gal, G., Gorfine, M., Hipsey, M.R., and Carmel, Y. (2011) Sensitivity analysis for complex ecological models – A new approach. *Environ. Model. Softw.* **26**: 124–134.

McVicar, T.R., Van Niel, T.G., Li, L.T., Roderick, M.L., Rayner, D.P., Ricciardulli, L., and Donohue, R.J. (2008) Wind speed climatology and trends for Australia, 1975-2006: Capturing the stilling phenomenon and comparison with near-surface reanalysis output. *Geophys. Res. Lett.* **35**: L20403.

McVicar, T.R., Roderick, M.L., Donohue, R.J., Li, L.T., Van Niel, T.G., Thomas, A., et al. (2012) Global review and synthesis of trends in observed terrestrial near-surface wind speeds: Implications for evaporation. *J. Hydrol.* **416-417**: 182–205.

Mimikou, M.A., Baltas, E., Varanou, E., and Pantazis, K. (2000) Regional impacts of climate change on water resources quantity and quality indicators. *J. Hydrol.* **234**: 95–109.

Mooij, W.M., Janse, J.H., Senerpont Domis, L.N., Hülsmann, S., and Ibelings, B.W. (2007) Predicting the effect of climate change on temperate shallow lakes with the ecosystem model PCLake. *Hydrobiologia* **584**: 443–454.

Newcombe, G., House, J., Ho, L., Baker, P., and Burch, M.D. (2010) Management strategies for Cyanobacteria (blue-green algae): a guide for water utilities Water Quality Research Australia Limited.

Paerl, H.W. and Paul, V.J. (2012) Climate change: links to global expansion of harmful cyanobacteria. *Water Res.* **46**: 1349–63.

R Development Core Team (2011) R: A language and environment for statistical computing. R Foundation for Statistical Computing, Vienna, Austria.

Read, J.S., Hamilton, D.P., Jones, I.D., Muraoka, K., Winslow, L.A., Kroiss, R., et al. (2011) Derivation of lake mixing and stratification indices from high-resolution lake buoy data. *Environ. Model. Softw.* **26**: 1325–1336.

Reynolds, C.S. (1984) The Ecology of Freshwater Phytoplankton Cambridge University Press, Cambridge, UK.

Rigosi, A., Carey, C.C., Ibelings, B.W., and Brookes, J.D. (2014) The interaction between climate warming and eutrophication to promote cyanobacteria is dependent on trophic state and varies among taxa. *Limnol. Ocean.* **59**: 99–114.

Rigosi, A., Wickramaratne, C., Brookes, J.D., van der Linden, L., Ibelings, B.W., Carey, C.C., et al. (2015) Impact of Climate Change on the Ecology of Algal Blooms Water Research Foundation, Denver, Colorado, USA.

Robarts, R.D. and Zohary, T. (1987) Temperature Effects on Photosynthetic Capacity, Respiration, and Growth-Rates of Bloom-Forming Cyanobacteria. *New Zeal. J. Mar. Freshw. Res.* **21**: 391–399.

Romero, J., Antenucci, J., and Okley, P. (2005) Happy Valley Reservoir Modelling Study - Final Report Centre for Water Research, University of Western Australia.

Saloranta, T., Forsius, M., Järvinen, M., and Arvola, L. (2009) Impacts of projected climate change on the thermodynamics of a shallow and a deep lake in Finland: model simulations and Bayesian uncertainty analysis. *Hydrol. Res.* **40**: 234.

Saltelli, A. (2002) Making best use of model evaluations to compute sensitivity indices. *Comput. Phys. Commun.* **145**: 280–297.

Schlabing, D., Eder, M., Frassl, M., Rinke, K., and B, A. (2005) A Vector-Autoregressive " co-shiftable " Weathergenerator for Hydrodynamic Modeling of Lakes. 2005.

Schlabing, D., Frassl, M. a., Eder, M.M., Rinke, K., and Bárdossy, A. (2014) Use of a weather generator for simulating climate change effects on ecosystems: A case study on Lake Constance. *Environ. Model. Softw.* **61**: 326–338.

Schladow, S.G. and Hamilton, D.P.D. (1997) Prediction of water quality in lakes and reservoirs: Part II-Model calibration, sensitivity analysis and application. *Ecol. Modell.* **96**: 111–123.

Taylor, K.E., Stouffer, R.J., and Meehl, G.A. (2012) An Overview of CMIP5 and the Experiment Design. *Bull. Am. Meteorol. Soc.* **93**: 485–498.

Thorne, O.M. and Fenner, R.A. (2008) Modelling the impacts of climate change on a water treatment plant in South Australia. *Water Sci. Technol. Water Supply* **8**: 305.

Trolle, D., Elliott, J. a, Mooij, W.M., Janse, J.H., Bolding, K., Hamilton, D.P., and Jeppesen, E. (2014) Advancing projections of phytoplankton responses to climate change through ensemble modelling. *Environ. Model. Softw.* **61**: 371–379.

Trolle, D., Hamilton, D.P., Pilditch, C. a., Duggan, I.C., and Jeppesen, E. (2011) Predicting the effects of climate change on trophic status of three morphologically varying lakes: Implications for lake restoration and management. *Environ. Model. Softw.* **26**: 354–370.

USCE (1995) CE-QUAL-R1: A numerical one-dimensional model of reservoir water quality; user's manual, Instruction Report E-82-1 (Revised Edition) Department of the Army, U.S. Corps Engineers, Washington D.C., USA.

Venables, W.N. and Ripley, B.D. (2002) Modern Applied Statistics with S 4th Ed. Springer, New York.

Westra, S., Thyer, M., Leonard, M., Kavetski, D., and Lambert, M. (2014) Impacts of Climate Change on Surface Water in the Onkaparinga Catchment Final Report Volume 1 : Hydrological Model Development and Sources of Uncertainty Goyder Institute for Water Research, Technical Report Series No. 14/22, Adelaide, South Australia.

Whitehead, P.G., Wilby, R.L., Battarbee, R.W., Kernan, M., and Wade, A.J. (2009) A review of the potential impacts of climate change on surface water quality. *Hydrol. Sci. J. - J. des Sci. Hydrol.* **54**: 101–123.

Woodbury, M., Baldo, M., Yates, D., and Kaatz, L. (2012) Joint Front Range Climate Change Vulnerability Study Water Research Foundation, Denver, Colorado, USA.

Yeo, I.K. and Johnson, R. (2000) A new family of power transformations to improve normality or symmetry. *Biometrika* **87**: 954–959.

Appendix 1 – R code for functions

clearSkyShortWave

```
clearSkyShortWave <- function(chrn = 1, lat = -35, alt = 0.05,
                              solcon = 1361.5,
                              AC = 0.84056972,
                              AB = -1.22495736,
                              K = 0.05702292){
  # solar constant in w/m2
  # Contracted Nelder-Mead direct search function minimizer output
  # See: clearSkyShortWave to Happy Valley Pyranometer.R
  #   $par [1]  0.84056972 -1.22495736  0.05702292
  #   $value [1] 1019.662 (sum absolute error as minimised)
  #   $counts  function   168
  #   $convergence [1] 0 (0 = converged)
  if(length(chrn)!=1) stop("single time only, use vectorized function: clearSkyShortWave.v")
  require(chron)
  yr <- as.numeric(levels(years(chrn)))
  mth <- as.numeric(months(chrn))
  dy <- as.numeric(days(chrn))
  tm <- 60*as.numeric(hours(chrn)) + minutes(chrn)

  if(leap.year(yr)) {diy <- 366} else {diy <- 365}
  doy <- julian(mth, dy, yr,
                origin.= c(month = 1, day = 1, year = yr))+1
  soldec <-   23.45*sin((360*(284+doy)/diy)*(pi/180)) # deg
  k1   <-  (-(tan(lat*(pi/180))*tan(soldec*(pi/180))))
  if(k1 > 1){dha <- 0} else if(k1 < 0-1){dha <- 180} else
    dha <- acos(-(tan(lat*pi/180)*
                    tan(soldec*pi/180)))*(180/pi) # deg sunset from S
  daylength   <- 8*dha # daylength in minutes
  tmha <- (tm-720)*0.25  # deg
  k2 <- 360*doy/diy # deg
  solorbrad <- 1.0001 + 0.034221*cos(k2*pi/180) +
    0.00128*sin(k2*pi/180) - 0.000719*cos(2*k2*pi/180)+
    0.000077*sin(2*k2*pi/180)
  coszen <- (sin(soldec*pi/180)*sin(lat*pi/180)+
               cos(soldec*pi/180)*cos(lat*pi/180)*
               cos(tmha*pi/180)) # deg
  Iotm <- solcon*solorbrad*coszen*1000/60 # W/m^2
  Iotm <- max(0,Iotm)

  TR <- AC+AB*exp(-K/coszen)
  Dir_PAR <- TR*Iotm*coszen
  TD <- 0.2710-0.2939*TR
  Dif_PAR <- Iotm*TD*coszen
  CS_PAR <- Dif_PAR + Dir_PAR
  as.numeric(CS_PAR) # W/m^2
}
```

clearSkyShortWave.v

```
clearSkyShortWave.v <- Vectorize(clearSkyShortWave)
```

AveSolarRadiation

```
AveSolarRadiation <- function(date = '2012-01-01', lat = -35, alt = 0.05){
  require(chron)
  tms <- chron(dates. = chron(rep(date, 145), format = 'y-m-d'), times. = seq(from = 0, to =
1, by = 1/144))
  mean(clearSkyShortWave.v(tms, lat = lat, alt = alt), na.rm = T)
}
```

AveSolarRadiation.v

```
AveSolarRadiation.v <- Vectorize(AveSolarRadiation)
```

cloudCoverFromSRdev

```
cloudCoverFromSRdev <- function(obsSR,idealSR, idealScale = 1, geom = 1.01, minThreshold =
3.5){
  obsSR[obsSR<idealSR*(1/minThreshold)] <-
idealSR[obsSR<idealSR*(1/minThreshold)]*(1/minThreshold)
 obsSR[obsSR>idealSR*idealScale] <- idealSR[obsSR>idealSR*idealScale]*idealScale
  maxScale <- (idealSR*idealScale) - idealSR*(1/minThreshold)
  obsSRscaled <- 1 - (geom^(obsSR - idealSR*(1/minThreshold))/(geom^maxScale))
  obsSRscaled
}
```

cloudCoverFromSR.MtBoldGLM

```
cloudCoverFromSR.MtBoldGLM <- function(obsSR,idealSR,idealScale = 1.049597, geom = 1.012686,
minThreshold = 4.447259){
  # function using parameters estimated for GLM MtBold met inputs
  # by quantile mapping to HVR observations
  # Leon van der Linden
  obsSR[obsSR<idealSR*(1/minThreshold)] <-
idealSR[obsSR<idealSR*(1/minThreshold)]*(1/minThreshold)
  obsSR[obsSR>idealSR*idealScale] <- idealSR[obsSR>idealSR*idealScale]*idealScale
  maxScale <- (idealSR*idealScale) - idealSR*(1/minThreshold)
  obsSRscaled <-
    1 - (geom^(obsSR - idealSR*(1/minThreshold))/(geom^maxScale))
  obsSRscaled
}
```

GOYDER INSTITUTE
FOR WATER RESEARCH

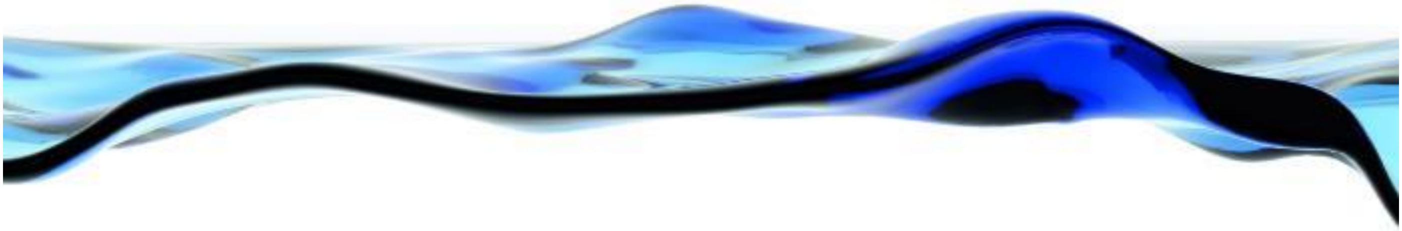

The Goyder Institute for Water Research is a partnership between the South Australian Government through the Department of Environment, Water and Natural Resources, CSIRO, Flinders University, the University of Adelaide and the University of South Australia.